Harnessing RIG-I in the tumor microenvironment for therapeutic breast cancer treatment

By

David Len Elion

Dissertation

Submitted to the Faculty of the

Graduate School of Vanderbilt University

in partial fulfillment of the requirements

For the degree of

DOCTOR OF PHILOSOPHY

in

Cancer Biology

December 14, 2019

Nashville, Tennessee

Approved:

Justin Balko, Pharm.D., Ph.D.

Jin Chen, M.D., Ph.D.

Rebecca Cook, Ph.D.

Barbara Fingleton, Ph.D.

John Wilson, Ph.D.

This work is dedicated to all breast cancer patients and their families, including my amazing, beautiful aunts Sharon Donaldson (1961-2018) and Iola Williams (1939-2019). I love you.

And to my dad, David Lee Elion Jr. (1939-2006)

And to my parents Bettye Baptist Wilson and Jesse Wilson for all of your continuous love and support

ACKNOWLEDGEMENTS

None of the work in this dissertation would have been possible without the unending support, training and mentorship from my advisor Dr. Rebecca Cook, who, from day one in her lab, has given me the tools and opportunity to learn and grow as a scientist. I want to express my deepest gratitude to Dr. Cook for arming me with the navigation and resources to complete my graduate training and for always continuing to encourage me and be a positive and uplifting voice and teacher throughout my journey.

I would also like to thank Donna Hicks and past members of the Cook laboratory, including Bushra Rahman, Dr. Michelle Williams and Dr. Thomas Werfel, who never hesitated to support, inspire and help me during my graduate training. I would also like to thank Dr. Linda Sealy and Dr. Jin Chen, who have been like second mentors to me during my graduate training, always willingly giving me advice, encouragement and perspective in conducting research, as well as in life and career development. I want to thank other members of my committee, Dr. Barbara Fingleton and Dr. John Wilson for always extending to me their guidance, resources and support, and also Dr. Justin Balko, who in addition to continuously lending his knowledge and guidance, also provided me with tools and resources to do research.

I want to thank current and past members of the Balko, Wilson, Rathmell, and Kim laboratories for all of their advice and help in completing this work including, Margaret Axelrod, Dr. Susan Opalenik, Dr. Jamaal James, Dr. Mellissa Nixon, Max Jacobson, Dr. Sema Sevimli, Diana Contreras, Matt Madden, and Dr. Michael Korrer.

I want to thank the Initiative for Maximizing Student Diversity (IMSD) program, Dr. Linda Sealy and Dr. Roger Chalkley, and Dr. Christina Keeton, as well as the T32 Microenvironmental Infuences in Cancer training grant, Dr. Jin Chen, for giving me the resources, knowledge, and training to succeed in graduate school, and I also want to thank the National Cancer Institute for their pre-doctoral fellowship (F31) funding. I additionally want to thank the leaders of the Cancer Biology Program, Dr. Jin Chen and Dr. Ann Richmond, as well as all our collaborators, Dr. John Wilson, Dr. Anna Pyle (Yale University), and Violeta Sanchez and Dr. Paula Gonzalez-Ericsson (Pathology Core, Breast SPORE VUMC).

Finally, I want to thank my family, my parents Bettye Wilson, Jesse Wilson, and David Lee Elion Jr. (deceased), as well as my grandparents, aunts, uncles and cousins, for your love, your teaching, your guidance, and unwavering support, and for always inspiring me to progress, to be a better person, to strive to reach my goals, and to strive to help others.

TABLE OF CONTENTS

LIST OF FIGURES

CHAPTER I

INTRODUCTION

Work presented in this chapter is published in *Oncotarget*:

"Harnessing RIG-I and intrinsic immunity in the tumor microenvironment for therapeutic cancer treatment," June 2018 [Volume 9, Number 48]

"Activation of RIG-I signaling to increase the pro-inflammatory phenotype of a tumor," March 2019 [Volume 10, Number 24]

Overview

Numerous reports demonstrate that most cell populations, including tumor cells, express receptors that recognize and respond to viral nucleotide motifs, referred to as pattern recognition receptors (PRRs). PRRs are important elements of innate immunity, which, once activated, initiate signaling pathways that generate a pro-inflammatory microenvironment that becomes replete with lymphocytes. Therapeutic approaches that use non-infectious methods to activate PRR signaling within the tumor microenvironment (TME) are gaining momentum as a strategy to prime tumors for cancer vaccine and immune checkpoint inhibitor (ICI) therapies. We recently investigated the PRR known as retinoic acid-inducible gene (RIG)-I in models of estrogen receptor positive (ER+), HER2 amplified (HER2+) and triple negative (TNBC) breast cancers, testing the possibility that, when appropriately delivered and modulated, RIG-I agonists might have a robust therapeutic effect, as is currently being explored for therapies targeting other PRRs, e.g. STING.

RIG-I is a cytosolic RNA helicase, recognizing RNA motifs specific to certain viruses. A decade of RIG-I research has culminated in the development of synthetic

non-infectious RIG-I agonists, comprised of minimal stem-loop RNA (SLR) sequences harboring a 5′ -triphosphate motif, capable of potent RIG-I activation in cultured tumor cells and in mice *in vivo*. Delivery of SLR sequences to cultured breast cancer cells activated RIG-I signaling and induced immunogenic programs of breast cancer cell death, demonstrating that RIG-I signaling has important therapeutic consequences that occur in a breast cancer cell intrinsic manner. Interestingly, we also found that RIG-I activation using SLR sequences induced expression of pro-inflammatory and T-cell recruiting cytokines in breast cancer cells, supporting the hypothesis that therapeutic RIG-I activation might recruit tumor infiltrating lymphocytes (TILs) and prime the TME for ICI response.

The effective delivery of SLR sequences to the TME *in vivo* was enabled by recent advances in nanoparticle (NP)-mediated delivery of RNA interference (RNAi) technologies. We focused on a previously described NP design strategy used with siRNAs, based on its proven *in vivo* protection of siRNA sequences, longer circulating half-life, increased uptake of siRNA by tumor cells, and enhanced endosomal release of siRNA cargo into the cytoplasm of tumor cells. Adapting this NP design for use with SLR sequences, we found that RIG-I activation in tumor cells *in vivo* resulted in increased expression of pro-inflammatory cytokines and increased tumor cell death. Additionally, SLR treatment resulted in potent TIL recruitment to the TME, and primed otherwise insensitive tumors for sensitivity to anti-PD-L1 treatment. Importantly, we found that RIG-I signaling in breast cancer cells increases activation and tumor cell-directed killing in adjacent T-lymphocytes, indicating an increase in T-cell mediated immunity following RIG-I activation in breast cancer .

These findings support clinical translation of RIG-I agonists, which is currently underway (NCT03065023) using the RIG-I agonist from Merck, MK-4621, in advanced and recurrent tumors. Another clinical trial recently opened (NCT03739138) to identify the therapeutic effects of MK-4621 with anti-PD-1 (Pembrolizumab) in patients with advanced and recurrent tumors. These trials are supported by our data demonstrating that RIG-I agonists increase ICI response in breast cancers through at least two mechanisms, tumor intrinsic apoptosis and enhanced immunogenicity of the TME. It is anticipated that, although RIG-I agonists are only in earliest phases of exploration as cancer treatment strategy, the field will move forward at a rapid pace, based on the vast potential for its success in immune-oncology.

Pattern recognition receptors in cancer

The immune system is capable of targeted tumor cell killing through the process of immunosurveillance. Although tumors often develop ways to escape immunosurveillance, the growing interest and understanding of molecular interactions that occur between the tumor and the immune system have resulted in treatment strategies aimed at harnessing the immune system to target cancers. Recent advances in tumor immunology have produced immune checkpoint inhibitors (ICIs), cancer treatments designed to relieve the checkpoint restraints on adaptive immunity (1). ICIs have revolutionized treatments for many types of cancer (1–3). Despite these successes, not all patients respond to ICI therapy, for reasons that are varied and incompletely understood. It is thought that ICIs may be less effective in tumors that are

poorly immunogenic, as defined by low levels of tumor infiltrating lymphocytes (TILs), minimal cross-presentation of tumor neoantigens, and high levels of immune suppressive leukocytes such as regulatory T-cells (TRegs), tumor associated macrophages (TAMs) and myeloid derived suppressor cells (MDSCs) (4–7). Innovative strategies to increase immunogenicity in tumors are being explored through a variety of approaches. One emerging strategy is based on activation of innate immunity in the tumor microenvironment (TME) (8, 9). Innate immunity is a powerful arm of the immune system responsible for rapid anti-microbial immunity, often inducing programmed cell death of an infected cell. Innate immunity functions beyond the infected cell as well, by modulating the expression of cytokines and chemokines that recruit T-lymphocytes to the affected tissue, enhance antigen presentation, and increase cross-priming to antigen-specific T-cells (8, 10). This idea is being explored extensively in regard to the pattern recognition receptor (PRR) known as Stimulator of Interferon Genes (STING) (11, 12). Synthetic STING ligands potently induce anti-tumor immunity in several cancers, including breast cancer, chronic lymphocytic leukemia, colon cancer, and squamous cell carcinoma (13–17). However, there is increasing evidence that STING signaling might be defective in some cancers, due to mutations, promoter methylation, and decreased expression of STING pathway effectors (18, 19), thus limiting their potential efficacy in the tumor cell compartment of the TME. However, other cells of the TME, particularly cells of the immune compartment, may retain STING signaling even when the STING pathway is defective within the tumor cells, per se, allowing STING ligands to induce innate immunity within the TME under these circumstances (20).

Viral nucleic acid sensors, such as the RNA helicase known as retinoic acid-inducible gene I (RIG-I, encoded by the gene DDX58) (21), are expressed in most cells of the human body, including tumor cells (22). When infected by an RNA virus, double-stranded RNA replication intermediates derived from the virus bind to RIG-I (23–26) and activate a RIG-I inflammasome leading to pyroptosis, a highly immunogenic mechanism of programmed cell death (27–29). A hallmark of pyroptosis is the formation of pores in the plasma membrane [30], leading to hypotonic cell swelling and leakage of intracellular contents, including danger associated molecular patterns (DAMPs), into the microenvironment. RIG-I signaling simultaneously induces expression of pro-inflammatory cytokines (8, 10). Together, DAMPs and pro-inflammatory cytokines stimulate a local acute inflammatory immune response aimed at removal of virus and virally-infected cells (31). Interestingly, viral nucleotide motifs can be mimicked using synthetic, non-infectious oligonucleotides. These RIG-I agonists are capable of triggering RIG-I signaling, pyroptosis, and acute inflammation (26, 32–35). In the cancer setting, RIG-I activation could thus provide a three-pronged attack: 1.) direct activation of tumor cell death; 2.) cytokine-mediated activation of innate immune effectors (e.g., macrophages, natural killer cells), and 3.) increased recruitment and cross priming of adaptive immune effectors (e.g., CD8+ T-lymphocytes) through a cytokine-enriched microenvironment and enhanced activity of professional antigen presenting cells [APCs, e.g., dendritic cells (DCs) or macrophages] (**Figure 1.1**). Synthetic RIG-I agonists are being explored as a therapeutic approach in a diverse range of cancers (27, 33, 34, 36). Here, we review studies of RIG-I signaling in the tumor microenvironment, and preclinical studies investigating RIG-I agonists for cancer treatment.

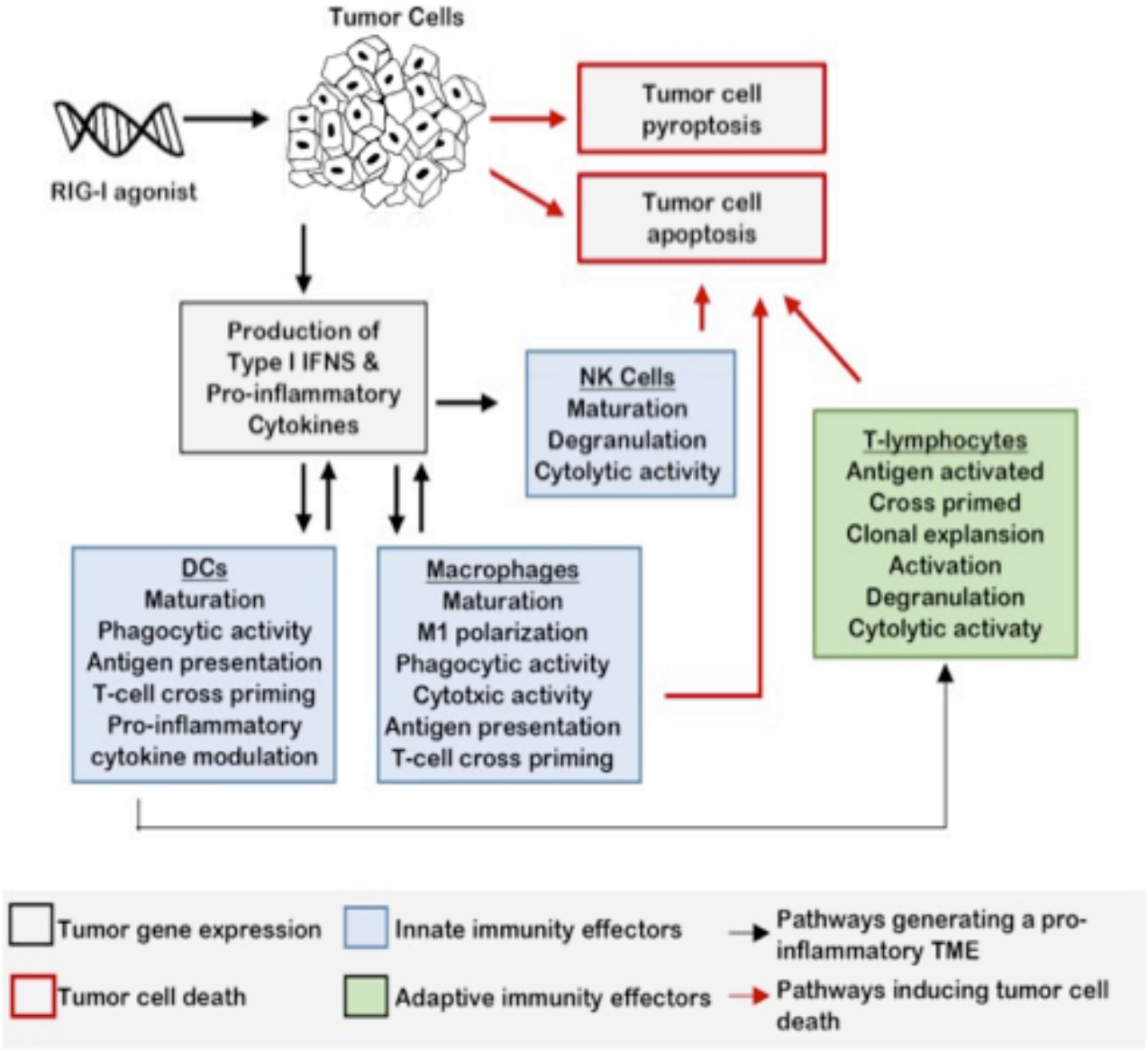

Figure 1.1 RLR activation signals innate immunity in the TME. When tumor cells are treated with an RIG-I mimetic, inflammatory cytokine and type I IFN expression is rapidly upregulated, inducing innate immune responses in the tumor microenvironment. The cytolytic activity of leukocytes, such NK cells and macrophages, is increased in response to this IFN-enriched microenvironment. Maturation and activation of macrophages and DCs result in enhanced antigen presentation to T-lymphocytes in tumor draining lymph nodes. T-regulatory cell differentiation is decreased by the pro-inflammatory microenvironment produced by RIG-I activation.

Activation of RLRs induces pro-inflammatory signaling in a cell-intrinsic manner

RIG-I was first identified as a cytosolic DExD/H box RNA helicase activated in response to certain RNA viruses (21). RIG-I is activated upon recognition of its ligand, double-stranded RNA sequences modified with a 5′ -triphosphate (5′ -3pRNA) or 5′ -diphosphate (5′ -2pRNA) motif (24, 26, 27, 37). RIG-I activation may occur in response to other RNA motifs, including blunt dsRNAs (38), monomeric RNA within defective human immunodeficiency virus (HIV)-1 particles (39), cytoplasmic long non-coding RNAs (40), small nuclear RNAs (41–44), or endogenous retroviral transcripts. In addition to the DexD/H box RNA helicase domain, RIG-I is characterized by an amino-terminal Caspase Activation and Recruitment Domain (CARD) domain, and a Carboxy-Terminal Domain (CTD) (45–47). Once activated by its ligand, RIG-I undergoes an ATP-dependent conformational change, exposing its CARD domain for polyubiquitylation [48] by ubiquitin ligases such as TRIM25, Riplet and others (49–52). Once polyubiquitylated, a mitochondrial signalosome, comprised of the proteins WHIP, PPP6C and TRIM14, recruits RIG-I to the mitochondrial surface where the CARD domain of RIG-I interacts with the CARD domain of Mitochondrial Anti-Viral Signaling (MAVS), a requisite RIG-I co-factor (49, 53–55).

Once engaged, MAVS signaling activates three kinases that serve as regulators of inflammation, Inhibitor of κB-Kinase (IKK)-γ, TANK-Binding Kinase (TBK)-1 and IKK-ε (56–58). These kinases phosphorylate Interferon (IFN) Regulatory Factor (IRF)-1, IRF-3, IRF-7, and Nuclear Factor (NF)-κB (59–61), transcription factors that drive expression of a pro-inflammatory transcriptional program that includes type I IFNs and pro-

inflammatory cytokines (45, 62). Importantly, IFN-α, IFN-β, and other pro-inflammatory cytokines produced in response to RIG-I activation drive a feed-forward signaling loop that maintains high expression levels of RIG-I, IFNs and additional pro-inflammatory IFN-stimulated genes (ISGs), by maintaining phosphorylation and activation of the transcription factors IRF-3, IRF-7, and NF-κB, and by phosphorylation of the transcription factor Signal Transducer and Activator of Transcription (STAT)-1, which occurs in response to IFN-α/β receptor (IFNAR)-mediated activation of JAK-STAT signaling (**Figure 1.2**) (62). This feed-forward signaling model amplifies inflammatory cytokine production in the infected and neighboring cells, while recruiting leukocytes to the infected area, including pro-inflammatory lymphocytes. Since a 'T-cell inflamed' microenvironment is often associated with an improved prognosis for several cancers, and correlates with increased tumor sensitivity to ICIs, the pro-inflammatory phenotype induced by RIG-I activation may be an attractive treatment approach to increase tumor immunogenicity and clinical success of ICIs.

Two RIG-I-like receptors (RLRs) with structural similarity to RIG-I have been identified. One of these RLRs, Melanoma Differentiation Associated (MDA)-5, harbors an amino-terminal CARD domain, a DexD/H box motif, and a CTD domain (63, 64). Like RIG-I, MDA-5 induces type I IFNs and other pro-inflammatory cytokines in response to viral nucleotides, albeit viral nucleotide motifs that are distinct from those that activate RIG-I. MDA-5 is activated by blunt-ended, long double-stranded RNA [e.g. polyinosinic-polycytidylic acid, or poly(I:C)], a ligand that also activated some Toll-Like Receptors (TLRs). In contrast to RIG-I and MDA-5, the other RLR known as Laboratory of Genetics and Physiology (LGP)-2 lacks the CARD domain shared by RIG-I and MDA-5,

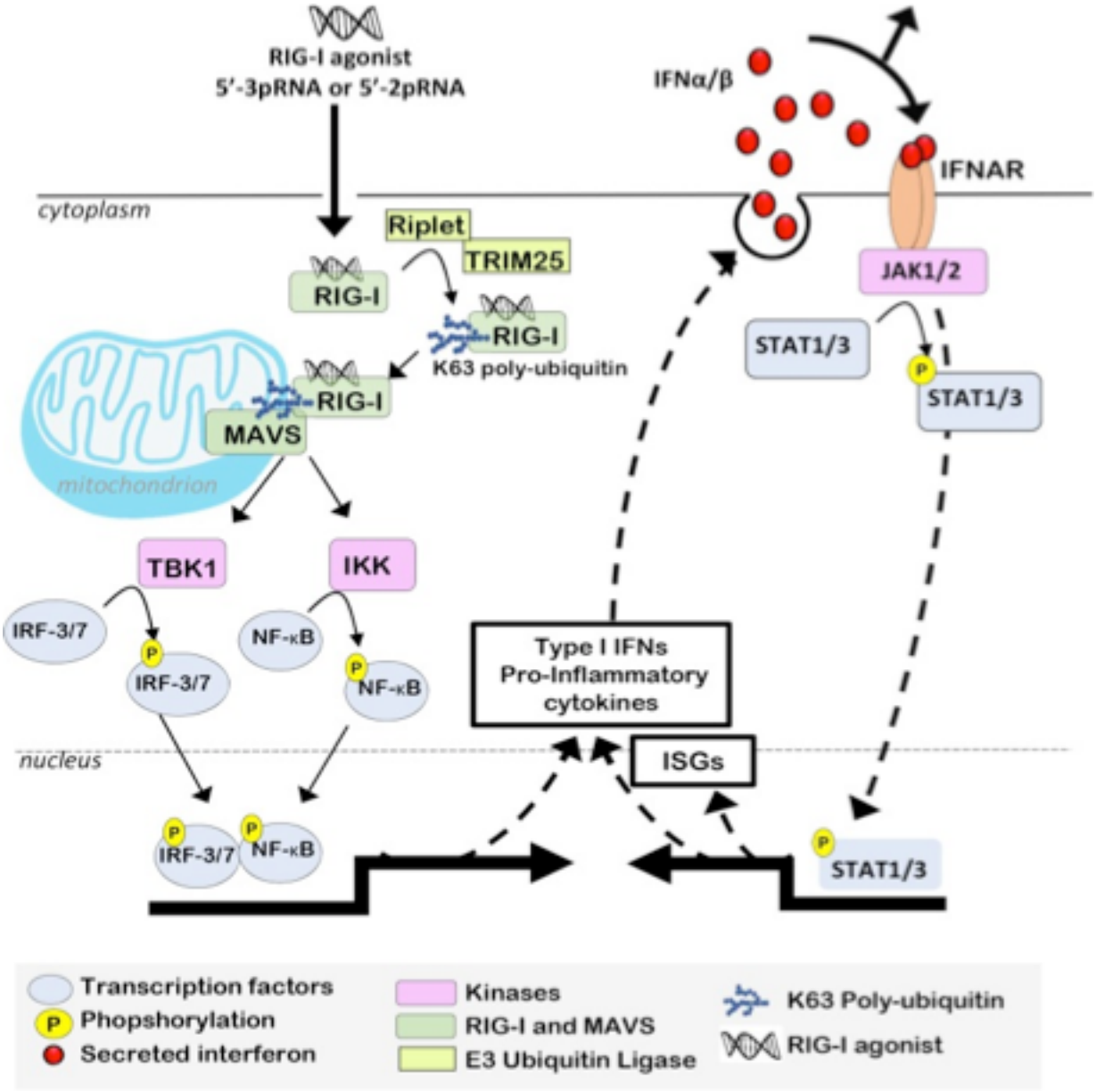

Figure 1.2 RIG-I activation induces Type I IFNs, which support pro-inflammatory transcriptional reprogramming. RIG-I binding to 5′ -3pRNA or 5′ -2pRNA induces a conformational change, allowing RIG-I CARD domains to be polyubiquitylated by E3 ligases (e.g., Riplet or TRIM25). Polyubiquitylated RIG-I is recruited to mitochondria outer membranes, where it interacts with MAVS, which then activates IKK-ε, IKK-γ, and TBK1, kinases responsible for phosphorylation/activation of transcription factors (ATF-1, c-Jun, CBP, IRF-3, NF-κB). These transcription factors induce an expression profile that includes Type I I IFNs and additional pro-inflammatory cytokines. Type I IFNs bind to IFNAR, activating the intracellular tyrosine kinase JAK1/2, which in turn phosphorylates pro-inflammatory STAT transcription factors, thus driving expression of additional ISGs and amplifying the IFN-inducible positive feedback loop to support and maintain a pro-inflammatory microenvironment.

but is otherwise similar to the other RLRs (65). Without the CARD domain, LGP-2 is unable to interact directly with MAVS to initiate a pro-inflammatory response. There are reports suggesting that LGP-2 activation interferes with RIG-I signaling, but that MDA-5 signaling may be enhanced by LGP2 (48, 66–69). The implications of LGP2 expression and signaling in the context of cancer therapy, and how LGP2 might affect therapeutic responses to RIG-I agonists, are currently unclear.

RLR signaling potently activates programmed cell death

In the context of viral infection, RIG-I signaling is capable of inducing programmed cell death (PCD) as a mechanism to eliminate virally-infected cells. Cellular mechanisms by which RIG-I induces PCD include activation of the intrinsic apoptosis pathway, the extrinsic apoptosis pathway, and a type of programmed necrosis termed 'pyroptosis.' The molecular factors governing the mode of RIG-I mediated cell death may depend to some extent on cell type. For example, RLR activation in keratinocytes, melanoma cells, glioblastoma cells, and many leukemia cells cause mitochondrial outer membrane permeabilization (MOMP), cytochrome-C release from mitochondria, and activation of caspase-9 and Apaf-1, the irreversible molecular switch that governs the intrinsic apoptotic pathway (27). However, RIG-I signaling in pancreatic and prostate cancer cells robustly induces expression of several factors that activate the extrinsic apoptotic pathway, including Fas, Fas Ligand, Tumor Necrosis Factor (TNF), TNF-related apoptosis-inducing ligand (TRAIL), and the TRAIL receptors Death Receptor (DR)-4 and DR-5, causing caspase-8 activation and extrinsic apoptosis. The mechanism by which RIG-I signaling upregulates TRAIL, FAS and other extrinsic

apoptosis-activating factors are not entirely clear, although it is likely that IFN signaling is involved, given that Fas, TRAIL, and caspase-8 are known ISGs (70, 71).

Another mode of programmed cell death induced upon RIG-I activation is termed "pyroptosis," an immunogenic form of cell death occurring in response to activation of the inflammasome, a multi-protein holoenzyme comprised of capsase-1 oligomers, adaptor proteins known as ASC (Apoptosis-associated Speck with a Caspase-recruitment domain), and a molecular sensor of pathogens, such as RIG-I (Figure (**Figure 1.3**). RIG-I can interact, via its CARD domain, with the CARD domains of inflammasome components (72), resulting in auto-cleavage and activation of caspase-1 (29, 73), which then allows proteolysis of the pro-inflammatory cytokines interleukin (IL)-1β and IL-18 (73), which amplify inflammatory signaling in the local environment while activating natural killer (NK) cells and recruiting leukocytes to the affected tissue. Caspase-1 activation also results in cleavage of Gasdermin-D, removing the auto-inhibitory domain from Gasdermin-D to allow oligomerization at the plasma membrane and pore formation. Plasma membrane permeabilization by Gasdermin-D pores allows water to enter and swell the cell, a hallmark of necrosis. Once membrane integrity is lost, intracellular contents, including DAMPs, permeate the extracellular environment, inducing danger responses in neighboring cells, which amplifies the inflammatory response.

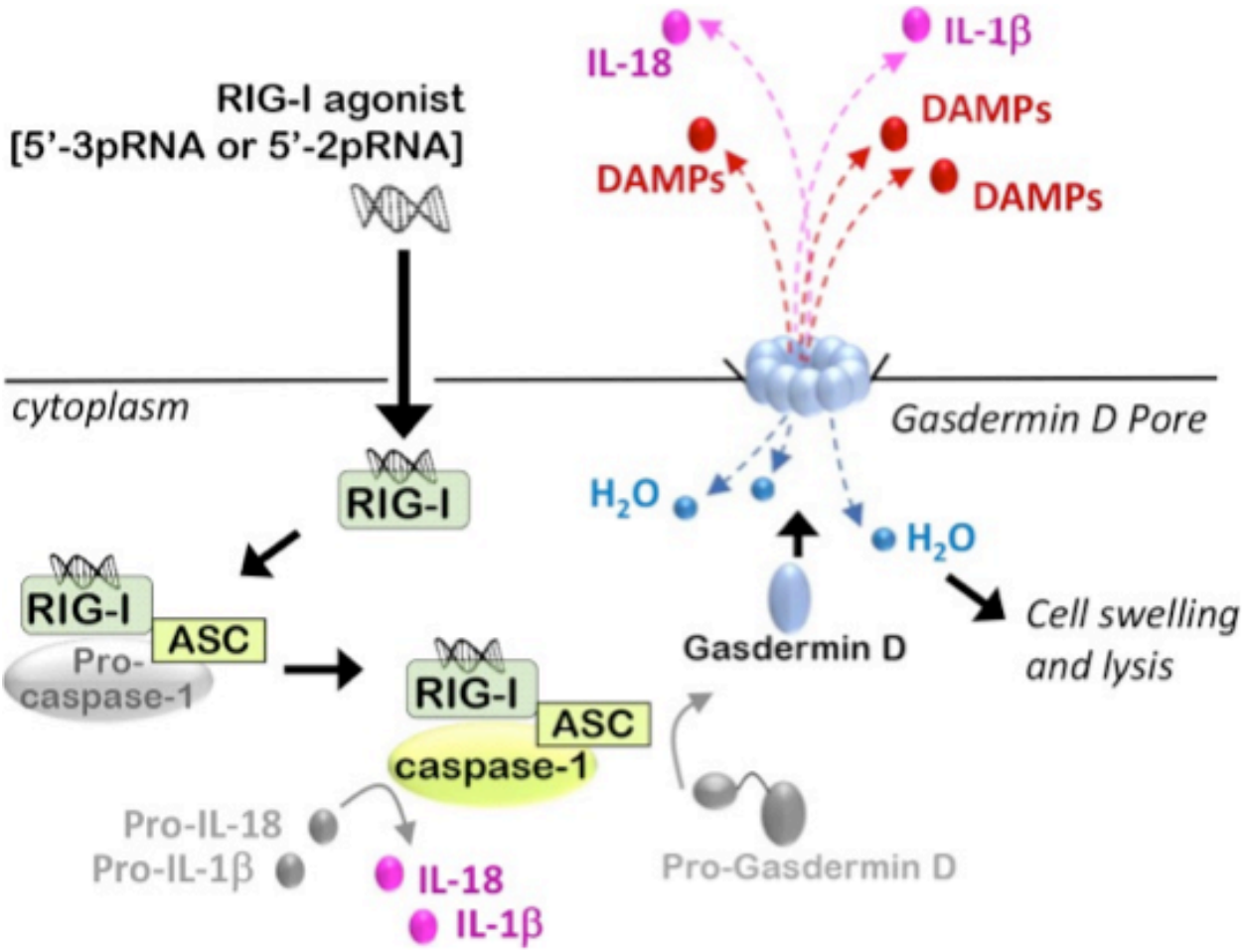

Figure 1.3 RIG-I activation induces immunogenic modes of programmed cell death. Activated RIG-I recruits the inflammasome adaptor protein ASC, which facilitates binding and oligomerization of Caspase-1, leading to caspase-1 auto-cleavage and activation. Caspase-1 cleaves protein precursors of IL-1β and IL-18 to generate their mature, pro-inflammatory isoforms, which are then secreted. Caspase-1 activity also drives cleavage of the auto-inhibitory domain from Gasdermin-D, liberation the amino-terminal pore-forming domain of Gasdermin-D to translocate to the plasma membrane and oligomerize, forming pores that initiate hypotonic cellular swelling and lysis, followed by release of DAMPs into the extracellular space, thus inducing an inflammatory response from surrounding cells.

RLR signaling in tumor cells affects the complex tumor microenvironment

The capacity for RIG-I signaling to induce cell death, while inducing pro-inflammatory responses, makes therapeutic use of RIG-I mimetics a highly attractive option in cancers. A growing number of studies show that the molecular responses to RIG-I or RLR signaling are retained in tumor cells and in non-tumor cells of the tumor microenvironment, and support innate immune responses against tumor cells (34). For example, RIG-I activation in ovarian cancer cells enables NK-mediated tumor cell killing in culture (36). Further, RIG-I signaling within the tumor cell increases phagocytosis of the affected tumor cell by professional APCs, including macrophages and DCs, thus providing tumor antigens for presentation to lymphocytes (32). At the same time, the IFN-enriched microenvironment generated by tumor cell RIG-I signaling increases expression of major histocompatibility complex (MHC)-II antigen presentation molecules in macrophages and DCs, which may further increase tumor antigen cross-presentation. In support of this idea, it is reported that DCs presented pancreatic cancer-derived antigens more robustly to T-cells if RIG-I signaling was activated in pancreatic cancer cells prior to their co-culture with DCs (32, 36). Similar results were observed upon RIG-I activation ovarian cancer cells prior to co-culture with macrophages (74).

RLR agonists are gaining traction as a possible cancer treatment in pre-clinical studies

Through direct activation of intrinsic immunity in cancer cells, and accompanying indirect activation of leukocytes in the TME, synthetic RIG-I mimetics are under investigation for cancer treatment in pre-clinical studies in hepatocellular carcinoma

(75), leukemias (76), melanomas (27), prostate cancers (77) and others. RIG-I agonists that are stable and functional *in vivo* are under current development. For example, a minimal 5′ -triphophosphorylated stem-loop RNA (SLR) sequence for intra-venous delivery to mice was recently reported (25). The stem-loop structure enhances structural stability of the complex, a key determinant of RIG-I ligand potency. Delivery of SLR sequences to mice *in vivo* activated RIG-I signaling, IFN induction, and expression of genes required for potent anti-viral immunity, although this RIG-I mimetic has not yet been studied in tumors grown *in vivo*. A pre-clinical compound specific for RIG-I is RGT100 (Merck/Rigontec), currently in phase I clinical trials for treatment of advanced solid tumors and lymphomas (NCT03065023), although peer-reviewed preclinical reports for RGT100 were not identified, to our knowledge. Another compound which activates RIG-I by unknown mechanisms is SB-9200 (78), which is currently under investigation as an anti-viral agent, but has not yet been tested in the pre-clinical setting of cancer treatment.

In addition to RIG-I specific mimetics, synthetic RLR mimetics are being investigated in pre-clinical and early clinical studies. The compound Hiltonol [polyinosinic-polycytidylic acid stabilized with poly-l-lysine and carboxymethylcellulose (poly-ICLC)] (79, 80) was tested in combination with chemotherapy for patients with Stage IV anaplastic astrocytoma, resulting in increased overall survival (OS) to >8 years, versus the expected survival of two years on conventional chemotherapy alone (81). Another trial tested poly-ICLC in combination with radiation and temozolomide in newly diagnosed adult glioblastoma patients. In these studies, intramuscular poly-ICLC increased OS to 18.3 months from 14.6 months (82–84). Further, poly-ICLC is being

tested as a tumor vaccine adjuvant in several cancer types, with a growing number of successes in Phase I and II clinical trials for gliomas (85), breast cancer (86), pancreatic cancer (87), ovarian cancer (88, 89), multiple myeloma (90), and others, highlighting the potential advances that Poly-ICLC may achieve across a spectrum of cancers. Although poly-ICLC potently activates MDA-5, it also activates Toll-like Receptor (TLR)-3, making the specific contributions of RLR signaling to the therapeutic effects of poly-ICLC, and to patient outcome, difficult to dissect.

The future of RLR agonists in cancer

Exciting innovations within the field of RIG-I agonists are emerging. For example, a powerful, bimodal application of RNAi-based silencing of intra-tumoral gene targets using a 5′-triphosphate modified dsRNA sequence would allow for RIG-I activation and simultaneous gene targeting. This approach was demonstrated in melanomas, using 5′-3p-siRNA sequences specific to the anti-apoptotic gene BCL2. Delivery of this construct to cells potently stimulated IFN production and NK activation, while enhancing tumor cell killing through Bcl-2 ablation (34). This concept was validated using a 5′-3p-siRNA targeting transforming growth factor (TGF)-β in pancreatic cancer cells, resulting in tumor cell apoptosis, IFN induction, and enhanced CD8+ T cell responses (36). A similar approach was used in models of non-small cell lung cancer, using 5′-3p-siRNA sequences against vascular endothelial growth factor (VEGF), resulting in reduced tumor angiogenesis while enhancing anti-tumor immunity (91). Defining the most appropriate gene silencing target may be a difficult task, but the use

of siRNA paves the pathway for targeting certain oncogenes (e.g., MYC) that are currently 'undruggable.'

Despite the potential success of RIG-I and RLR agonists, the immune system is powerful and incompletely understood, warranting cautious optimism and thorough examination of the caveats associated with innate immune activation, including possible on-target induction of autoimmunity, or induction of a cytokine 'storm' which could pose a threat to patient safety (92–94). It is important to note that, since RIG-I is expressed in most cells of the human body, the consequences of RIG-I activation might be widespread, driving symptoms like fatigue, depression and cognitive impairment. In ICI-based therapies, these side-effects are generally managed by corticosteroid immunosuppression.

Delivery of small nucleotide sequences to tumor cells and leukocytes within the TME is another major obstacle to the widespread utility of RIG-I or RLR-based therapeutics in the cancer setting. Studies aimed at generating stable, specific and potent RIG-I ligands that retain functionality *in vivo* have been reported only recently. For example, a study employing a minimal 5′-triphophosphorylated stem-loop RNA (SLR) sequence delivered by intra-venous delivery to mice activated in RIG-I signaling, IFN induction, and expression of genes required for potent anti-viral immunity *in vivo*. A recently described 'conditional' RIG-I ligand, in which the 5′-triphosphorylated terminus of the RNA duplex remained shielded until release by predetermined molecular cues *in vivo*, could enhance delivery of RIG-I agonist to tumors, and minimize RIG-I activation outside of the TME (95). However, the efficacy of RIG-I ligands,

including SLRs and conditional RIG-I ligands, not yet been tested in animal models of cancer (25).

In summary, therapeutic RIG-I and RLR agonists are emerging as a novel approach to engage the immune system in the fight against cancer. Importantly, RIG-I signaling directly promotes tumor cell killing through three distinct modes of action: intrinsic apoptosis, extrinsic apoptosis, and pyroptosis. Further, simultaneous activation of the innate and adaptive arms of the immune system may generate durable therapeutic responses. The multi-faceted mechanisms by which RLR agonists eliminate cancer cells represent the well-rounded arsenal of weapons required to fight aggressive and metastatic cancers effectively.

CHAPTER II

THERAPEUTICALLY ACTIVE RIG-I AGONIST INDUCES IMMUNOGENIC TUMOR CELL KILLING IN BREAST CANCERS

Work presented in this chapter is published with the same title in Cancer Research, November 2018 [Volume 78, Number 21]

Abstract

Cancer immunotherapies that remove checkpoint restraints on adaptive immunity are gaining clinical momentum but have not achieved widespread success in breast cancers, a tumor type considered poorly immunogenic and which harbors a decreased presence of tumor-infiltrating lymphocytes. Approaches that activate innate immunity in breast cancer cells and the tumor microenvironment are of increasing interest, based on their ability to induce immunogenic tumor cell death, type I IFNs, and lymphocyte-recruiting chemokines. In agreement with reports in other cancers, we observe loss, downregulation, or mutation of the innate viral nucleotide sensor retinoic acid-inducible gene I (RIG-I/DDX58) in only 1% of clinical breast cancers, suggesting potentially widespread applicability for therapeutic RIG-I agonists that activate innate immunity. This was tested using an engineered RIG-I agonist in a breast cancer cell panel representing each of three major clinical breast cancer subtypes. Treatment with RIG-I agonist resulted in upregulation and mitochondrial localization of RIG-I and activation of pro-inflammatory transcription factors STAT1 and NF-κB. RIG-I agonist triggered the extrinsic apoptosis pathway and pyroptosis, a highly immunogenic form of cell death in breast cancer cells. RIG-I agonist also induced expression of lymphocyte-recruiting chemokines and type I IFN, confirming that cell death and cytokine modulation occur in

a tumor cell–intrinsic manner. Importantly, RIG-I activation in breast tumors increased tumor lymphocytes and decreased tumor growth and metastasis. Overall, these findings demonstrate successful therapeutic delivery of a synthetic RIG-I agonist to induce tumor cell killing and to modulate the tumor microenvironment *in vivo*.

Introduction

Breast cancer is the most frequently diagnosed cancer in women (96). Despite advances in early detection and treatment, breast cancer remains the second leading cause of cancer-related deaths for women. With an eye toward new treatment strategies, recent attention has focused on immune-checkpoint inhibitors (ICI), antibodies that block regulatory receptors that dampen adaptive immunity (e.g., PD-1, PD-L1, CTLA-4). ICI-mediated inhibition of checkpoint receptors releases regulatory restraints on adaptive immunity, permitting a pro-inflammatory lymphocytic response against tumor neoantigens, and resulting in robust and durable antitumor immune responses (1). ICI treatments have seen remarkable success in cases of melanoma and lung cancer (1–3). However, ICI response rates reported in breast cancer clinical trials have thus far been disappointing, achieving success in only a fraction of patients (97-99). The relatively diminished response to ICIs in breast cancer is not completely understood, but may relate to fewer tumor-infiltrating lymphocytes (TIL) (100-101), a decreased mutational burden (4-5), limited or absent expression of antigen presentation machinery on tumor cells (6), or enhanced expression of counter-regulatory factors in breast cancers as compared with what is seen in other cancer types (7). A fraction of the highly aggressive triple-negative breast cancer (TNBC) subtypes, which on average

harbor a greater number of TILs and a greater mutational burden than the other clinical breast cancer subtypes, have shown greater response to ICI over those breast cancer subtypes expressing estrogen receptor (ER+) or harboring HER2 gene amplification (HER2+). Further, decreased TILs within the aggressive TNBC subtype predict poor outcome and decreased response to ICI. Interestingly, certain chemotherapeutic regimens increase TILs in breast cancers, which often correlates with improved response to treatment. Therefore, a new treatment paradigm may be needed in breast cancers to promote de novo inflammation to instigate antitumor immunity, or to enable efficacy of existing ICIs. It is possible that treatment strategies that increase TILs improve antigen presentation or increase inflammatory cytokines in the tumor microenvironment might improve immunogenicity of all breast cancer subtypes.

Pattern recognition receptors (PRR) of the innate immune system, which recognize conserved pathogen-associated molecular patterns (PAMP; e.g., viral nucleotide motifs), are gaining interest as a potential treatment strategy (8-9). PRR activation by their viral nucleotide ligand induces pro-inflammatory transcription factors, including NF-κB, signal transduction and transcription, and interferon regulatory factors (IRF), which drive production of IFNs and other pro-inflammatory cytokines that orchestrate antimicrobial innate immune responses and stimulate adaptive immunity (8, 10). Certain PRRs are expressed in nearly every cell in the human body, including cancer cells, suggesting that some PRRs might be leveraged therapeutically as part of a cancer treatment strategy. This idea is being explored extensively in regard to the PRR known as stimulator of interferon genes (STING) (11-12). Synthetic STING ligands potently induce type I IFNs and support antitumor immunity across a variety of cancers,

including breast, CLL, colon, and squamous cell carcinoma (13–17). However, there is increasing evidence that STING signaling is defective in many cancers, including breast some breast cancers, due to mutations, promoter methylation, and decreased expression of genes in the STING pathway (18-19).

Retinoic acid-inducible gene I (RIG-I) is another PRR, playing a key role in recognizing RNA viruses. In contrast to the frequent STING pathway alterations seen in breast cancers, alterations in the RIG-I gene DDX58 have been infrequently reported, and DDX58 promoter methylation was not significantly higher in breast tumor versus normal breast tissue (18). RIG-I recognizes double-stranded viral RNAs (dsRNA) containing two or three 5′ -phosphates (23–26). RIG-I activation by its ligand causes RIG-I translocation to mitochondria, where it interacts with its binding partner Mitochondrial antiviral signaling (MAVS) to activate signaling pathways that produce pro-inflammatory cytokines (53). Importantly, RIG-I activation also promotes the elimination of virally infected cells through apoptotic pathways (27-29). These attributes make RIG-I mimetics an attractive therapeutic approach in immune oncology.

Therapeutic efficacy of RIG-I mimetics has been seen in several cancer cell lines originating from a variety of tissues, although the impact of RIG-I activation in breast cancers is relatively understudied as compared with other cancers. Further, the use of RIG-I agonists as a cancer treatment requires a specific and potent RIG-I ligand that is functional *in vivo*, which has only recently been reported in a study using a minimal 5′ -triphophosphorylated stem-loop RNA (SLR) sequence for intravenous delivery to mice (25). The stem-loop structure enhances structural stability of the complex, a key determinant of RIG-I ligand potency. Delivery of SLR sequences to mice *in vivo*

activated in RIG-I signaling, IFN induction, and expression of genes required for potent antiviral immunity. However, the efficacy of RIG-I ligands, including SLRs, in animal models of cancer has not yet been tested.

We tested the hypothesis that RIG-I–mediated activation of innate immune responses might be therapeutically efficacious in breast cancers, while increasing the inflammatory phenotype of breast cancers. We demonstrate here that RIG-I activation in breast cancer cells resulted in tumor cell–intrinsic tumor cell death due in part to activation of pyroptosis and induced expression of inflammatory cytokines, leukocyte-recruiting chemokines, and increased expression of major histocompatibility (MHC)-I components. Delivery of synthetic RIG-I ligands to breast tumors *in vivo* recapitulated these results, recruiting leukocytes to the tumor microenvironment and decreasing tumor growth and metastasis.

Materials and Methods

Generation of SLR20

Oligoribonucleotides sequence OH-SLR20 (5′ -GGACGUACGUUUCGACGUACGUCC) was synthesized on an automated MerMade synthesizer (BioAutomation) using standard phosphoramidite chemistry. The hydroxylated oligonucleotide was deprotected and gel purified as previously described (34). Triphosphorylated oligoribonucleotide SLR20 (5′ ppp-GGACGUACGUUUCGACGUACGUCC) was synthesized as described (35), deprotected, and gel purified. The triphosphorylation state and purity were confirmed using mass spectrometry. The oligonucleotides were resuspended in RNA storage

buffer (10 mmol/L MOPS pH 7, 1 mmol/L EDTA) and snap cooled to ensure hairpin formation, as previously described (28).

Cell line authentication

The human cell lines MCF-7, BT474, and murine cell line 4T1 were purchased from ATCC in 2015. All cells were maintained at low passage in DMEM with 10% fetal bovine serum and 1% antibiotics and antimyotics. Cell identity was verified by ATCC using genotyping with a Multiplex STR assay. All cell lines were screened monthly for Mycoplasma. Cells were used within 20 passages for each experiment.

Cell culture

SLR20 and OH-SLR20 were delivered to cells in serum-free Opti-MEM media at a final concentration of 0.25 μmol/L using lipofectamine 2000 (Invitrogen). Where indicated, cells were treated with staurosporine (Cell Signaling Technology) at a final concentration of 1 μmol/L in serum-free Opti-MEM. Cells expressing shRNA against RIG-I were generated by transduction with pLKO lentiviral particles (Sigma-Aldrich) harboring shRNA sequences against human or mouse RIG-I (DDX58) and selected with puromycin (2 μg/mL). Cells were treated with inhibitors for caspase-9 (Z-LEHD-FMK, BD Pharmingen), caspase-10 (Z-AEVD-FMK, Cayman Chemical), and caspase-1 (Ac-YVAD-CHO, Cayman Chemical) at a final concentration of 5 μmol/L.

Western analysis

Whole-cell lysate was harvested by homogenization of cells in ice-cold lysis buffer [50 mmol/L Tris pH 7.4, 100 mmol/L NaF, 120 mmol/L NaCl, 0.5% nonidet P-40, 100 μmol/L Na3VO4, 1 × protease inhibitor cocktail (Roche), 0.5 μM MG132 (Selleck Chem)]. Mitochondrial and cell membrane extracts were harvested from cells using the Cell Fractionation Kit (Cell Signaling Technologies) according to the manufacturer's instructions. Lysates (20 μg protein measured by BCA assay) were resolved on 4% to 12% polyacrylamide gels (Novex) and transferred to nitrocellulose membranes (iBlot), blocked in 3% gelatin in TBS-T (Tris-buffered saline, 0.1% Tween-20), incubated in primary antibodies from Cell Signaling Technologies: (RIG-I (D14G6, 1:1,000), MAVS (3993, 1:1,000), SOD2 (D3 × 8F, 1:1,000), p65 (D14E12, 1:1,000), P-p65 Y701 (D4A7, 1:1,000), STAT1 (D1K9Y, 1:1,000), P-STAT1 S536 (93H1, 1:1,000), PARP (9542, 1:1,000), caspase-1 (2225, 1:1,000), cleaved caspase-1 (D57A2, 1:1,000), gasdermin-D (96458, 1:1,000), Rab11 (7100, 1:1,000); β-actin (Sigma-Aldrich, AC-15, 1:10,000); and E-cadherin (BD Transduction Laboratories, 610182, 1:1,000). Secondary antibodies were from PerkinElmer [goat anti-rabbit (1:5,000) and goat anti-mouse (1:10,000)]. Western blots were developed with ECL substrate (Thermo Fisher Scientific).

Cytofluorescence

Live cells were incubated in MitoTracker Red (Invitrogen) for 45 minutes to stain mitochondria then 100% methanol fixed, blocked in TBS-T 3% gelatin and stained with rabbit anti–RIG-I (1:100, Cell Signaling Technology) and goat anti-rabbit Alexa Fluor 488 (1:1,000, Invitrogen). For apoptotic analysis, live cells were stained with Annexin V,

AlexaFluor-488 conjugate (1:500, Invitrogen) for 4 hours before imaging. For pyroptotic studies, live cells were stained in propidium iodide (PI; Sigma-Aldrich, 1:1,000) for 1 hour before imaging.

Generation of nanoparticles for intratumoral delivery

Amphiphilic diblock copolymer composed of a 10.3 kDa dimethylaminoethyl methacrylate (DMAEMA) first block and a 31.0 kDa, 35% DMAEMA, 39% butyl methacrylate (BMA), and 26% propylacrylic acid (PAA) second block were synthesized as previously described (36). Dry amphiphilic diblock polymer was dissolved into ethanol at 50 mg/mL, rapidly diluted into phosphate buffer (pH 7.0, 100 mmol/L) to 10 mg/mL, concentrated, and buffer was exchanged into PBS (Gibco) using 3 kDa molecular weight cutoff centrifugal filtration columns (Ambion, Millipore) and sterile filtered. Polymer concentration was measured by absorbance at 310 nm (Synergy H1 microplate reader, BioTek). Concentrated polymer solution was rapidly mixed with SLR20 (or OH-SLR20) at a charge ratio of 5:1 (N:P) for 30 minutes and diluted into PBS (pH 7.4, Gibco) to 20 μg of SLR and 400 μg of polymer in 50 μL total volume.

Animal studies

All studies were performed in accordance with Association for Assessment and Accreditation of Laboratory Animal Care International (AAALAC) guidelines and were approved by the Institutional Animal Care and Use Committee at Vanderbilt University. All mice were housed in pathogen-free conditions. Left inguinal mammary fat pads of wild-type (WT) female Balb/c mice or athymic (nu/nu) Balb/c mice (Jackson Labs) were

injected with 106 4T1 cells. Mice were randomized into treatment groups when tumors reached 50 to 100 mm3. Intratumoral injection of nanoparticle in 50 μL of saline (or saline without nanoparticle) was performed at 48-hour intervals for a total of 3 treatments, or at 72- to 96-hour intervals for a total of 4 treatments. Intraperitoneal injection of InVivoMab αPD-L1 (B7-H1) and control IgG2b κ from Bio X Cell were delivered at 25 mg/kg in sterile saline twice weekly for 10 days. Mice were monitored daily, and tumor volume was measured with calipers twice weekly for up to 25 days.

Histologic analyses

Lungs and tumors were formalin-fixed and paraffin-embedded, and sections (5 μm) were stained with hematoxylin and eosin. In situ TUNEL analysis was performed on paraffin-embedded sections using the ApopTag kit (Millipore). IHC was performed using the following antibodies: RIG-I (Invitrogen, PA5-20276, 1:400), P-STAT1 (Cell Signaling Technology, 9167, 1:100), Ki67 (Biocare Medical, CFM325B, 1:100), CD45 (Abcam, ab10558, 1:5,000), F4/80 (Bio-Rad, MCA497GA, 1:100), CD4 (eBioscience, 14-0195-82, 1:1,000), CD8 (eBioscience, 14-0195-82, 1:100), TRAIL (GeneTex, 6TX11700, 1:800). Immunodetection was performed using the Vectastain kit (Vector Laboratories) according to the manufacturer's instructions.

RNA isolation and expression analyses

Total RNA was extracted using NucleoSpin RNA (Machery-Nagel), reverse transcribed (iScript cDNA Synthesis; Bio-Rad), and using for qPCR with iTaq Universal SYBR Green (Bio-Rad) on a Bio-Rad CFX96 thermocycler. Gene expression is normalized to

36B4. The following primers were obtained from Integrated DNA Technologies: IFNB1 [forward 5′ -TGCTCTCCTGTTGTGCTTCTCC; reverse 5′ -GTTCATCCTGTCCTTGAGGCAGT]; Ifnb1 [forward 5′ -CAGCTCCAAGAAAGGACGAAC; reverse 5′ -GGCAGTGTAACTCTTCTGCAT]; HLA-A [forward 5′ -GCGGCTACTACAACCAGAGC; reverse 5′ -GATGTAATCCTTGCCGTCGT]; TNF [forward 5′ -CCTCTCTCTAATCAGCCCTCTG; reverse 5′ -GAGGACCTGGGAGTAGATGAG]; Tnf [forward 5′ -CCCTCACACTCAGATCATCTTCT; reverse 5′ -GCTACGACGTGGGCTACAG]; TNFSF10 [forward 5′ -TGCGTGCTGATCGTGATCTTC; reverse 5′ -GCTCGTTGGTAAAGTACACGTA]; Tnfsf10 [forward 5′ -ATGGTGATTTGCATAGTGCTCC; reverse 5′ -GCAAGCAGGGTCTGTTCAAGA]. Other genes were analyzed via PCR array (RT2 Profiler Array, Qiagen).

Cytokine array

Cells (1 × 106) were seeded. After 24 hours, cells were transfected with SLR20 or OH-SLR20 as described above. Cell culture media were removed 32 hours after transfection, filtered with a 0.2 micron strainer, and immediately added to blocked membranes from Human Cytokine Antibody Array C1000 (RayBiotech), and processed according to the manufacturer's instructions. Chemiluminescent cytokine arrays were imaged digitally using Amersham Imager 600 (GE Healthcare).

Statistical analysis

Experimental groups were compared with controls using Student unpaired, two-tailed t test. Multiple groups were compared across a single condition using one-way analysis of variance (ANOVA). $P < 0.05$ was used to define significant differences from the null hypothesis. qPCR array data sets were compared using multiple t tests with an FDR cutoff of 0.05.

Ethics statement

Animals were housed under pathogen-free conditions, and experiments were performed in accordance with AAALAC guidelines and with Vanderbilt University Institutional Animal Care and Use Committee approval.

Results

Breast cancer cell autonomous RIG-I signaling is activated by a synthetic RIG-I mimetic

To assess the potential applicability of a RIG-I agonist in breast cancer, we examined RIG-I/DDX58 expression in a clinical invasive breast cancer data set curated by The Cancer Genome Atlas (TCGA) (105). We found genomic DDX58 deletion in only 1 of 817 tumors and mRNA downregulation in only 8 of 817 tumors (**Figure 2.1.A**), suggesting that loss of RIG-I expression is a rare event. Similar results were produced upon the analysis of 2509 breast tumors from the METABRIC invasive breast cancer data set (**Figure 2.2.A**) (106). Whole-exome sequencing data identified 3 non-recurrent

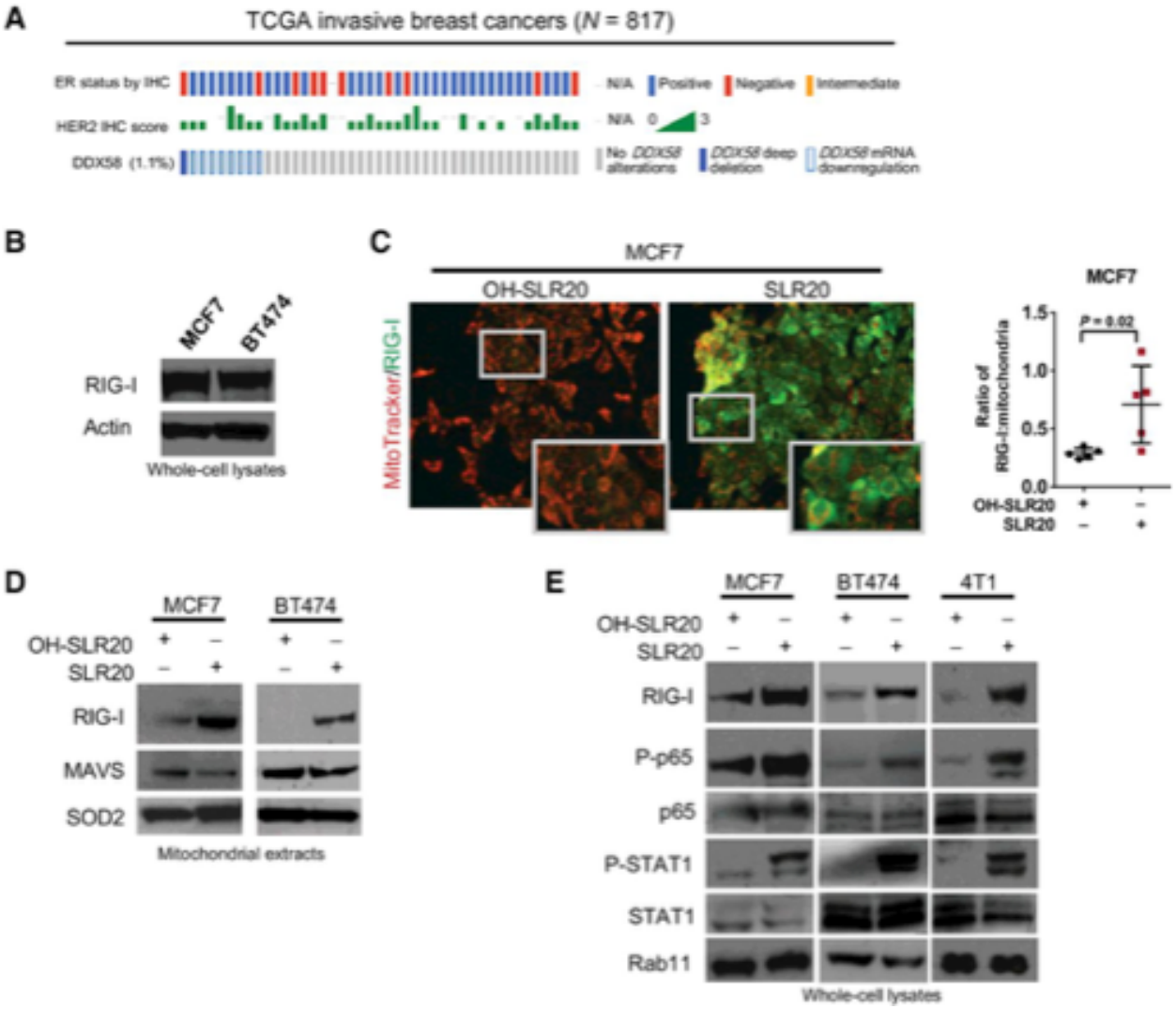

Figure 2.1 RIG-I/DDX58 is expressed in breast cancers and is activated by the RIG-I agonist SLR20. A, TCGA-curated clinical data set of invasive breast cancers (N = 817; ref. 37) was assessed for samples harboring genomic DDX58 loss (solid blue) and/or DDX58 mRNA downregulation (defined as <−1 SD from the mean DDX58 expression among the entire data set and shown in blue outline). Reported scores for IHC analysis of ER and HER2 corresponding to each clinical specimen are shown. B, Whole-cell lysates were assessed by Western analysis using the antibodies indicated to the left of each blot. C, Sixteen hours after transfection with OH-SLR20 and SLR20, cells were fixed, assessed by immunofluorescence to detect RIG-I (green fluorescence), and counterstained with MitoTracker Red (red fluorescence). Left, representative images are shown. The inset shows a high-power magnification of the boxed area within each respective panel. Right, the ratio of RIG-I staining to MitoTracker is shown. MitoTracker staining was quantified as the number of red fluorescent pixels per 40× field using ImageJ. RIG-I immunofluorescent staining was quantified as the number of green fluorescent pixels per 40× field. Each point represents the average value of three random fields per sample, N = 5 samples. Midlines and error bars show average ± SD. P value was calculated using Student's unpaired t-test. D, Mitochondrial fractions of cells were assessed by Western analysis 18 hours after transfection, using the antibodies shown on the left of each panel. Representative images are shown. N = 3. E, Whole-cell lysates collected 12 hours after transfection were assessed by Western analysis using the antibodies shown on the left of each panel. Representative images are shown. N = 3.

missense mutations within DDX58, and no recurrent, truncating, or in-frame mutations (**Figure 2.2.B**), suggesting that RIG-I/DDX58 is rarely lost or mutated in breast cancers. Western analysis confirmed RIG-I expression in two human breast cancer cell lines, MCF7 (ER+), and BT474 (HER2 amplified) (**Figure 2.1.B**), but not in HER2-amplified, ER+ MDA-MB-361 cells (**Figure 2.3.A**). To determine if RIG-I signaling pathways are functional in breast cancer cells, we used a previously described synthetic minimal RIG-I agonist composed of a double-stranded, triphosphorylated 20-base pair stem-loop RNA, which was then modified with a 5′ triphosphate sequence (SLR20) (107). Previous studies demonstrated that SLRs containing the 5′-ppp motif, but not those lacking the motif, activate type I IFN production via RIG-I/MAVS signaling. We transfected SLR20 (and the non-phosphorylated, but otherwise identical sequence, OH-SLR20) into MCF7 cells and measured RIG-I expression and distribution by immunofluorescence. RIG-I expression was robustly increased in cells transfected with the RIG-I ligand SLR20 as compared with the control ligand OH-SLR20 (**Figure 2.1.C**). Counterstaining of mitochondria demonstrated mitochondrial localization of RIG-I in many cells following SLR20 treatment. Further, analysis of mitochondrial cell fractions by Western analysis confirmed mitochondrial RIG-I localization in MCF7 and BT474 cells transfected with SLR20, but not OH-SLR20 (**Figure 2.1.D**). Western analysis confirmed RIG-I upregulation following transfection with SLR20 in MCF7, BT474, and mouse 4T1 cells, a mammary tumor line used as a model of aggressive, metastatic, and poorly immunogenic TNBC (**Figure 2.1.E**). Importantly, SLR20 increased phosphorylation of the pro-inflammatory transcription factors p65 (an NF-κB subunit)

A

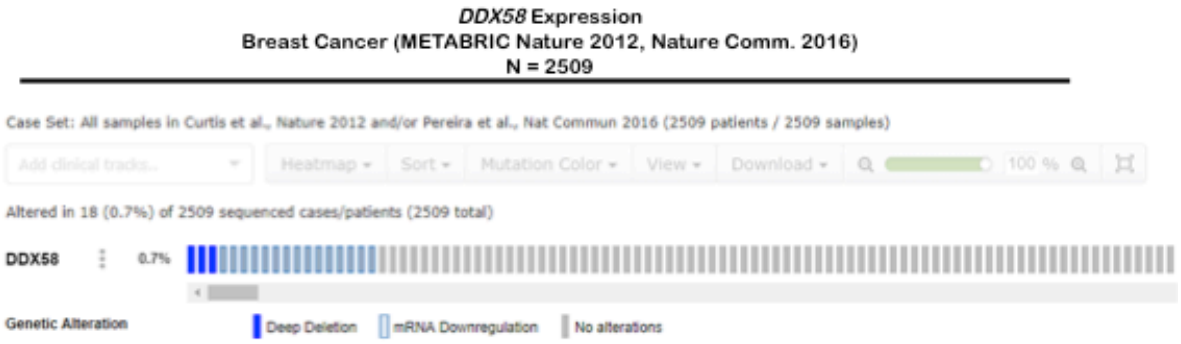

B

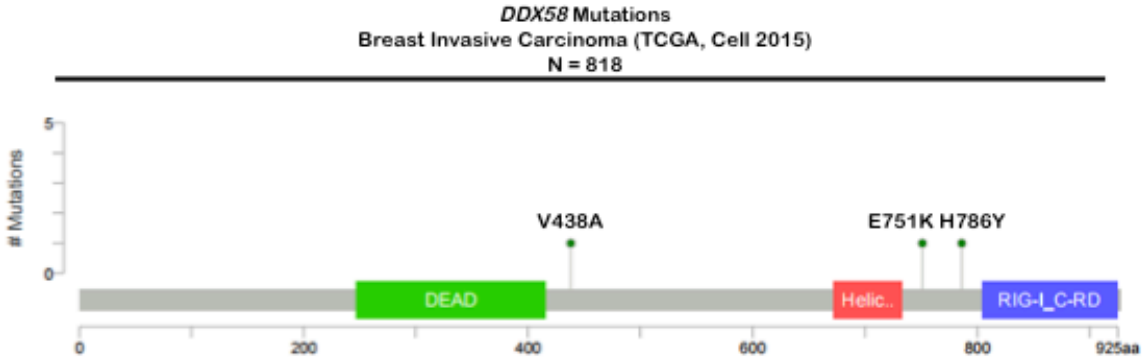

Figure 2.2 RIG-I/DDX58 is rarely lost or mutated in breast cancers. A. METABRIC-curated clinical dataset of invasive breast cancers (N = 817, Ref. here) was assessed for samples harboring genomic loss (solid blue boxes) or mRNA down-regulation (defined as < -2 S.D. from the mean DDX58 expression among the entire dataset, and shown in blue outline). B. A lollipop graph was used to show the relative positioning of DDX58 missense mutations found in a TCGA-curated clinical dataset of invasive breast tumors (N = 817). No recurrent mutations were identified.

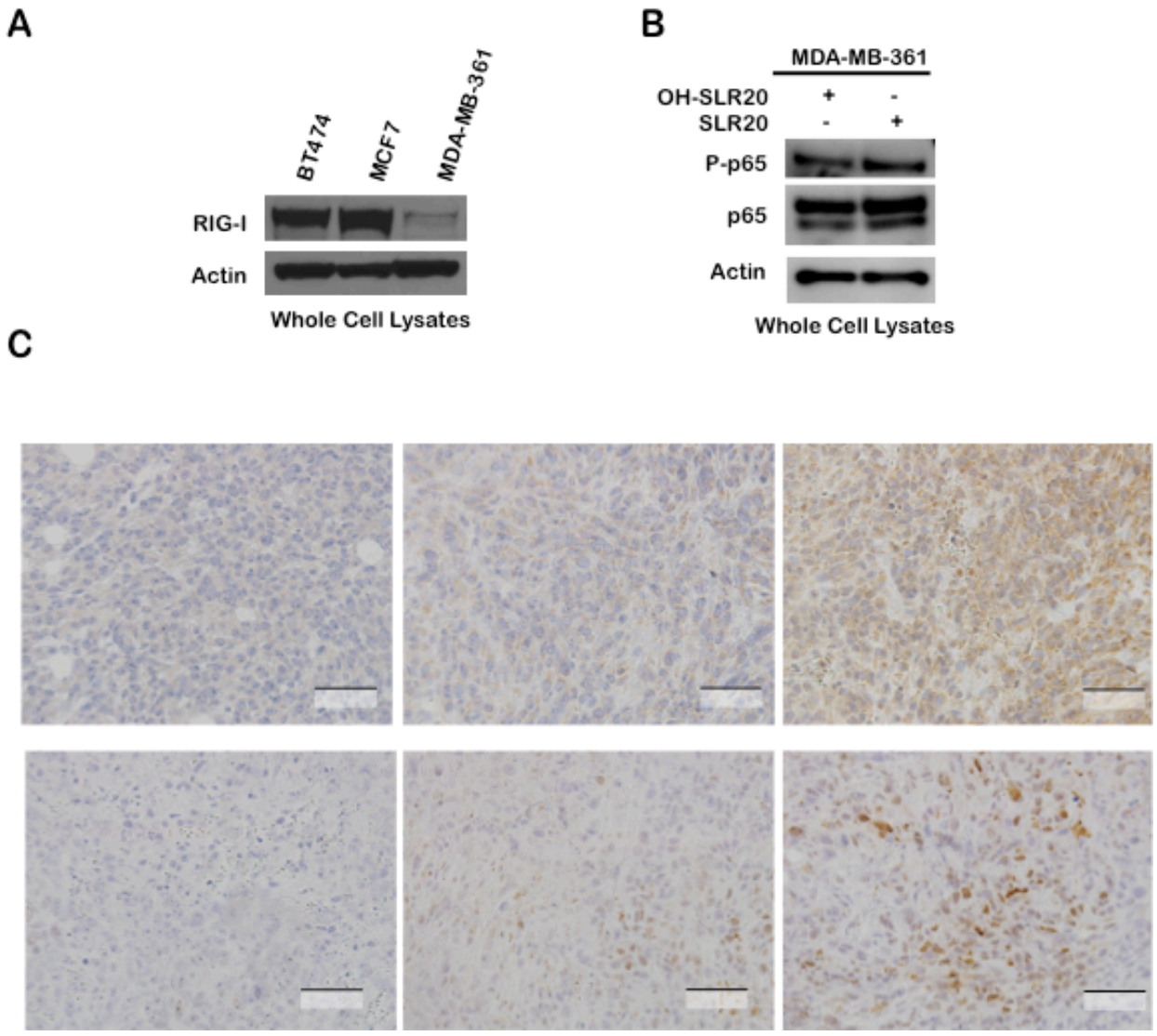

Figure 2.3 MDA-MB361 is RIG-I deficient. A. Western analysis of whole cell lysates harvested from BT474, MCF7, and MDA-MB-361 cells using antibodies indicated at the left of each panel. B. Western analysis of whole cell lysates harvested from MDA-MB-361 cells transfected with SLR20 or OH-SLR20 at 12 hours after transfection. C. Immunohistochemistry was used to measure RIG-I and P-STAT1 in tumors harvested at day 5. Representative Images are shown. N = 5.

and STAT1 in MCF7, BT474, and 4T1 cells. Importantly, SLR20 did not affect P-p65 in MDA-MB-361 cells, which lack RIG-I expression (**Figure 2.3.B**). These data support use of these breast cancer cell lines, and the SLR20 agonist, to model the therapeutic impact of RIG-I signaling in breast cancer.

A nanoparticle-based approach for RIG-I activation *in vivo* decreases breast tumor growth and metastasis

A recent study examining SLR delivery *in vivo* confirmed rapid induction of type I IFNs following delivery of a 10-bp SLR sequence (SLR10) (25). However, the impact of RIG-I activation in the complex breast tumor microenvironment has not been explored. We used a nanoparticle-based platform previously optimized for oligonucleotide delivery *in vivo* for intratumoral (i.t.) treatment of breast tumors with SLR20 (**Figure 2.4.A**). These pH-responsive nanoparticles (NP) were composed of amphiphilic diblock copolymers formulated with a hydrophobic core-forming block that is endosomolytic and drives micellar assembly, and a polycationic corona for electrostatic complexation with oligonucleotide (i.e., SLR20), as described previously (104). This formulation has been shown to maximize cytoplasmic delivery of oligonucleotides, an ideal scenario for cytoplasmic RIG-I activation by SLR20. NPs were delivered i.t. to 4T1 mammary tumors grown in WT Balb/c female mice when tumors reached 50 to 100 mm3. As an additional control, a third group of tumor-bearing mice were treated by i.t. injection of saline, the vehicle in which NPs were delivered. A total of 3 treatments were administered (days 0, 2, and 4) (**Figure 2.4.B**). IHC of tumors collected at day 5 (24 hours after final treatment) revealed RIG-I protein upregulation in 4T1 tumors treated with SLR20 NPs

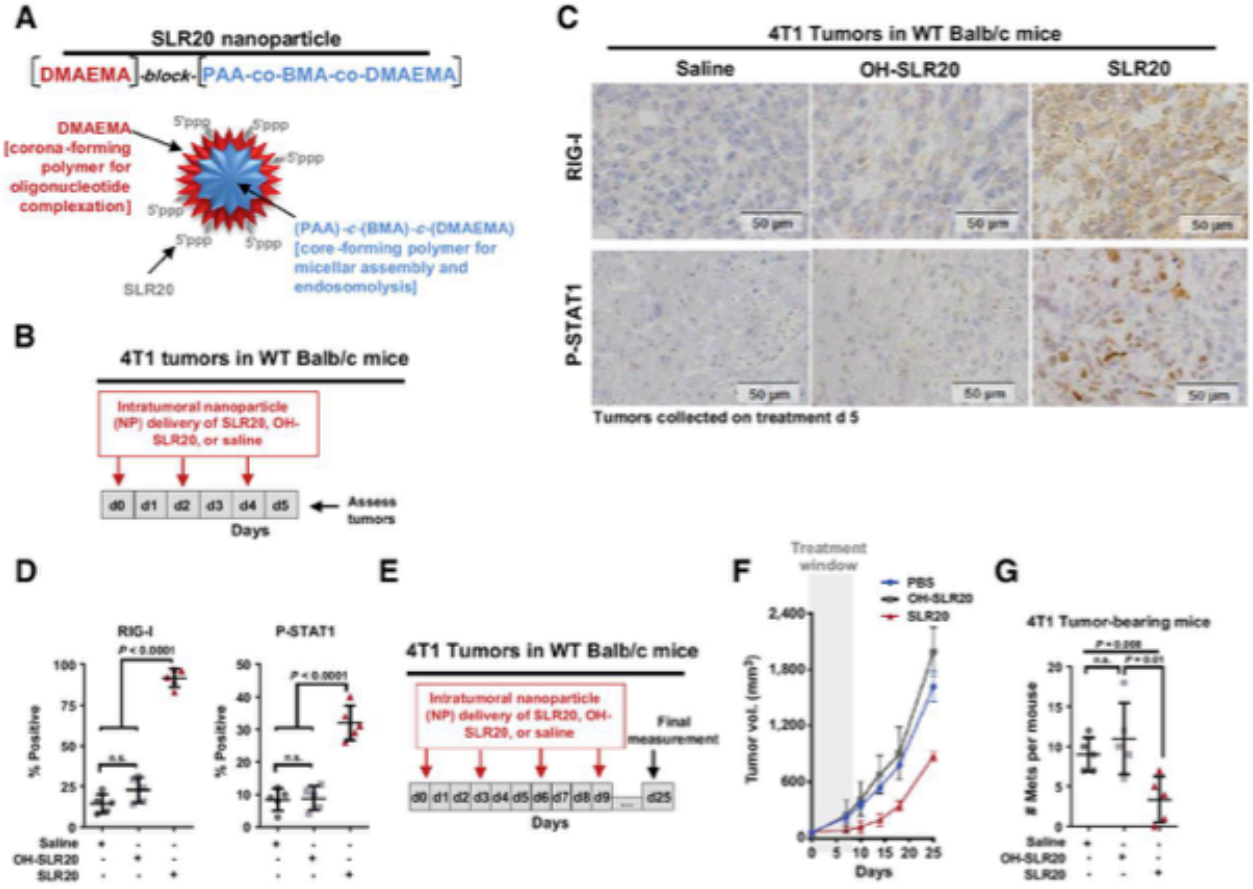

Figure 2.4 RIG-I agonist SLR20 induces RIG-I signaling and impairs tumor progression in vivo. A, Schematic representation of nanoparticle formulation used to treat tumor-bearing mice in vivo. B, Schematic of treatment strategy for intratumoral nanoparticle delivery of SLR20 (or OH-SLR20) to WT Balb/c mice harboring 4T1 mammary tumors. Saline was delivered intratumorally as a control. C and D, IHC was used to measure RIG-I and P-STAT1 in tumors harvested at day 14. B, Representative images are shown. N = 5. C, IHC staining for RIG-I and P-STAT1 was quantitated. Each point represents the average of three random fields per sample, N = 5. Midlines show average (±SD). P values were calculated using Student t test. E, Schematic of treatment strategy for intratumoral nanoparticle delivery of SLR20 (or OH-SLR20) to WT Balb/c mice harboring 4T1 mammary tumors. Saline was delivered intratumorally as a control. Tumors were measured throughout treatment (days 0–9) and for 16 days after treatment ceased (days 10–25). Tumors were collected on day 25 (16 days after the final treatment). F, Tumor volume was measured beginning at treatment day 1. N = 10 per group through day 5. N = 5 per group from days 6 to 25. G, Lungs harvested at day 25 were assessed histologically for metastatic lesions. Each point represents the number of metastases per individual mouse. Midlines represent the average (± SD); Student's t-test. n.s., non-significant.

over saline-treated or OH-SLR20 NP-treated tumors (**Figures 2.4.C–D** and **Figure 2.3.C**). Further, tumors treated with SLR20 NPs, but not OH-SLR20 NPs, exhibited a 3-fold increase in phosphorylation of STAT1 (**Figure 2.4.C** and **D**), confirming RIG-I signaling in SLR20-treated tumors *in vivo*.

We used a slightly modified treatment scheme to assess the therapeutic impact of SLR20-NP on tumor growth. Tumors were treated on days 0, 3, 6, and 9 with i.t. delivery of SLR20 NPs, at which point treatment stopped and tumor volume was monitored through day 25 (**Figure 2.4.E**). Tumors treated with SLR20 NPs did not increase in volume during the treatment window (days 0–9), while tumors treated with saline or with OH-SLR20 NPs increased nearly 4-fold (**Figure 2.4.F**). Once treatment was complete, tumors treated with SLR20 resumed volumetric increase, but still grew at a diminished rate as compared with tumors treated with OH-SLR20 NPs or with saline. Lungs harvested from mice on day 25 revealed a decreased number of lung metastases in the SLR20-treated mice as compared with control groups (**Figure 2.4.G**). Treatment extended through treatment day 25 (**Figure 2.5.A**) resulted in sustained tumor growth inhibition in response to SLR20 (**Figure 2.5.B**).

RIG-I signaling induces breast cancer cell death through tumor cell–intrinsic pathways

We investigated potential mechanisms responsible for decreased tumor growth and metastasis following treatment with SLR20 NPs, first measuring Ki67-positive cells r

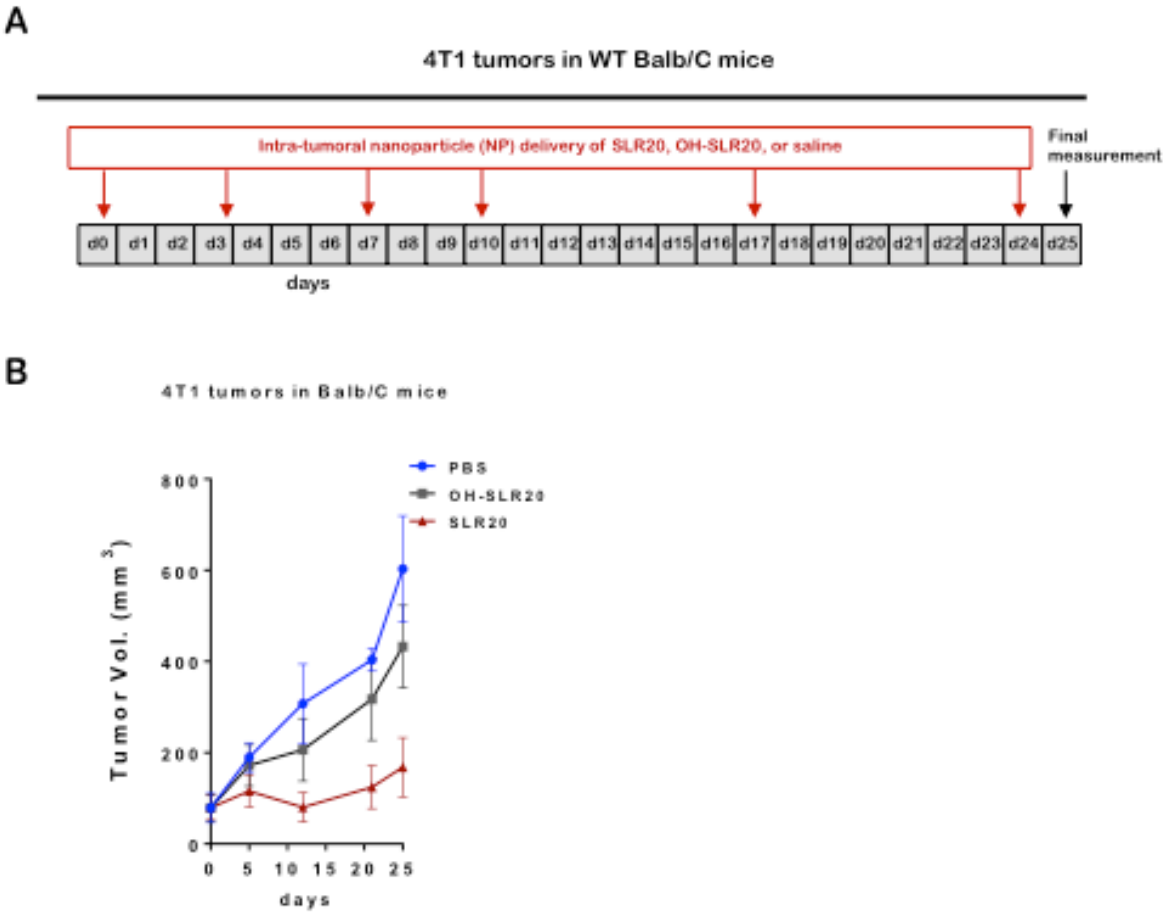

Figure 2.5. SLR20 inhibits tumor growth
A. Schematic of treatment strategy for intra-tumoral nanoparticle delivery of SLR20 (or OH-SLR20) to WT Balb/C mice harboring 4T1 mammary tumors. Saline was delivered intratumorally as a control. Tumors were measured throughout treatment. B. Tumor volume was measured beginning at treatment day 0. N = 7-8 per group.

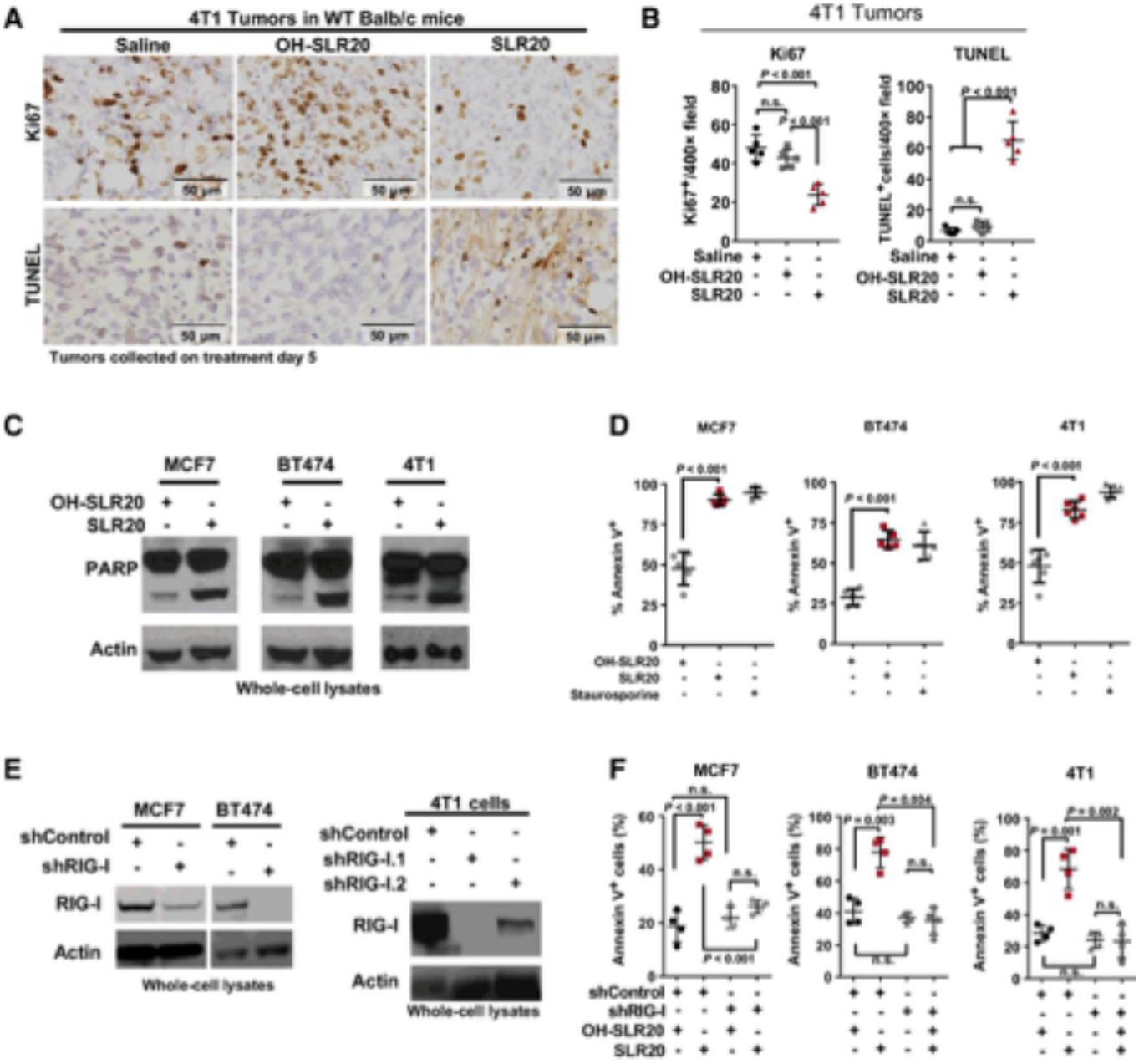

Figure 2.6 RIG-I agonist SLR20 induces tumor cell apoptosis. A and B, histologic analysis of tumor sections using IHC against Ki67 and TUNEL analysis. B, Representative images are shown. N = 5. C, The number of Ki67+ cells and TUNEL+ cells per 400× field was quantitated. Each point represents the average of three random fields per sample, N = 5. Midlines show average (± SD). P values were calculated using Student t test. C, Western analysis of whole-cell lysates harvested 12 hours after transfection, using antibodies indicated on the left of each panel. D, Cells were transfected, and after 18 hours, cells were stained with Annexin V-AlexaFluor488 for 4 hours. AlexaFluor488+ cells were imaged by fluorescence microscopy. The number of Annexin V+ cells per well was counted. Each point shown represents the average of two experimental replicates, N = 5. Midlines represent the average (± SD). P values were calculated using Student t test. Staurosporine treatment (1 μmol/L) was performed in parallel as a positive control for induction of apoptosis/Annexin V staining. E, Western analysis of whole-cell lysates using antibodies shown on left of each panel. F, Cells were transfected and stained with Annexin V-FITC as shown in D. n.s., non-significant.

by IHC as a marker of cell proliferation (**Figure 2.6.A**; **Figure 2.7.A**). Assessing 4T1 tumors collected on treatment day 5, we found a decreased percentage of Ki67+ tumor cells in samples treated with SLR20 NPs as compared with samples treated with OH-SLR20-NPs or with saline (**Figure 2.6.B**). Conversely, tumor cell death, measured by terminal dUTP nick-end labeling (TUNEL) analysis (**Figure 2.6.A**), was increased 5-fold in samples treated with SLR20 NPs (**Figure 2.6.B**). RIG-I signaling is capable of inducing programmed cell death in many cell types, including some cancer cell types (75), although this possibility remains unclear in breast cancers. Therefore, we transfected MCF7, BT474, and 4T1 cells in culture with SLR20, assessing cells 12 hours after transfection for PARP cleavage, a molecular marker of cell death. Cleaved PARP was increased in cells transfected with SLR20 versus OH-SLR20 (**Figure 2.6.C**). Annexin V-FITC staining was used to enumerate apoptotic cells, revealing increased Annexin V+ cells following SLR20 treatment in MCF7, BT474, and 4T1 cells (**Figure 2.6.D**), but not in MDA-MB-361 cells, which lack RIG-I expression (**Figure 2.7.B**). Importantly, knockdown of RIG-I in MCF7, BT474, and 4T1 cells using shRNA sequences against RIG-I (**Figure 2.6.E**) abrogated the increased Annexin V staining in response to SLR20 (**Figure 2.6.F**), while SLR20 remained capable of inducing Annexin V staining in cells expressing nontargeting shRNA sequences. These findings demonstrate that SLR20 activates RIG-I signaling in breast cancer cells, inducing cell death in a tumor cell–intrinsic manner.

RIG-I signaling in breast cancer cells induces extrinsic apoptosis and pyroptosis

Because RIG-I signaling is reported to induce apoptosis through several distinct pathways, including intrinsic apoptosis, extrinsic apoptosis, and pyroptosis pathways across a variety of cell types (29), it is unclear by which pathway RIG-I induces cell death in breast cancers. We investigated this using an apoptosis expression array, assessing expression changes in 84 genes associated with the intrinsic and extrinsic apoptosis pathways. RNA harvested from BT474 cells collected 16 hours after transfection harbored changes in 18 of the 84 genes assessed. Genes arranged in order of expression fold change revealed that genes regulating intrinsic apoptosis (e.g., BAD, BAX, CASP9) were downregulated, while expression of genes regulating the extrinsic apoptosis pathway (TNFSF10, FAS, CASP10, CASP8) were upregulated (**Figure 2.8.A**), suggesting that the extrinsic apoptosis pathway might be activated in response to RIG-I signaling in breast cancer cells. We confirmed that SLR20 induced expression of the extrinsic apoptotic factor TNFSF10 in MCF7, BT474, and 4T1 cells (**Figure 2.8.B**). Additionally, 4T1 tumors treated in vivo with SLR20 NPs were assessed by IHC for expression of the Tnfsf10 gene product, TRAIL. Although TRAIL was expressed at only low levels in 4T1 tumors treated with saline or with OH-SLR20 NPs (**Figure 2.8.C**), TRAIL protein levels were markedly upregulated in samples treated with SLR20 NPs.

These data suggest that RIG-I might activate the extrinsic apoptosis pathway in breast cancer cells but do not rule out that RIG-I signaling might also induce breast cancer cells to undergo pyroptosis, an inflammatory type of programmed cell death that requires activation of caspase-1 and oligomerization of gasdermin D on the cell

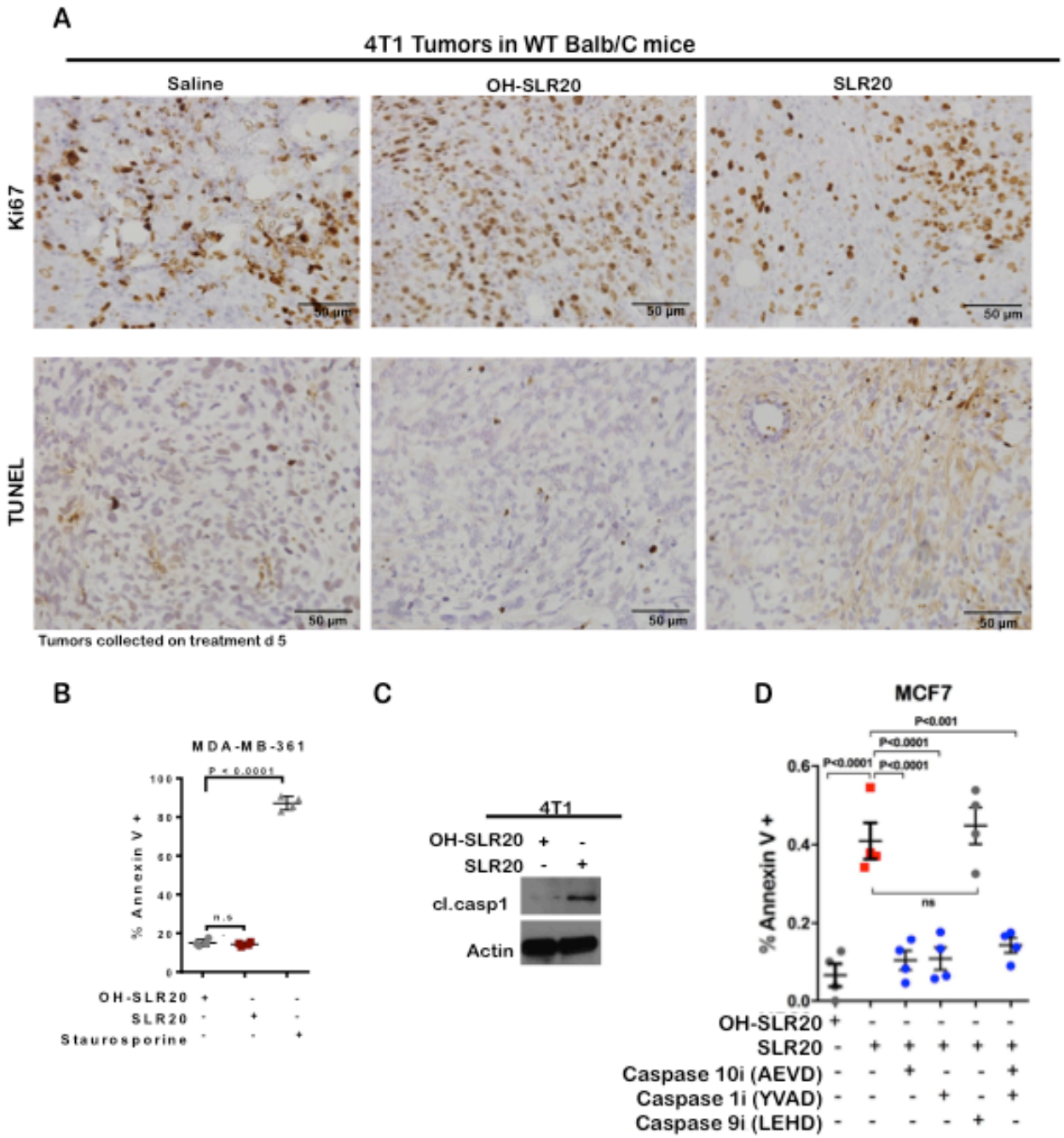

Figure 2.7 Caspase-1 cleavage is increased by RIG-I signaling A. Immunohistochemistry was used to measure Ki67 and TUNEL+ cells in tumors harvested at day 5. Representative Images are shown. N = 5. B. Immunohistochemistry was used to measure Ki67 and TUNEL+ cells in tumors harvested at day 5. Representative Images are shown. N = 5. C. Western analysis of whole cell lysates collected 16 hours after transfection using antibodies indicated at the left of each panel. D. MCF7 Cells were transfected, and after 16 h, total RNA was assessed by RT-qPCR to measure expression of the indicated genes involved in pyroptosis. Each point represents the average of three experimental replicates, N = 3. Midlines are average ± S.D. Student's t-test.

membrane (30). Western analysis of MCF7 and BT474 cells transfected with SLR20 revealed potent activation of caspase-1 (**Figure 2.8.D**) and localization of gasdermin D to cell membranes (**Figure 2.8.E**). These findings were confirmed in 4T1 cells (**Figure 2.7.C**). Upregulation of CASP1 and CASP4 (encoding another mediator of pyroptosis, caspase-4) was seen in BT474 cells transfected with SLR20 (**Figure 2.8.F**). Importantly, Casp1 levels were increased in 4T1 tumors treated in vivo with SLR20 NPs, but not in tumors treated with OH-SLR20 NPs (**Figure 2.8.G**), suggesting the RIG-I–mediated activation of pyroptotic signaling pathway may be maintained even within the complex tumor microenvironment.

Next, we used a selective inhibitor of caspase-10, AEVD-FMK, to block the extrinsic apoptotic pathway, resulting in a moderate, but significant, diminution of Annexin V+ cells following treatment with SLR20 (**Figure 2.8.H**). In contrast, the caspase-9 inhibitor Z-LEHD-FMK, which blocks activation of the intrinsic apoptotic pathway, had little impact on Annexin V staining in cells transfected with SLR20. We also tested an inhibitor of caspase-1, Z-YVAD-FMK, to block the pyroptosis pathway in SLR20-transfected cells, resulting in partial inhibition of Annexin V staining. These results were confirmed in MCF7 cells (**Figure 2.7.D**). Interestingly, the combination of the caspase-10 inhibitor with the caspase-1 inhibitor produced a greater reduction in Annexin V staining in BT474 cells as compared with either inhibitor used alone (**Figure 2.8.H**), consistent with the idea that these two inhibitors operate through distinct pathways in BT474 cells, and suggesting that RIG-I signaling in breast cancer cells may use both the intrinsic apoptosis pathway and pyroptosis to potently induce programmed cell death. Because pyroptosis produces pores in the plasma membrane (30), making

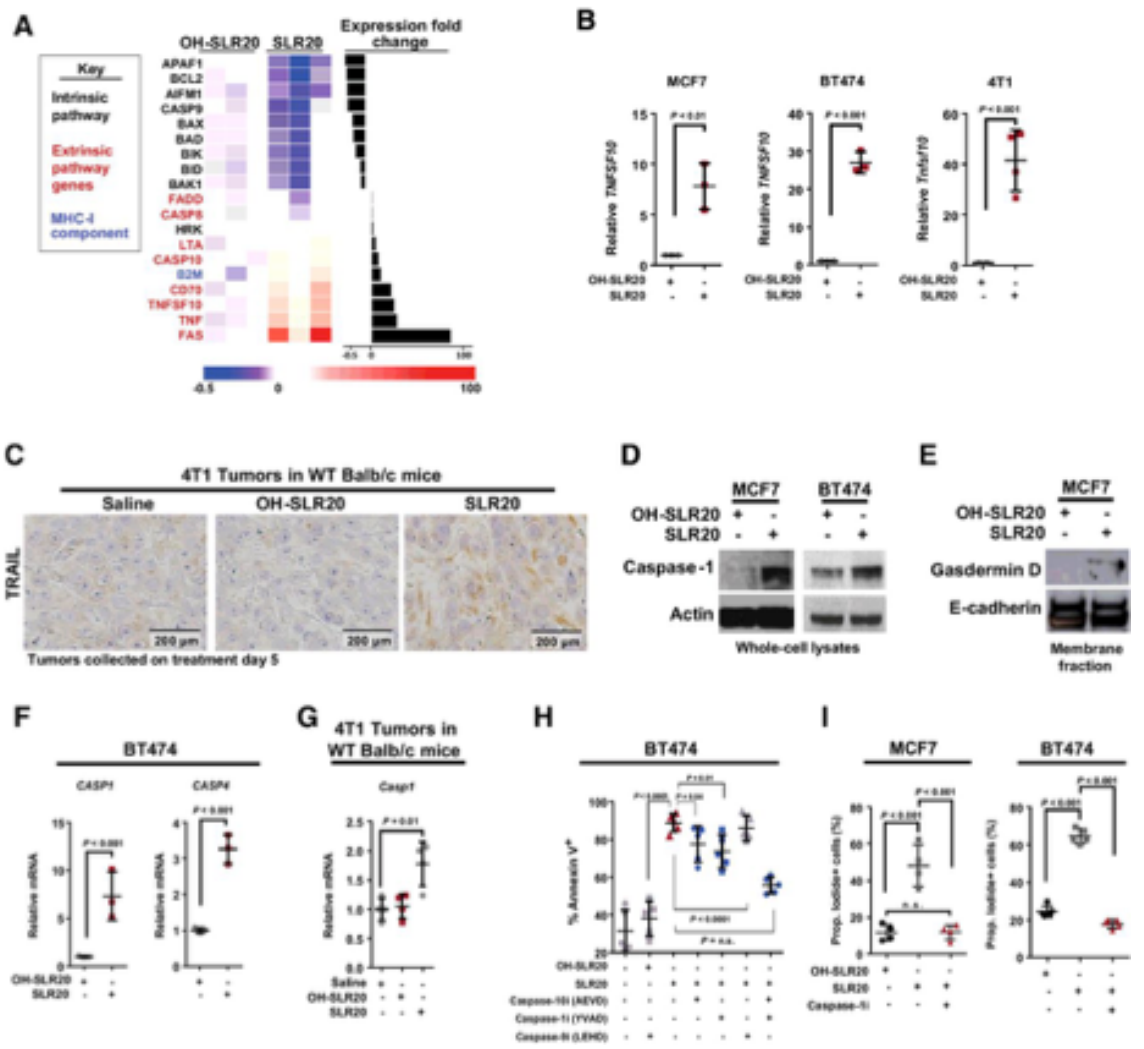

Figure 2.8 RIG-I signaling in breast cancer cells induces extrinsic apoptosis and pyroptosis. A, BT474 cells were transfected with SLR20 or OH-SLR20. After 12 hours, RNA was collected and assessed for expression of genes within the intrinsic and extrinsic apoptosis pathway (RT2 Profiler Apoptosis Array). Relative gene-expression values were calculated using the ddCT method, correcting for expression of ACTB and GAPDH, and are shown as expression relative to the average value for each gene in OH-SLR20-transfected cells, as shown in the heat map. Genes (listed at left) were ranked in order of expression fold change, as shown on the right. B, Cells were transfected, and after 12 hours, total RNA was assessed by RT-qPCR to measure expression of the indicated genes involved in pyroptosis. Each point represents the average of three experimental replicates, N = 3. Midlines are average ± SD. Student t test. C, IHC analysis to detect TRAIL in 4T1 tumors harvested on treatment day 5. D and E, Western analysis of whole-cell lysates (D) or membrane fractions (E) harvested 16 hours after transfection using the antibodies shown on left of each panel. F, Cells were transfected, and after 12 hours, total RNA was assessed by RT-qPCR to measure expression of the indicated genes involved in pyroptosis. Each point represents the average of three experimental replicates, N = 3. Midlines are average ±SD. Student t test. G, RNA harvested from 4T1 tumors collected on treatment day 5 was assessed by RT-qPCR for Casp1 gene expression as described in C. H and I, Cells were transfected and immediately treated with caspase-specific inhibitors (each used at 10 µmol/L). After 18 hours, cells were stained with Annexin V-AlexFluor488 for 4 hours (H) or PI for 10 minutes (I). AlexaFluor488+ and PI+ cells were imaged by fluorescence microscopy. The number of fluorescent cells per well was counted. Each point shown represents the average of two experimental replicates, N = 5 (H) and N = 4–5 (I). Midlines represent the average (±SD). P values use Student's t-test.

them permeable to PI, we stained MCF7 and BT474 cells with PI at 12 hours after transfection with OH-SLR20 or SLR20, finding a robust increase in PI+ staining when cells were transfected with SLR20 (**Figure 2.8.I**). However, PI staining was completely abolished in MCF7 and BT474 cells pretreated with the caspase-1 inhibitor, confirming that pyroptosis is induced by SLR20 in breast cancer cells.

RIG-I signaling increases breast tumor-infiltrating leukocytes

In contrast to the intrinsic apoptosis pathway, which is considered an immunologically silent form of programmed cell death, pyroptosis is thought to be an immunogenic form of cell death that may recruit inflammatory leukocytes to the site of a viral infection through cytokine modulation, while increasing immunogenicity of the infected cell through increased expression of the major histocompatibility complex (MHC)-I, the antigen presentation machinery expressed on most nucleated cells. Consistent with this idea, both MCF7 and BT474 breast cancer cells transfected with SLR20 showed upregulation of HLAB (**Figure 2.9.A**), encoding a key MHC-I component. The gene B2M, encoding another key MHC-I component, β2 microglobulin, was similarly upregulated in BT474 cells (**Figure 2.8.A**).

We assessed leukocyte recruitment to 4T1 mammary tumors grown in immune-competent Balb/c mice following treatment with SLR20 NPs. IHC analysis for CD45, a pan-leukocyte marker, revealed substantially increased CD45+ cells in tumors treated with SLR20 NPs versus saline or OH-SLR20 NPs (**Figure 2.9.B** and **Figure 2.10**). Further, IHC analysis using antibodies against F4/80 (a mature macrophage marker),

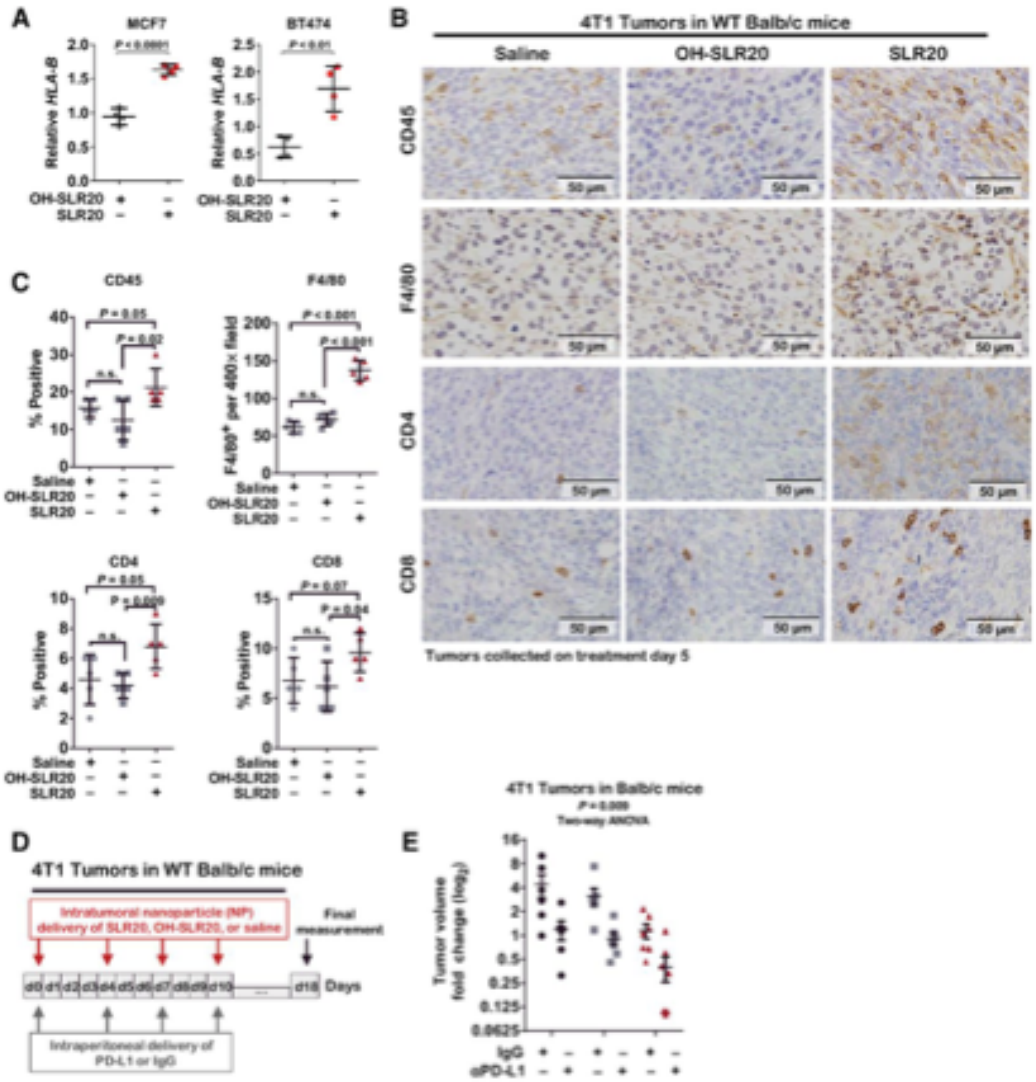

Figure 2.9 RIG-I signaling induces immunogenic cell death and increases tumor leukocyte infiltration. A, Cells were transfected, and after 12 hours, total RNA was assessed by RT-qPCR to measure expression of the MHC Class II gene HLAB. Each point represents the average of three experimental replicates, N = 3. Midlines are average ± SD. Student t test. B and C, histologic analysis of tumor sections using IHC against F4/80analysis. B, Representative images are shown. N = 5. C, The number of CD45+, F4/80+, CD4+, and CD8+ cells per 400× field was quantitated. Each point represents the average of three random fields per sample, N = 5. Midlines show average (±SD). P values were calculated using Student t test. D, Schematic of treatment strategy for intraperitoneal delivery of αPD-L1 or IgG, and intratumoral nanoparticle delivery of SLR20 (or OH-SLR20, or saline) to WT Balb/c mice harboring 4T1 mammary tumors. Tumors were measured throughout treatment (days 1–10) and for 8 days after treatment ceased (days 11–18). E, Tumor volume was measured beginning at treatment day 1. N = 7 to 8 per group. n.s., non-significant.

CD4 (a marker of helper T lymphocytes), and CD8, a marker of cytotoxic T lymphocytes (CTL), natural killer T cells (NK-T) and inflammatory dendritic cell (DC)with SLR20 NPs versus saline or OH-SLR20 NPs (**Figure 2.9.B** and **Figure 2.10**). Further, IHC analysis using antibodies against F4/80 (a mature macrophage marker), CD4 (a marker of helper T lymphocytes), and CD8, a marker of cytotoxic T lymphocytes (CTL), natural killer T cells (NK-T) and inflammatory dendritic cell (DC) populations, were each increased in tumors treated with SLR20 NPs as compared with saline OH-SLR20 NP-treated tumors (**Figure 2.9.B** and **C**). These data suggest that RIG-I activation results in active recruitment of leukocytes to the TME, consistent with a more immunogenic tumor microenvironment. Consistent with this notion, we found that SLR20 delivery to 4T1 tumors grown in immune-compromised athymic Balb/c (nu/nu) mice displayed more rapid resurgence of tumor growth once the SLR20 treatment was discontinued (**Figure 2.11**). This use of the RIG-I ligand to generate a more immunogenic tumor microenvironment was tested more directly using SLR20 in combination with the ICI, αPD-L1. Tumor-bearing WT Balb/c mice were randomized into groups to receive treatment with SLR20, OH-SLR20, or saline and were randomized further into groups receiving αPD-L1 or an isotype-matched control IgG (**Figure 2.9.D**). Tumors were treated twice weekly through treatment day 10 and monitored through treatment day 18. We found that tumors treated with SLR20 alone grew at a slower rate than tumors treated with OH-SLR20 or with saline (**Figure 2.9.E**). Tumor growth was inhibited by treatment with αPD-L1 alone. However, the combination of SLR20 with αPD-L1 decreased tumor growth to a greater extent than either agent alone, and to a greater extent than αPD-L1 in combination with the control OH-SLR20 NP. These findings are

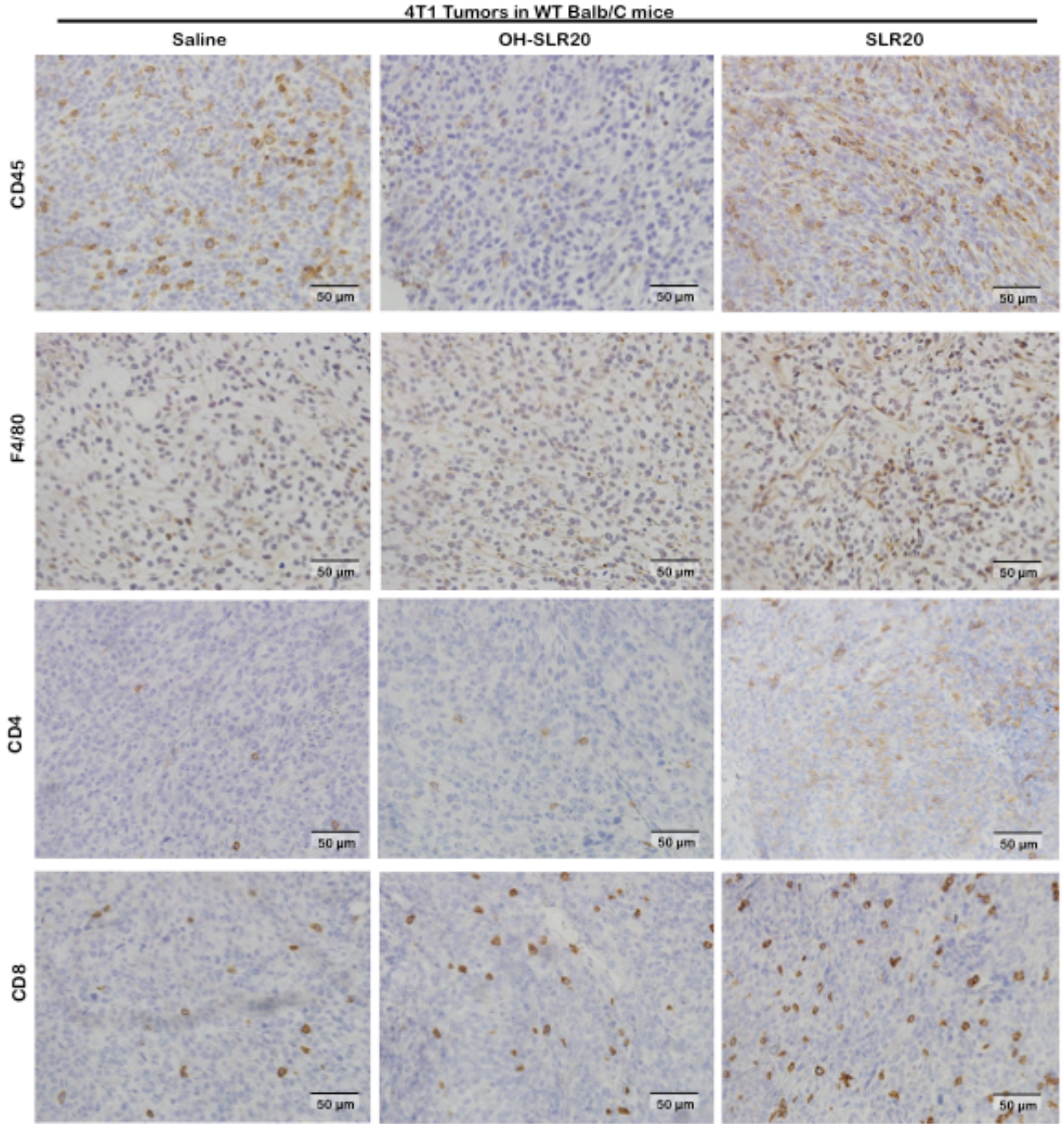

Figure 2.10 Leukocyte infiltration is increased by SLR20. Immunohistochemistry was used to measure CD45, F4/80, CD4, and CD8 in tumors harvested at day 5. Representative Images are shown. N = 5.

consistent with the idea that SLR20 increases the immunogenicity of the tumor microenvironment in this model of breast cancer.

Cytokine and chemokine modulation by RIG-I signaling in breast cancer cells

Like many PRRs, RIG-I induces expression of inflammatory cytokines required for lymphocyte recruitment (32). Therefore, we measured expression of IFNB1 in MCF7, BT474, and 4T1 cells following transfection with SLR20, revealing IFNB1 upregulation (**Figure 2.13.A**). Notably, Ifnb1 upregulation was also seen in 4T1 tumors treated in vivo with SLR20 NPs (**Figure 2.13.B**). SLR20-mediated upregulation of IFN1B was impaired in MCF7 and BT474 cells expressing RIG-I-directed shRNA sequences (**Figure 2.13.C**; **Figure 2.12**). This suggests that RIG-I signaling in breast cancer cells might be capable of activating in trans the antigen presenting cells, such as macrophages, within the tumor microenvironment. We tested this hypothesis by harvesting cultured media from 4T1 cells transfected with SLR20 or OH-SLR20, and adding the cultured media to macrophage-derived Raw264.7 cells. After 30 minutes of exposure to cultured media harvested from 4T1 cells treated with SLR20, we found phosphorylation of the proinflammatory transcription factor STAT1 (**Figure 2.14.A**). Induction of TNF gene expression following transfection with SLR20 also was seen in MCF7, BT474, and 4T1 (**Figure 2.13.D**), but not in cells expressing RIG-I shRNA sequences (**Figure 2.14.B**). To confirm that these gene-expression changes were seen at the protein level, we assessed cultured media harvested from MCF7 cells 48 hours after transfection with SLR20 by cytokine array analysis. Although this array did not carry IFNβ, we observed

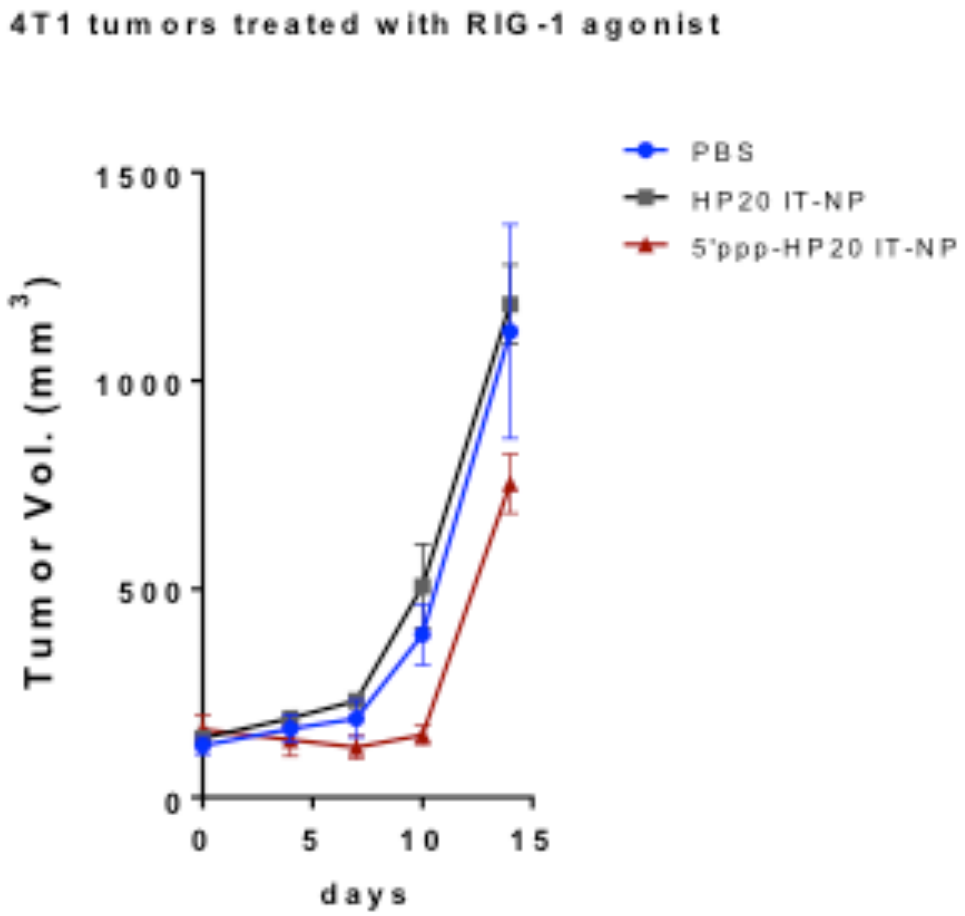

Figure 2.11 RIG-I reduces tumor growth in immune-compromised mice. 4T1 mouse mammary tumors were grown orthotopically in athymic Balb/C (nu/nu) female mice. Tumor-bearing mice were randomized into treatment groups for intratumoral delivery of SLR20 (or OH-SLR20, or saline) on treatment days 1, 5, and 9. Tumors were measured throughout treatment (days 1-10) and for 5 days after treatment ceased (days 10-15). N = 7 per group.

increased protein levels of TNFα and TNFβ in the cultured media harvested from SLR20 transfected MCF7 cells (**Figure 2.13.E**). Additionally, MCF7 cells transfected with SLR20 harbored increased protein expression of several IFNβ-inducible chemokines known to recruit T lymphocytes, including chemokine (C-C) motif ligand (CCL)-3, CCL5, CCL13, C-X-C motif chemokine ligand 11 (CXCL11), lymphotactin/C-motif ligand (XCL1) and interleukin (IL)-8.

Discussion

Although RIG-I–dependent anticancer immunity has been reported in several cancers, including pancreatic cancer, hepatocellular carcinoma (75), leukemias (76), and melanomas (27), little is known regarding RIG-I signaling in breast cancers. We used a synthetic agonist to activate the innate immune effector RIG-I in breast cancer cells in culture and in vivo, resulting in decreased tumor growth, decreased metastasis, increased TILs, and induction of tumor cell death via pyroptosis, an immunogenic form of cell death. These results suggest that RIG-I signaling remains intact in breast cancer cells and can be exploited to increase tumor cell death and, perhaps, tumor immunogenicity. Similar results have been reported from preclinical tumor models and clinical trials in cancers assessing the STING-mediated DNA/viral-sensing pathway (13, 14, 17), although STING signaling reportedly may be defective in a variety of cancers (18-19). Nonetheless, these findings suggest that the developing field of RIG-I mimetics and the wider field of innate anti-cancer immunity may yield novel treatment strategies for breast cancers, which historically have not benefited to the same extent as other cancers from recent breakthroughs in immuno-oncology.

The data shown herein are the first (to our knowledge) showing that RIG-I signaling provides a therapeutic benefit in breast cancer cells, per se, and in a mouse model of breast cancer in vivo. Interestingly, a previous report identified RIG-I/DDX58 as belonging to an antimetastatic gene signature in breast cancer cells (108); however, the significance of this interesting finding remains unclear. Our findings here are consistent with a previous report using poly(I:C), a double-stranded RNA that binds to a RIG-I like receptor known as MDA5, as well as Toll-like receptor 3 (TLR3), to demonstrate that viral-sensing RNA helicases can activate pro-inflammatory signaling pathways that can be exploited therapeutically in breast cancers (109). We have built upon these important early studies by investigating models of each of the three major clinical subtypes of breast cancer, including poorly immunogenic ER+ breast cancers, and highly aggressive TNBCs (96). We have also studied the impact of RIG-I signaling in the context of an immune-competent mouse model, finding that RIG-I signaling not only induces tumor cell death and cytokine modulation, but also increases tumor infiltration by leukocytes, a significant finding given that increased TILs predict a better outcome for patients with breast cancer and correlates with increased response to ICIs (97, 100-101).

Although pro-inflammatory cytokines, such as those induced by RIG-I signaling, support antitumor immunity, these are likely to have multifaceted effects on antitumor immunity, depending on their expression dose and duration. For example, type I IFNs promote DC maturation and T-cell priming during an antitumor immune response, but prolonged IFN exposure induces regulatory factors that restrain inflammation and antitumor immunity, such as PD-L1, IDO-1, and others. This has been shown in the

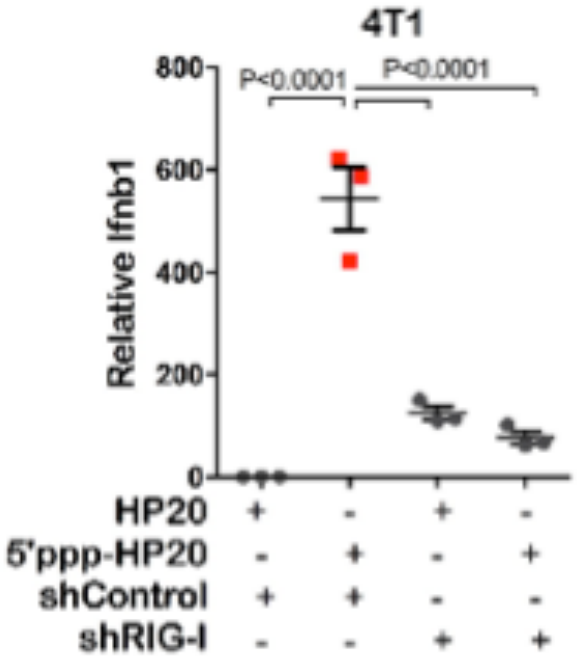

Figure 2.12 RIG-I shRNA reduces type I IFN induction in 4T1 cells. Cells were transfected, and after 16 h, total RNA was assessed by RT-qPCR to measure expression of the indicated gene.. Each point represents the average of three experimental replicates, N = 3. Midlines are average ± S.D. Student's t-test.

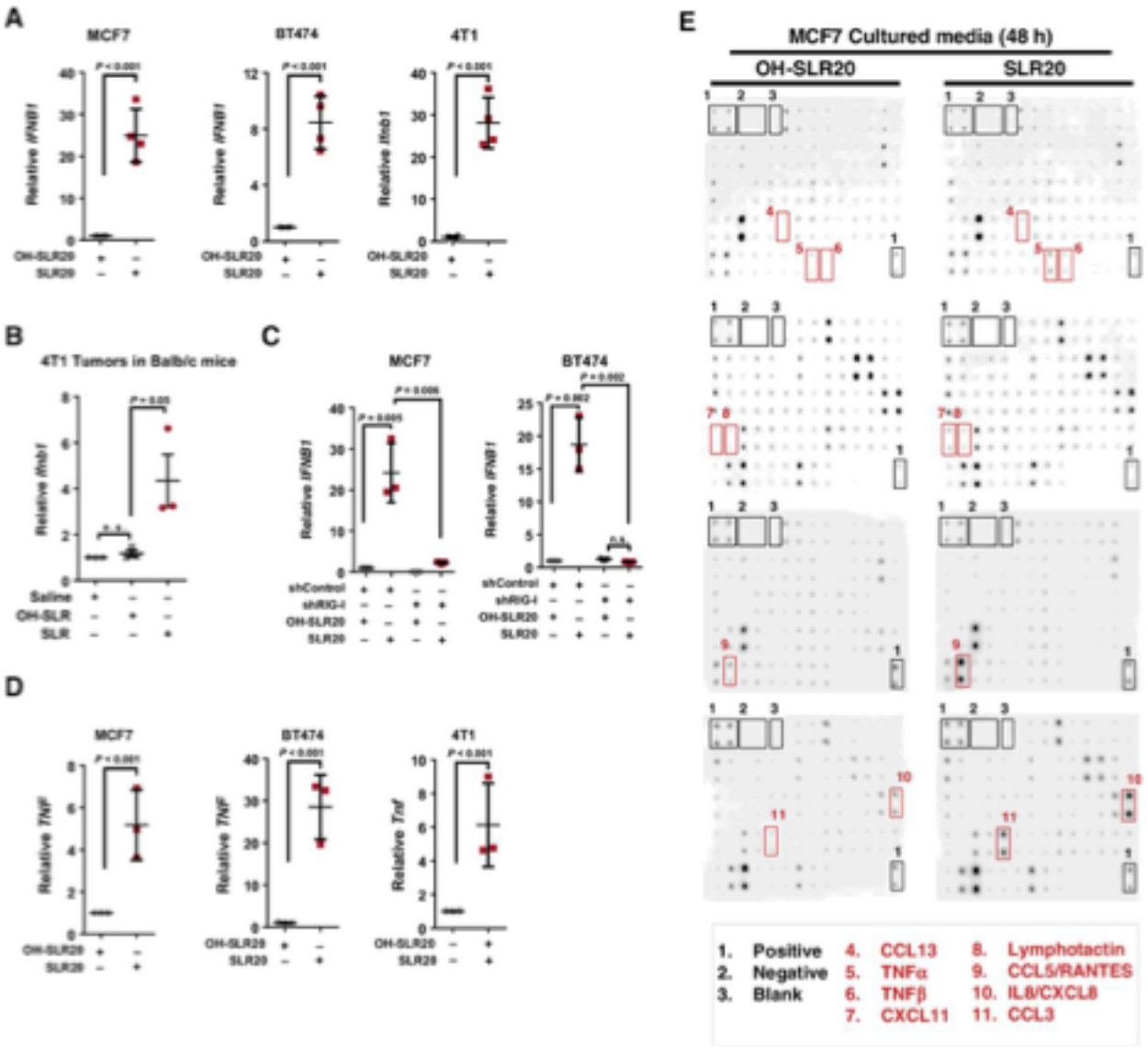

Figure 2.13 RIG-I signaling induces expression of proinflammatory cytokines from breast cancer cells. A–D, Cells were transfected, and after 12 hours, total RNA was assessed by RT-qPCR to measure expression of the indicated genes. Each point represents the average of three experimental replicates, N = 3. Midlines are average ± SD. Student t test. E, Cytokine array assessing cultured media harvested from MCF7 cells 48 hours after transfection. Representative images are shown.

context of therapeutic STING signaling in tumors, causing sustained induction of type I IFNs, which ultimately recruited immune-suppressive myeloid-derived suppressor cells (MDSC) to the tumor microenvironment (110). Further, studies demonstrating that RIG-I may respond to endogenous “unshielded” long noncoding RNAs (lnRNA) or genomically incorporated retroviral sequences, derived from neighboring tumor-associated fibroblasts and delivered to tumor cells through exosomal transport, may actually increase tumor cell growth, treatment resistance and malignant progression (111), despite production of inflammatory cytokines. These observations support further investigation into the longer-term consequences of RIG-I signaling in tumors. Future studies also need to consider the potential risk for unrestrained inflammation, because RIG-I is expressed in virtually all cell types, and RIG-I activation induces feed-forward signaling to amplify RIG-I and IFN-responsive genes. Recently described conditional RIG-I agonists, in which the 5′ -triphosphorylated terminus of the RNA duplex remains shielded until release by predetermined molecular cues, may help enrich delivery of RIG-I agonist to the target tissue (95).

In summary, we demonstrate that RIG-I signaling induces immunogenic tumor cell death and upregulates expression of MHC-I components, pro-inflammatory cytokines, and chemokines in ER+ breast cancer cells, HER2+ breast cancer cells, and TNBC cells, resulting in inhibition of tumor growth and increased TILs in vivo. These findings suggest that RIG-I activation using a synthetic agonist activates innate immunity in breast cancer cells increases immunogenicity of breast cancers and may be a feasible treatment approach for treatment of breast cancers, including those with lower mutational burden that are considered poor candidates for immunotherapy.

A

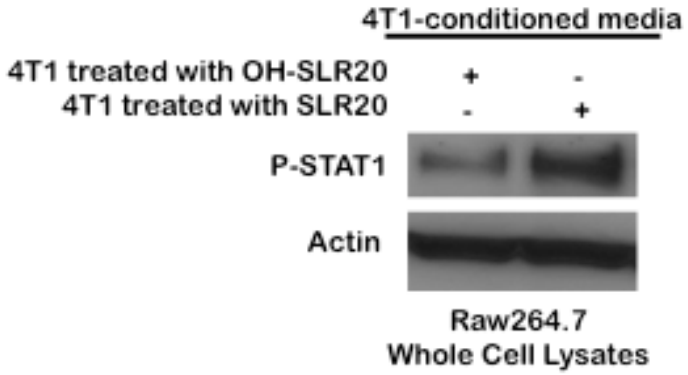

B

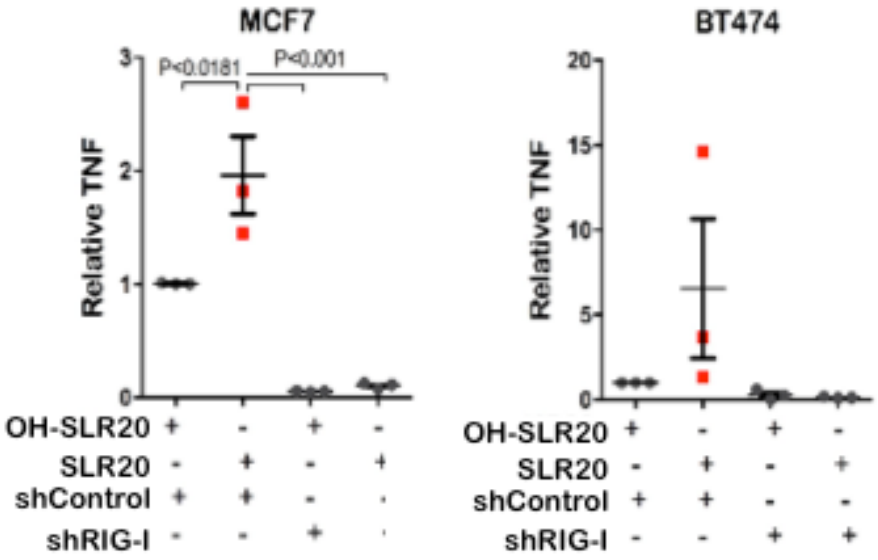

Figure 2.14 RIG-I shRNA decreases the induction of TNF. A. 4T1 cells were transfected with SLR20 or OH-SLR20. At 4 hours after transfection, 4T1 cells were washed 5 times, then cultured in serum-free media for 16 hours. 4T1-cultured supernatant was collected, passed through a 0.2mm filter, then added neat to cultures of Raw264.7 cells for 30 minutes. Western analysis of RAW264.7 whole cell lysates was used to measure P-STAT1. B. Cells were transfected, and after 16 h, total RNA was assessed by RT-qPCR to measure expression of the indicated gene.. Each point represents the average of three experimental replicates, N = 3. Midlines are average ± S.D. Student's T-test.

CHAPTER III

THERAPEUTIC RIG-I ACTIVATION PROMOTES TUMOR-DIRECTED T-CELL RESPONSES AND ANTI-TUMOR ADAPTIVE IMMUNITY IN BREAST CANCERS

Abstract

RIG-I is a cytoplasmic RNA helicase expressed in most cells of the body, functioning to sense viral oligonucleotide motifs, then activate innate immune responses to combat viral infection. RIG-I expression and activity is retained in most cancer cells, and in cells of the tumor microenvironment. These observations support a growing research interest in potential use of synthetic RIG-I agonists in cancer therapy. Recent studies showed that RIG-I agonist treatment induced breast tumor cell death through two tumor cell-intrinsic mechanisms, pyroptosis and extrinsic apoptosis. However, the impact of tumor RIG-I signaling on tumor cell-lymphocyte crosstalk and adaptive anti-tumor immunity remain unclear. We report that the RIG-I agonist SLR20 activated RIG-I signaling in tumor cells, resulting in increased Fas expression. Interestingly, T-cells co-cultured with SLR20-treated tumor cells upregulated Fas ligand (FasL) expression. Further, SLR20-treated tumor cells were more susceptible to Fas-mediated lysis by CD8+ T-cells. Antigen-specific lysis of ovalbumin-expressing mammary tumor cells by T-cells from transgenic OT-1 mice was enhanced when tumor cells were pre-treated with SLR20, which potently upregulated the antigen presenting machinery on tumor cells. Notably, molecular markers of T-cell activation were increased upon co-culture of T-cells with SLR20-treated breast cancer cells, or with conditioned media collected from SLR20-treated breast cancer cells. Immunization of wild-type mice with 4T1 mammary

cancer cell lysates did not affect future 4T1 tumor formation, but the addition of SLR20 as a vaccine adjuvant resulted in reduced growth of future tumors and increased tumor-cell reactive lymphocytes. Collectively, these findings indicate that therapeutic RIG-I signaling operates at the interface of innate and adaptive immunity within breast tumors to redirect T-cell responses in the TME and promote adaptive anti-tumor immunity.

Introduction

T-cell mediated responses are an important component in the success of cancer immunotherapies, including cancer vaccines, Chimeric Antigen Receptor (CAR)-T cells, and immune checkpoint inhibitors (1,89, 112). Use of immunotherapies in breast cancer treatment is not yet widespread, due in part to the immunological challenges that characterize many breast cancers, including immunosuppressive cytokines [e.g., transforming growth factor (TGF)-β, Interleuken (IL)-10] in the breast tumor microenvironment (TME), and immunosuppressive leukocyte populations [(e.g., regulatory CD4 T-cells (T_{Reg}s) and Myeloid Derived Suppressor Cells (MDSCs)] (112-113). Estrogen Receptor(ER)+ breast cancers often harbor a low burden of tumor infiltrating lymphocytes (TILs), which may be due to the relatively low mutational load of Estrogen Receptor(ER)+ breast cancers (4-5, 100-101). A direct relationship between TIL burden and tumor response to immunotherapy has been noted previously, posing another hurdle to overcome before immunotherapies can be adopted in ER+ breast cancers.

Although TILs may occur at a higher frequency in HER2-amplified (HER2+) and triple negative breast cancers (TNBC) over estrogen receptor (ER)+ tumors, these TILs

often bear molecular markers of exhaustion (e.g., LAG-3) or checkpoint induction (e.g. PD-1, CTLA-4, TIGIT), while lacking molecular markers of effector activity, [e.g., interferon (IFN)-γ, granzyme B] (113). Thus, breast cancers are often thought of as immunologically 'cold.' It is possible that recruitment of TILs to the TME that are not tolerogenic, anergized, or exhausted could change the breast TME to a more immunogenic state, increasing anti-tumor immunity and perhaps priming breast tumors for improved response to emerging immunotherapies.

There is growing evidence that innate immune responses remain intact within tumors, and can be harnessed to increase expression of pro-inflammatory cytokines, recruit TILs, and increase effector T-cell activity. Targeted activation of pattern recognition receptors (PRRs), the family of small cytoplasmic receptors that recognize intercellular pathogens and then trigger a pro-inflammatory immune response, is gaining increasing interest. Synthetic agonists are being produced that activate each PRR with specificity. Agonists of the PRR known as RIG-I mimic the viral nucleotide motif recognized by RIG-I, comprised of a short double-stranded (ds)-RNA capped with a 5' tri-phosphate motif (23-25). Agonists of RIG-I have shown anti-tumor effects in several preclinical cancer models in cell culture (ovarian and myeloid leukemia) (74, 76) and *in vivo* (melanoma, prostate, pancreatic, and breast) (27, 32, 77, 114). We recently used a 5' triphosphate labeled, 20-residue stem-loop RNA (SLR20) agonist to demonstrate that therapeutic RIG-I activation in breast cancer potently increased cell death in breast cancer cells, reducing mammary tumor growth and metastasis (114), while at the same time, increasing expression of pro-inflammatory cytokines.

Given that RIG-I signaling in breast cancer cells induces expression of pro-inflammatory cytokines, while inducing pyroptosis (114), a pro-inflammatory mode of programmed cell death, it is possible that RIG-I signaling in breast cancer cells might actively recruit TILs to the breast TME, while enhancing T-cell effector activity and diminishing T-cell checkpoint activation and/or exhaustion. This hypothesis was tested using SLR20, finding that RIG-I signaling in breast tumor cells promoted tumor cell crosstalk with T-cells, enhancing T-cell activation, and increasing both antigen-specific and Fas-mediated killing of tumor cells by T-cells.

Materials and Methods

Generation of SLR20

Oligoribonucleotides sequence OH-SLR20 (5′-GGACGUACGUUUCGACGUACGUCC) was synthesized on an automated MerMade synthesizer (BioAutomation) using standard phosphoramidite chemistry as described previously (34). Triphosphorylated oligoribonucleotide SLR20 (5′ppp-GGACGUACGUUUCGACGUACGUCC) was synthesized as described (35), deprotected, and gel purified. The triphosphorylation state and purity were confirmed using mass spectrometry. The oligonucleotides were resuspended in RNA storage buffer (10 mmol/L MOPS pH 7, 1 mmol/L EDTA) and snap cooled to ensure hairpin formation, as previously described (28).

Cell line authentication

The human cell lines MDA-MB231, BT474, and murine cell line 4T1 were purchased from ATCC in 2015. Cell identity was verified by ATCC using genotyping with a

Multiplex STR assay. MMTV-Neu primary mammary tumor cells were isolated from MMTV-Neu tumors in FVB mice and cultured. All cells were maintained at low passage in DMEM with 10% fetal bovine serum and 1% antibiotics and antimyotics. All cell lines were screened monthly for Mycoplasma. Cells were used within 20 passages for each experiment.

Cell culture

SLR20 and OH-SLR20 were delivered to cells in serum-free Opti-MEM media at a final concentration of 0.25 μmol/L using lipofectamine 2000 (Invitrogen). Cells expressing shRNA against RIG-I were generated by transduction with pLKO lentiviral particles (Sigma-Aldrich) harboring shRNA sequences against human or mouse RIG-I (DDX58) and selected with puromycin (2 μg/mL). Cell death of cultured cells was measured by adding propidium iodide (PI; Sigma-Aldrich, 1:1,000) to cultured media of live cells 1 hour before imaging by fluorescence microscopy. Where indicated, cells were treated with an anti-Fas (CD95) antibody (mouse anti-human, Biolegend, 305704, 1 μg/mL) or IgM control (Sigman-Aldrich, P6834, 1 μg/mL) for 1 hour. Apoptosis of cultured cells was measured by treating cells for 4 hours with Annexin V-Alexa Fluor 488 conjugates (1:500, Invitrogen), followed by fluorescence microscopy.

Western analysis

Whole-cell lysate was harvested by homogenization of cells in ice-cold lysis buffer [50 mmol/L Tris pH 7.4, 100 mmol/L NaF, 120 mmol/L NaCl, 0.5% nonidet P-40, 100 μmol/L Na3VO4, 1 × protease inhibitor cocktail (Roche), 0.5 μM MG132 (Selleck Chem)].

Lysates (20 μg protein measured by BCA assay) were resolved on 4% to 12% polyacrylamide gels (Novex) and transferred to nitrocellulose membranes (iBlot), blocked in 3% gelatin in TBS-T (Tris-buffered saline, 0.1% Tween-20), incubated in primary antibodies from Cell Signaling Technologies: RIG-I (D14G6, 1:1,000), STAT1 (D1K9Y, 1:1,000), P-STAT1 S536 (93H1, 1:1,000), PARP (9542, 1:1,000), Rab11 (7100, 1:1,000); β-actin (Sigma-Aldrich, AC-15, 1:10,000); and E-cadherin (BD Transduction Laboratories, 610182, 1:1,000). Western blots were developed with ECL substrate (Thermo Fisher Scientific).

Generation of nanoparticles for intratumoral delivery

Amphiphilic diblock copolymer composed of a 10.3 kDa dimethylaminoethyl methacrylate (DMAEMA) first block and a 31.0 kDa, 35% DMAEMA, 39% butyl methacrylate (BMA), and 26% propylacrylic acid (PAA) second block were synthesized as previously described (36). Dry amphiphilic diblock polymer was dissolved into ethanol at 50 mg/mL, rapidly diluted into phosphate buffer (pH 7.0, 100 mmol/L) to 10 mg/mL, concentrated, and buffer was exchanged into PBS (Gibco) using 3 kDa molecular weight cutoff centrifugal filtration columns (Ambion, Millipore) and sterile filtered. Polymer concentration was measured by absorbance at 310 nm (Synergy H1 microplate reader, BioTek). Concentrated polymer solution was rapidly mixed with SLR20 (or OH-SLR20) at a charge ratio of 5:1 (N:P) for 30 minutes and diluted into PBS (pH 7.4, Gibco) to 20 μg of SLR and 400 μg of polymer in 50 μL total volume.

Animal studies and immunization

All studies were performed in accordance with Association for Assessment and Accreditation of Laboratory Animal Care International (AAALAC) guidelines and were approved by the Institutional Animal Care and Use Committee at Vanderbilt University. All mice were housed in pathogen-free conditions. Left inguinal mammary fat pads of wild-type (WT) female Balb/c mice or athymic (nu/nu) Balb/c mice (Jackson Labs) were injected with 10^6 4T1 cells. Mice were randomized into treatment groups when tumors reached 50-100 mm^3. Intratumoral injection of nanoparticle in 50 μL of saline (or saline without nanoparticle) was performed at 48-hour intervals for a total of 3 treatments for 5 days. For vaccination studies, mice were co-injected (50 μL) intramuscularly with 4T1 lysates (1 x 10^6 cells freeze-thawed 3 times and sonicated) and a mixture of *in vivo*-JetPEI (1.2 μL) and SLR20 (10 μg), OH-SLR20 (10 μg), or vehicle (5% glucose solution prepared via manufacturer's instructions) at an N:P ratio of 6. After 8 days, 4T1 tumors were injected into the mammary fat pad in the same manner as specified above. Mice were monitored daily, and tumor volume was measured with calipers three times weekly for up to 16 days.

Histologic analyses

Tumors were formalin-fixed and paraffin-embedded, and sections (5 μm) were stained with hematoxylin and eosin. IHC was performed using the following antibodies: CD45 (Abcam, ab10558, 1:5000), CD3 (Abcam, ab16669, 1:800). Immunodetection was performed using the Vectastain kit (Vector Laboratories) according to the manufacturer's instructions.

RNA isolation and expression analyses

Total RNA was extracted using NucleoSpin RNA (Machery-Nagel), reverse transcribed (iScript cDNA Synthesis; Bio-Rad), and used for qPCR with iTaq Universal SYBR Green (Bio-Rad) on a Bio-Rad CFX96 thermocycler. Gene expression is normalized to *36B4*. The following primers were obtained from Integrated DNA Technologies: *IFNB1* [forward 5′-TGCTCTCCTGTTGTGCTTCTCC; reverse 5′-GTTCATCCTGTCCTTGAGGCAGT]; *Ifnb1* [forward 5′-CAGCTCCAAGAAAGGACGAAC; reverse 5′-GGCAGTGTAACTCTTCTGCAT]; *HLA-B* [forward 5′-GCGGCTACTACAACCAGAGC; reverse 5′-GATGTAATCCTTGCCGTCGT]; *FAS* [forward 5′-TCTGGTTCTTACGTCTGTTGC; reverse 5′-CTGTGCAGTCCCTAGCTTTCC]; *Fas* [forward 5′- TATCAAGGAGGCCCATTTTGC; reverse 5′-TGTTTCCACTTCTAAACCATGCT]; *FasI* [forward 5′-GCCCATGAATTACCCATGTCC; reverse 5′-ACAGATTTGTGTTGTGGTCCTT]. Other genes were analyzed via PCR array (RT^2 Profiler PCR Array Mouse T-Cell & B-Cell Activation, PAMM-053Z).

Flow Cytometry

Cells were washed with phosphate buffered saline (PBS) pH 7.4, incubated with Fc block (BioLegend, 101320), stained with fluorescent antibodies for 30 minutes, washed and counterstained with DAPI for live/dead cell detection. Antibodies used include the following: CD3 (BioLegend, 100210, 1:200), CD8 (BioLegend, 100722, 1:200), CD4 (BioLegend, 100422, 1:200), CD4 (BD Pharmingen, 553049, 1:200), CD25 (BioLegend,

101910, 1:200), CD44 (BioLegend, 103012, 1:200), CD69 (eBioscience, 12-0691-81, 1:200), FoxP3 (Invitrogen, FJK-16s, 12-5773-82, 1:200), H-2Kd (BioLegend, 114708, 1:200), HLA-A,-B,-C (BioLegend, 311415, 1:200), SIINFEKL (BioLegend, 141605, 1:200). Before anti-FoxP3 staining, splenocytes were fixed and permeabilized (Cytofix/Cytoperm, BD Biosciences). Flow cytometry samples were analyzed on a Life Technologies Attune NxT.

ELISA

Supernatant was collected 32 hours after isolated splenocytes were co-cultured with SLR20 or OH-SLR20 treated breast cancer cells. The supernatant was filtered (0.2 μm) and analyzed using an IFN-γ ELISA (RayBiotech, ELM-IFNg) per the manufacturer's instructions.

Splenic T-cell cultures

Spleens were minced in sterile PBS, and cultured 3 hours before collecting T-cells from the non-adherent population using the Miltenyi Biotec $CD8a^+$ T Cell Isolation Kit (130-104-075) and $CD4^+$ T Cell Isolation Kit (130-104-454). Breast cancer cells previously treated with OH-SLR20 or SLR20 were co-cultured with splenic $CD8^+$ T-cells a ratio of 5:1 (50,000 immune cells:10,000 breast cancer cells) for 2 hours, then cytotoxicity was measured using CytoTox 96 Non-Radioactive Cytotoxicity Assay (Promega) per manufacturer's instructions.

Statistical analysis

Experimental groups were compared with controls using Student unpaired, two-tailed T-test. Multiple groups were compared across a single condition using one-way analysis of variance (ANOVA). $P < 0.05$ was used to define significant differences from the null hypothesis. qPCR array data sets were compared using multiple T-tests with an FDR cutoff of 0.05.

Ethics statement

Animals were housed under pathogen-free conditions, and experiments were performed in accordance with AAALAC guidelines and with Vanderbilt University Institutional Animal Care and Use Committee approval.

Results

RIG-I signaling and cell death are activated in HER2+ and TNBC cells by a synthetic RIG-I agonist.

We assessed RIG-I activation and signaling in HER2+ breast cancer and TNBC cells using SLR20, a synthetic 20-residue dsRNA sequence with a stem-loop structure, and a 5’ tri-phosphate motif. As a negative control, we used the same double-stranded RNA sequence, but lacking the 5’ tri-phosphate motif (OH-SLR20). Human breast cancer cells BT474 (HER2+) and MDA-MB231 (TNBC) were transiently transfected with SLR20 or OH-SLR20. After 18 hours, western analysis revealed increased RIG-I expression and phosphorylation of the pro-inflammatory transcription factor Signal Transducer and Activator of Transcription (STAT)-1 (**Figure 3.1.A**), confirming agonist-induced RIG-I

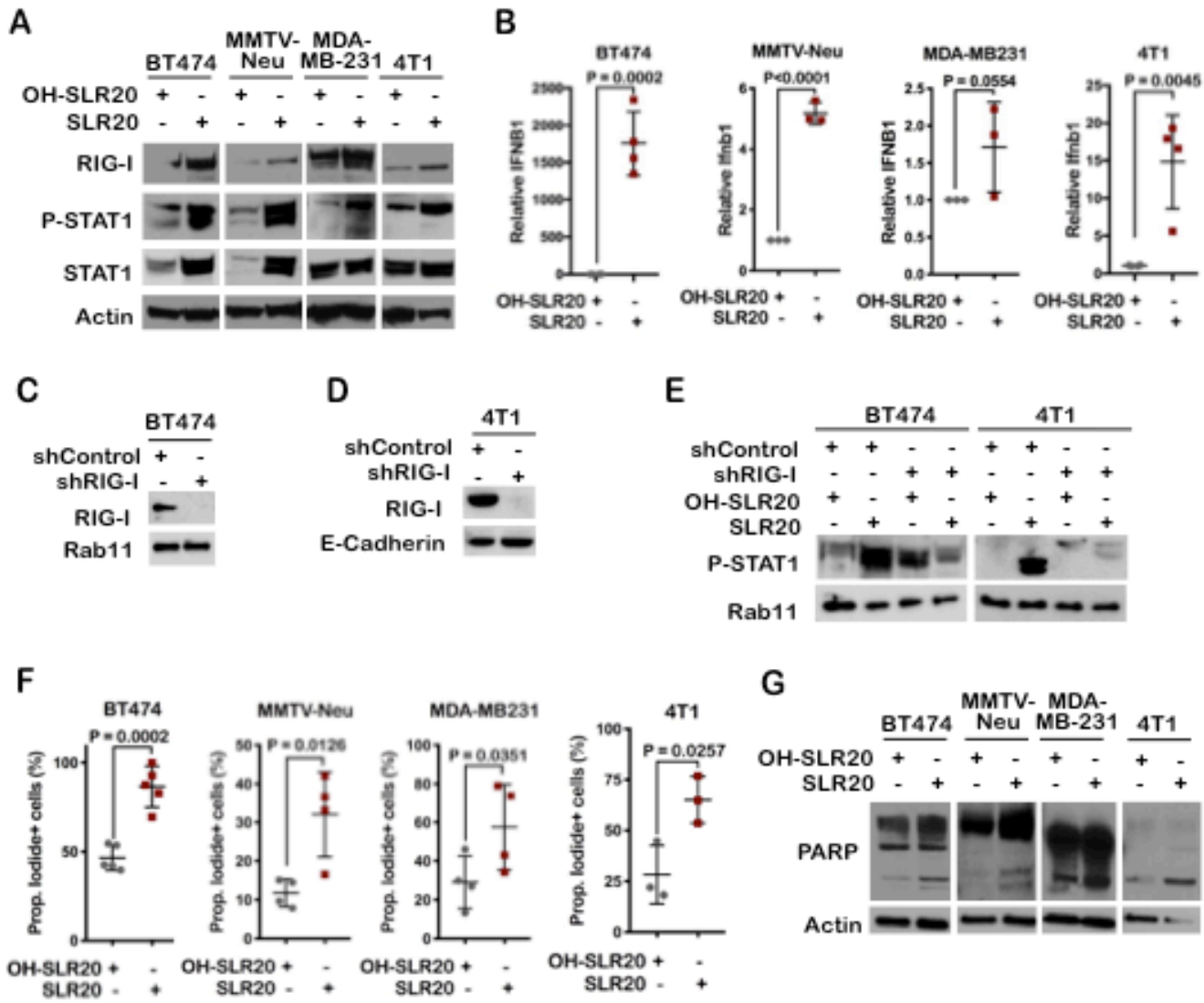

Figure 3.1 RIG-I agonist SLR20 induces pro-inflammatory signaling and activates cell death in HER2+ and triple negative breast cancer cells.

A. Whole-cell lysates were collected 18 hours after transfection and were assessed by Western analysis using the antibodies shown on the left of each panel. B. Cells were transfected, and after 18 hours, total RNA was assessed by RT-qPCR to measure the expression of *IFNB1*. Each point represents the average of three experimental replicates, N = 3-4. Midlines are the average ±SD. Student's t-test. C-D. Whole-cell lysates were collected and assessed by Western analysis using the antibodies shown on the left of each panel. E. Whole-cell lysates were collected 18 hours after transfection and were assessed by Western analysis using the antibodies shown on the left of each panel. F. PI^+ cells were imaged by fluorescence microscopy. The number of fluorescent cells per well was counted. Each point shown represents the average of two experimental replicates, N = 3-5. Midlines are the average ±SD. Student's t-test. G. Whole-cell lysates were collected 18 hours after transfection and were assessed by Western analysis using the antibodies shown on the left of each panel.

signaling. These results are consistent with previous studies in ER+ breast cancer cells, showing SLR20-medaited activation of RIG-I signaling (114). Transfection of mouse mammary tumor cells MMTV-Neu (HER2+) and 4T1 (TNBC) confirmed SLR20-induced activation of RIG-I signaling. SLR20 treatment induced the expression of type I IFN (*IFNB1*), a hallmark of RIG-I signaling, in BT474, MDA-MB-231, MMTV-Neu and 4T1 cells (**Figure 3.1.B**). We confirmed that the effects of SLR20 were due to RIG-I signaling by using cells with stable expression of shRNA sequences directed against RIG-I (shRIG-I), which diminished expression of RIG-I >90%, as measured by western blot (**Figure 3.1.C-D**). While BT474 and 4T1 cells expressing non-targeting shRNA sequences (shControl) showed potent P-STAT1 upon transfection with SLR20, cells expressing shRIG-I failed to induce P-STAT1 upon transfection with SLR20 (**Figure 3.1.E),** confirming molecular specificity of the response to SLR20. Previous reports demonstrated that ER+ breast cancer cells undergo two types of cell death in response to RIG-I signaling, pyroptosis and extrinsic apoptosis (114). To determine if SLR20 induces cell death in HER2+ cells (BT474 and MMTV-Neu) and TNBC cells (MDA-MB-231 and 4T1), we stained transfected cells with propidium iodide (PI), an indicator of cell membrane permeabilization, as would occur upon pyroptosis or necrosis. At 18 hours after transfection, cells transfected with SLR20 showed significantly increased PI staining as compared to cells transfected with OH-SLR20 (**Figure 3.1.F**). PARP cleavage, a molecular indicator of apoptosis, was also increased in HER2+ breast cancer and TNBC cell lines transfected with SLR20 (**Figure 3.1.G**), demonstrating the activation of cell death in HER2+ and TNBC cells treated with a RIG-I agonist.

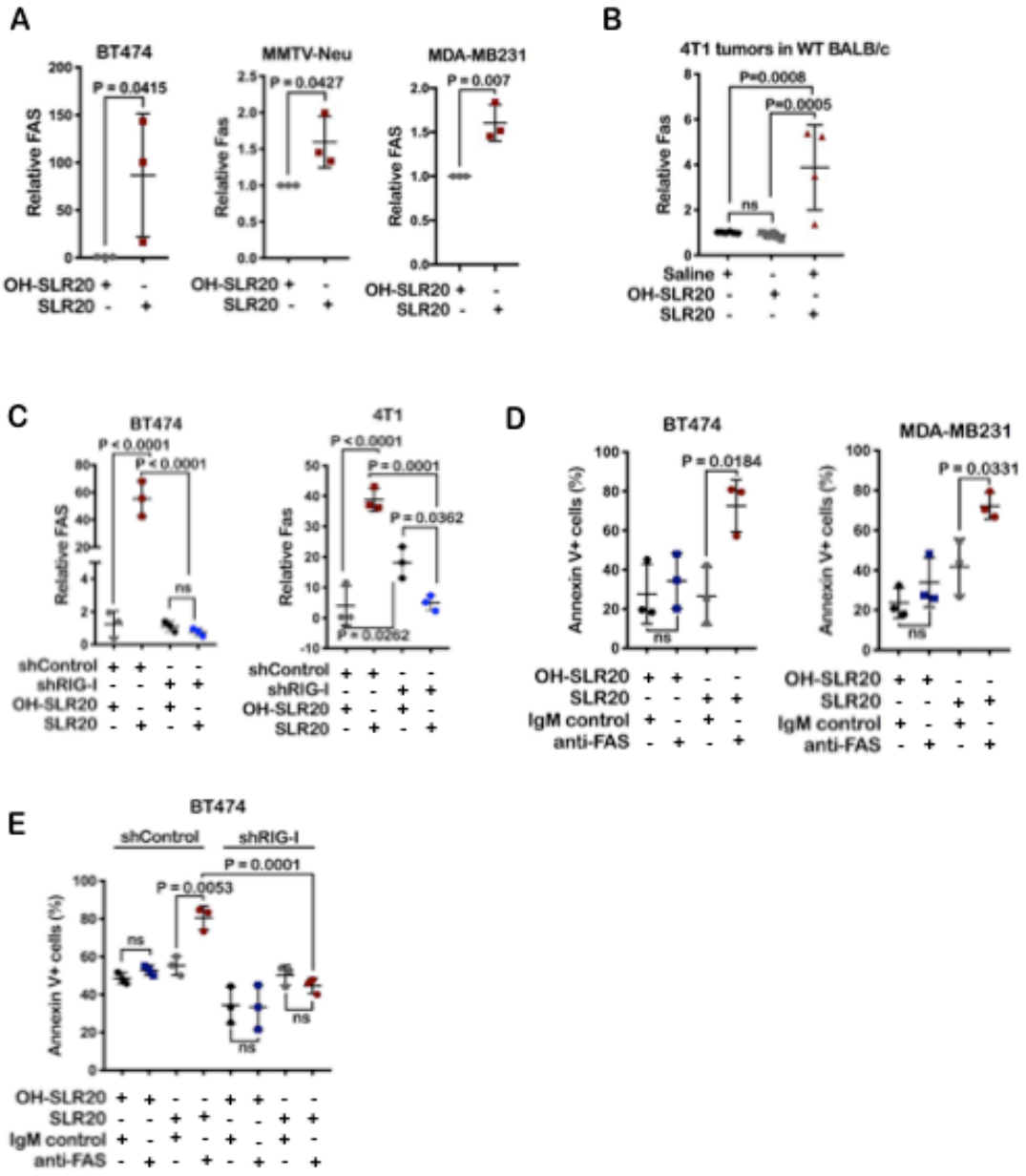

Figure 3.2 RIG-I signaling increases FAS expression and sensitivity to FAS-mediated cell death in breast cancer cells.

A. Cells were transfected, and after 18 hours, total RNA was assessed by RT-qPCR to measure the expression of *FAS*. Each point represents the average of three experimental replicates, N = 3. Midlines are the average ±SD. Student's t-test. B. RNA harvested from 4T1 tumors collected on treatment day 5 was assessed by RT-qPCR for *Fas* gene expression as described in A. One-way ANOVA. C. Cells were transfected, and after 18 hours, total RNA was assessed by RT-qPCR to measure the expression of *FAS*. Each point represents the average of three experimental replicates, N = 3. Midlines are the average ±SD. One-way ANOVA. D. Alexa Fluor 488^{+} cells were imaged by fluorescence microscopy. The number of fluorescent cells per well was counted. Each point shown represents the average of two experimental replicates, N = 3. Midlines are the average ±SD. One-way ANOVA E. AlexaFluor488+ cells were imaged by fluorescence microscopy. The number of fluorescent cells per well was counted. Each point shown represents the average of two experimental replicates, N = 3. Midlines are the average ±SD. One-way ANOVA.

Fas expression and sensitivity to Fas-mediated cell death is increased in RIG-I activated breast cancer cells.

Fas ligand (FasL) is expressed robustly on the cell surface of activated T-cells (115). T-cell FasL can engage its receptor, Fas, on the surface of tumor cells, activating Fas signaling, thus activating the extrinsic apoptosis pathway. We investigated the expression of Fas in HER2+ (BT474 and MMTV-Neu) and TNBC (MDA-MB-231) cell lines. At 18 h after transfection with SLR20, human *FAS* (and mouse *Fas*) gene expression was robustly elevated, as compared to cells transfected with OH-SLR20 (**Figure 3.2.A**). We assessed SLR20-induced *Fas* expression in vivo using 4T1 tumors grown in wild-type Balb/C mice. When tumors reached 50 mm^3 (treatment day 0, or d0), SLR20 was delivered to tumors via endosomolytic nanoparticles (np) by intra-tumoral injection, as described previously (114). Tumors were treated on d0, d2, and d4, then collected for analysis of *Fas* gene expression on d5 by quantitative reverse-transcription-polymerase chain reaction (qRT-PCR). Tumors collected 24 hours after final treatment with nanoparticle-SLR20 (npSLR20) displayed *Fas* gene upregulation compared to tumors treated with npOH-SLR20, or those treated with saline (**Figure 3.2.B**). Importantly, shRNA-mediated RIG-I knockdown in BT474 and 4T1 cells diminished SLR20-induced *FAS* upregulation (**Figure 3.2.C**), confirming that RIG-I signaling induces Fas expression in tumor cells.

Although these findings are consistent with previous reports describing Fas induction in other cancer cell types upon treatment with a RIG-I agonist, including pancreatic cancer (32), the consequences of RIG-I-induced Fas expression is not entirely clear. The impact of RIG-I mediated Fas induction on tumor cell sensitivity to

FasL-induced cell killing was investigated here, using an activating anti-human Fas monoclonal antibody (αFas mAb). HER2+ (BT474) and TNBC (MDA-MB-231) cells transfected with SLR20. 18 hours after transfection, cells were treated 24 hours with αFas mAb, or with a control mAb, followed by Annexin V staining to measure apoptotic cell death. SLR20 transfected cells treated with αFas mAb showed increased AnnexinV staining over OH-SLR20 transfected cells treated with αFas mAb (**Figure 3.2.D**), suggesting increased FAS sensitivity upon activation of RIG-I signaling. In contrast, SLR20 transfection in BT474 cells expressing shRIG-I failed to sensitize BT474 cells to cell death in response to the αFas mAb (**Figure 3.2.E**). Together, these studies show that RIG-I signaling increases Fas expression on HER2+ breast cancer and TNBC cells, sensitizing these cells to Fas-directed cell death.

RIG-I activation in breast cancer cells induces Fas ligand expression in lymphocytes

To measure the effect of tumor cell RIG-I signaling on FasL expression in neighboring lymphocytes, we harvested splenocytes from wild-type female FVB mice for co-culture with HER2+ MMTV-Neu cells, derived from a female FVB mouse. Only non-adherent splenocytes were used for co-culture, to enrich for lymphoid populations. Prior to co-culture with non-adherent splenocytes, MMTV-Neu cells were transfected with SLR20 or OH-SLR20, then thoroughly washed (**Supplementary Figure 3.3.A**). After 18 hours of co-culture, splenocytes were removed and assayed for *Fasl* mRNA expression, showing increased *Fasl* in splenocytes co-cultured with SLR20-transfected MMTV-Neu

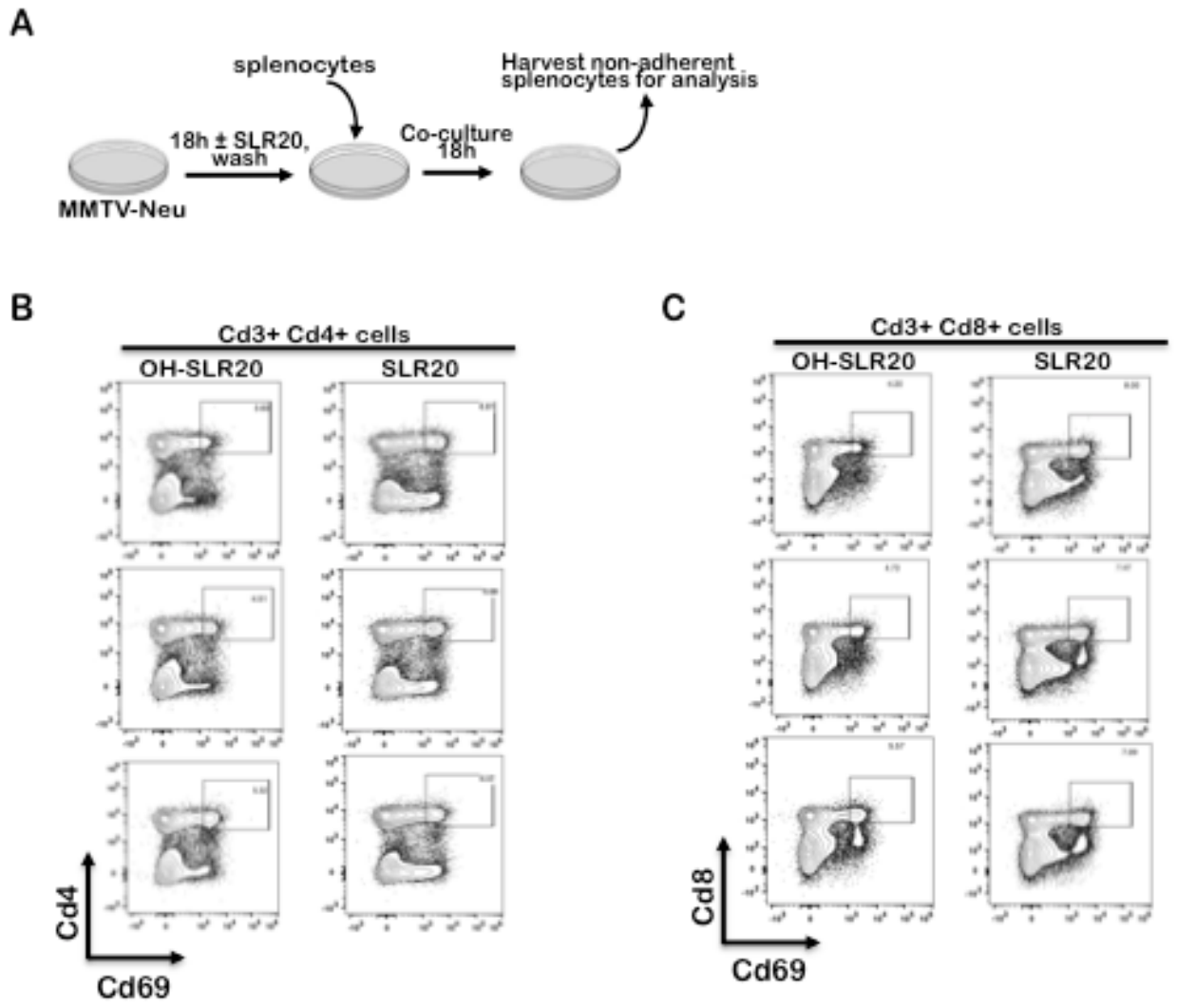

Figure 3.3 Activation marker CD69 is increased by RIG-I signaling A. Schematic of the experimental model used to measure the induction of *Fasl* in splenocytes. B-C. 18 hours after co-culture with treated breast cancer cells, $CD8^+$ and $CD4^+$ T-cells were assessed by flow cytometry to measure levels of activation marker CD69 on the cell surface. N=3. Student's t-test.

cells, but not those transfected with OH-SLR20 (**Figure 3.4.A**). Next, we transfected TNBC 4T1 cells (derived from a female Balb/C mouse). After 24 hours, cultured media was transferred from the transfected 4T1 cells to cultures of CD8+ T-cells enriched from wild-type Balb/C splenocytes (**Figure 3.4.B**). After 18 hours, *Fasl* expression was upregulated in CD8+ T-cells treated with media conditioned by SLR20-transfected 4T1 cells, but not media conditioned by OH-SLR20-transfected cells (**Figure 3.4.C**). These data suggests that RIG-I signaling in breast cancer cells, while upregulating expression of Fas on the tumor cell, simultaneously promotes FasL expression in adjacent T-lymphocytes, which may cooperate to produce robust, local tumor cell killing by T-cells. We tested this hypothesis using CD8+ T-cells harvested from Balb/C mice, which were immunized with 4T1 cell lysates. 4T1 lysates (generated by freeze-thaw) were delivered subcutaneously to WT Balb/C mice on days 1, 4, 7, and 10. CD8+ T-cells isolated from these mice were added in co-culture with 4T1 cells previously transfected with SLR20 or OH-SLR20 (**Figure 3.4.D**). After 2-hours of co-culture with CD8+ splenocytes, 4T1 cells transfected with OH-SLR20 showed similar cell death levels to what was seen with 4T1 cells cultured in the absence of CD8+ T-cells. However, cell death was upregulated 2-fold in SLR20-transfected 4T1 cells co-cultured with CD8+ T-cells (**Figure 3.4.E**). These findings are consistent with the idea that tumor cell RIG-I signaling coordinates cell death signaling pathways within both tumor cells and T-cells to drive tumor cell killing.

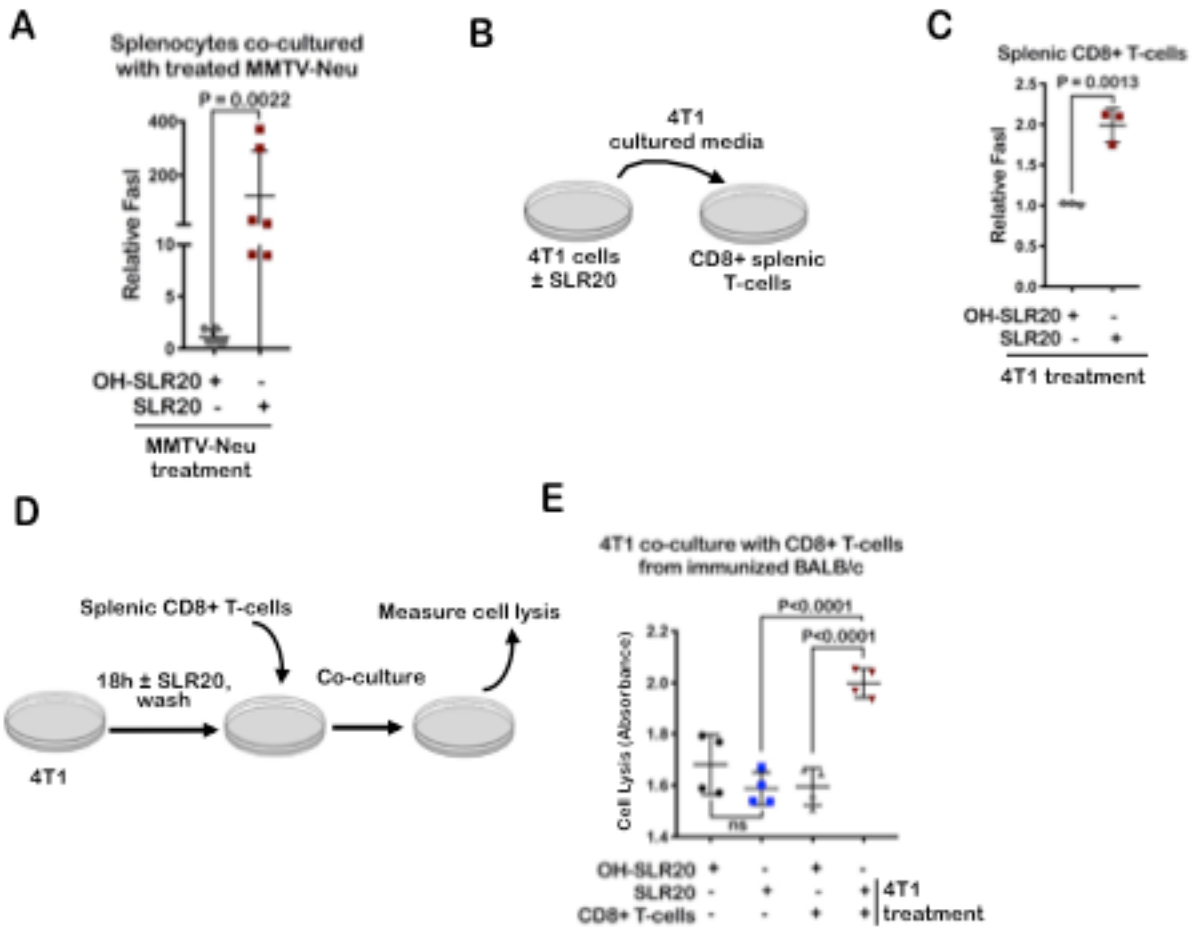

Figure 3.4 RIG-I signaling in breast cancer cells promotes leukocyte induction of FASL expression and leukocyte mediated tumor cell killing. A. RT-qPCR analysis of *Fasl* in splenocytes 18 hours after co-culture with breast cancer cells. Each point represents the average of two experimental replicates, N = 6. Midlines are the average ±SD. Student's t-test. B. Schematic of the experimental model used to measure the induction of *Fasl* in cytotoxic T-lymphocytes. C. RT-qPCR analysis of *Fasl* in $CD8^+$ T-cells after 18 hours of incubation in media conditioned by SLR20 or OH-SLR20 treated breast cancer cells. Each point represents the average of two experimental replicates, N = 3. Midlines are the average ±SD. Student's t-test. D. Schematic of the experimental model used to measure the cytotoxic T-lymphocyte mediated killing of breast cancer cells. E. Breast cancer cell (4T1) lysis following a 2 hour co-culture with $CD8^+$ T-lymphocytes. Lysis was quantified using a cytotoxicity assay that measures the release of LDH into the culture media following cell lysis. N = 4. Midlines are the average ±SD. One-way ANOVA.

RIG-I activation increases MHC-I expression and antigen presentation on breast cancer cells.

This idea was explored further, specifically focusing on tumor antigen-directed tumor cell killing by T-cells. Antigen presenting machinery in tumor cells is critical for tumor immune surveillance by T-cells. The major histocompatibility complex (MHC)-I is often downregulated in cancers in an effort to evade immune surveillance (116), although RIG-I signaling may enhance expression of MHC-I genes in some cancer cells. Expression of the MHC-I gene *HLA-B* was increased 50% in TNBC (MDA-MB-231) cells transfected with SLR20, versus transfection with OH-SLR20 (**Figure 3.5.A**). Cell surface expression of MHC-I components was measured by flow cytometry for H-2Kd in mouse cell lines MMTV-Neu and 4T1, revealing significantly increased percentage of H-2Kd+ cells following transfection with SLR20 (**Figure 3.5.B** and **Figures 3.6.A-B**). Similarly, flow cytometric analysis showed HLA-A,B,C (human MHC-I surface components) were increased in TNBC MDA-MB-231 cells transfected with SLR20 (**Figure 3.5.B** and **Figures 3.6.C**).

Given that MHC-I expression was higher in cells treated with the synthetic RIG-I agonist, we tested MHC-I antigen presentation capabilities in breast cancer cells transfected with SLR20, using E0771 mouse (C57BL/6) mammary tumor cells expressing the exogenous antigen, ovalbumin (E0771-Ova). Antigen processing of ovalbumin results in MHC-I presentation of the ovalbumin peptide fragment SIINFEKL. Therefore, we used flow cytometry to measure SIINFEKL presentation on E0771-Ova cells transfected with SLR20 or OH-SLR20, demonstrating an increased SIINFEKL+ population of cells upon transfection with SLR20 (**Figure 3.5.C** and **Figure 3.6.D**).

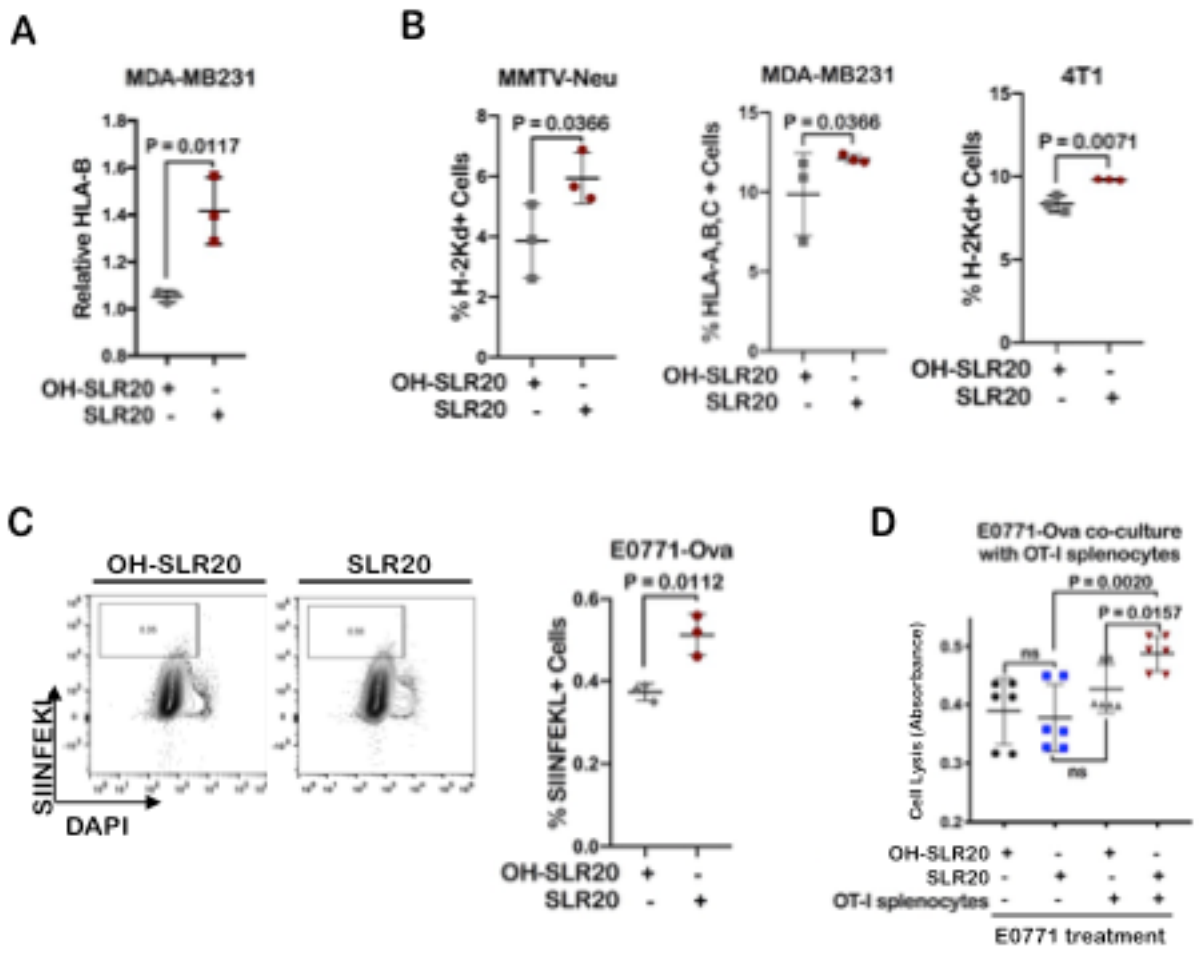

Figure 3.5 RIG-I signaling in breast cancer cells increases MHC-I expression and MHC-I mediated antigen presentation. A. Cells were transfected, and after 18 hours, total RNA was assessed by RT-qPCR to measure the expression of *HLA-B*. Each point represents the average of three experimental replicates, N = 3. Midlines are the average ±SD. Student's t-test. B. Cells were transfected for 18 hours and then assessed by flow cytometry to measure levels MHC-I. N=3. Student's t-test. C. Cells were transfected for 18 hours and then assessed by flow cytometry to measure levels SIINFEKL peptide on the cell surface. N=3. Student's t-test. D. Ovalbumin expressing breast cancer cell (E0771) lysis following a 2 hour co-culture with isolated OT-I splenocytes. Lysis was quantified using a cytotoxicity assay that measures the release of LDH into the culture media following cell lysis. N = 6. Midlines are the average ±SD. One-way ANOVA.

Further, CD8+ splenocytes enriched from transgenic OT-1 mice, which express an ovalbumin (SIINFEKL)-specific T-cell receptor, caused substantially higher levels of tumor cell lysis in E0771-Ova cells transfected with SLR20 (**Figure 3.5.D**). This result indicates that RIG-I activation within a tumor cell may coordinate signaling pathways within the tumor cell and neighboring T-cells to maximize tumor cell death.

RIG-I signaling in breast cancer cells induces markers of T-cell activation

To gain a broader understanding of how tumor cell RIG-I signaling might impact the phenotype of neighboring T-cells, we co-cultured splenocytes from FVB mice with MMTV-Neu (FVB) cells previously transfected with SLR20, then used flow cytometry to measure surface expression of the T-cell early activation marker CD69 on CD8+ and CD4+ T-cells (**Figure 3.7.A**). After 18 hours of co-culture, the percentage of CD3+CD8+ T-cells positive for CD69 was increased nearly 50% in co-cultures with SLR20-transfected MMTV-Neu cells (**Figure 3.7.B** and **Figures 3.3.B**). Similarly, the percentage of CD3+CD4+ T-cells positive for CD69 was increased following co-culture with SLR-20 transfected MMTV-Neu cells (**Figure 3.7.C** and **Figure 3.3.C**).

We expanded our analysis of lymphocyte activation markers using a gene expression array, profiling expression changes in 84 genes associated with T-cell activation. Cultured media from 4T1 cells transfected with SLR20 or OH-SLR20 was collected and added to splenic $CD4^+$ T-cells isolated from BALB/c mice. After 18 hours, $CD4^+$ T-cell mRNA was assessed by gene expression array, showing robust expression of genes involved in T-cell activation (*Cd3e*, *CD40lg*, *Map3k7*,), effector function (*Cd47*, *Csf2*, *Ifng*, *Icosl*), proliferation (*Il15*, *Cd74*, *Cxcr4, Cxcl12*) and negative regulation

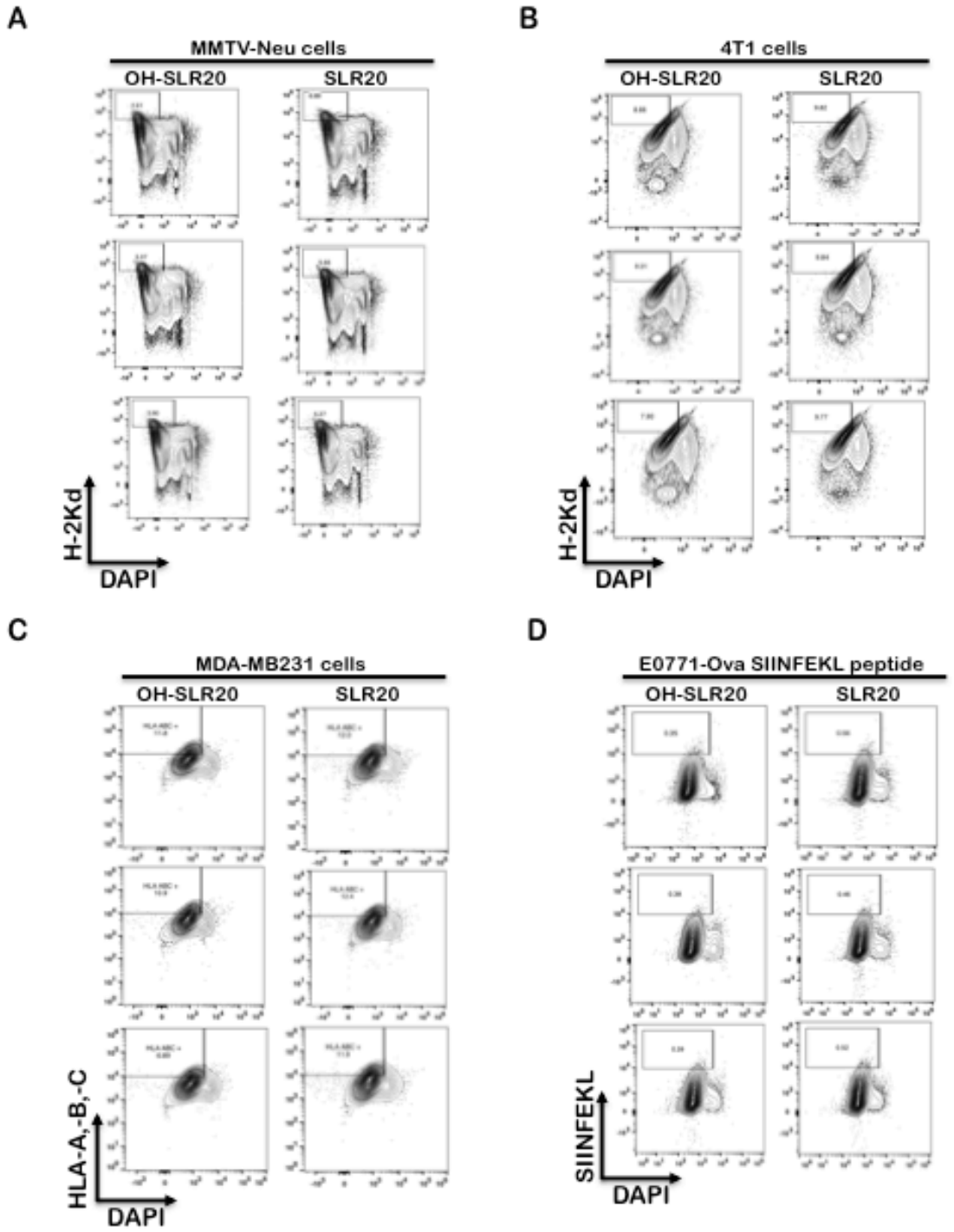

Figure 3.6 MHC-I is increased by RIG-I signaling in breast cancer cells. A-C. Cells were transfected for 18 hours and then assessed by flow cytometry to measure levels MHC-I. N=3. Student's t-test. D. Cells were transfected for 18 hours and then assessed by flow cytometry to measure levels SIINFEKL peptide on the cell surface. N=3. Student's t-test.

(*Lag3)* (**Figure 3.7.D**). Consistent with these findings, levels of IFN-γ were elevated in the media of BALB/c splenocytes co-cultured with SLR20-transfected 4T1 cells, as measured by an enzyme linked immunosorbant assay (ELISA)(**Figure 3.7.E**).

RIG-I activation stimulates anti-mammary tumor immunity *in vivo*

While these and previous results suggest that RIG-I signaling within the TME might acutely boost T-cell activity, the long-term effects of T-cell grooming by RIG-I remain unclear. To test this idea further, we used a modified vaccination approach, in which 4T1 cell lysates (generated by freeze-thaw) were delivered intramuscularly to tumor naïve Balb/C mice in combination with either SLR20 (1 mg/kg) or OH-SLR20. On day 16, anti-tumor activity of 4T1 splenocytes was assessed by co-culturing splenocytes with 4TI cells for 2 hours then measuring tumor cell lysis (**Figure 3.8.A**). Notably, lysis of 4T1 cells co-cultured with splenocytes from mice immunized with adjuvant SLR20 was nearly 40% higher than what was seen using splenocytes from control mice treated with OH-SLR20 (**Figure 3.9.A**). However, adjuvant SLR20 did not affect the proportions of splenic T-cell populations, including CD8+ T-cells, CD4+ T-cells, and T_{Reg}s (CD4+FoxP3+) (**Figure 3.9.B** and **Figures 3.8.B-D**).

We repeated this vaccination protocol, treating mice intramuscularly with 4T1 lysates, in combination with SLR20 (or OH-SLR20) on day 0, followed by orthotopic injection of live 4T1 mammary tumor cells on day 8 (**Figure 3.10.A**). In both groups, tumors formed in 100% of mice by day 14 (6 days after orthotopic injection of live tumor cells, N = 10). Tumor volume on day 16 was similar in mice pre-treated with saline, with 4T1 lysates plus saline, and 4T1 lysates plus OH-SLR20 (**Figure 3.10.B**). However,

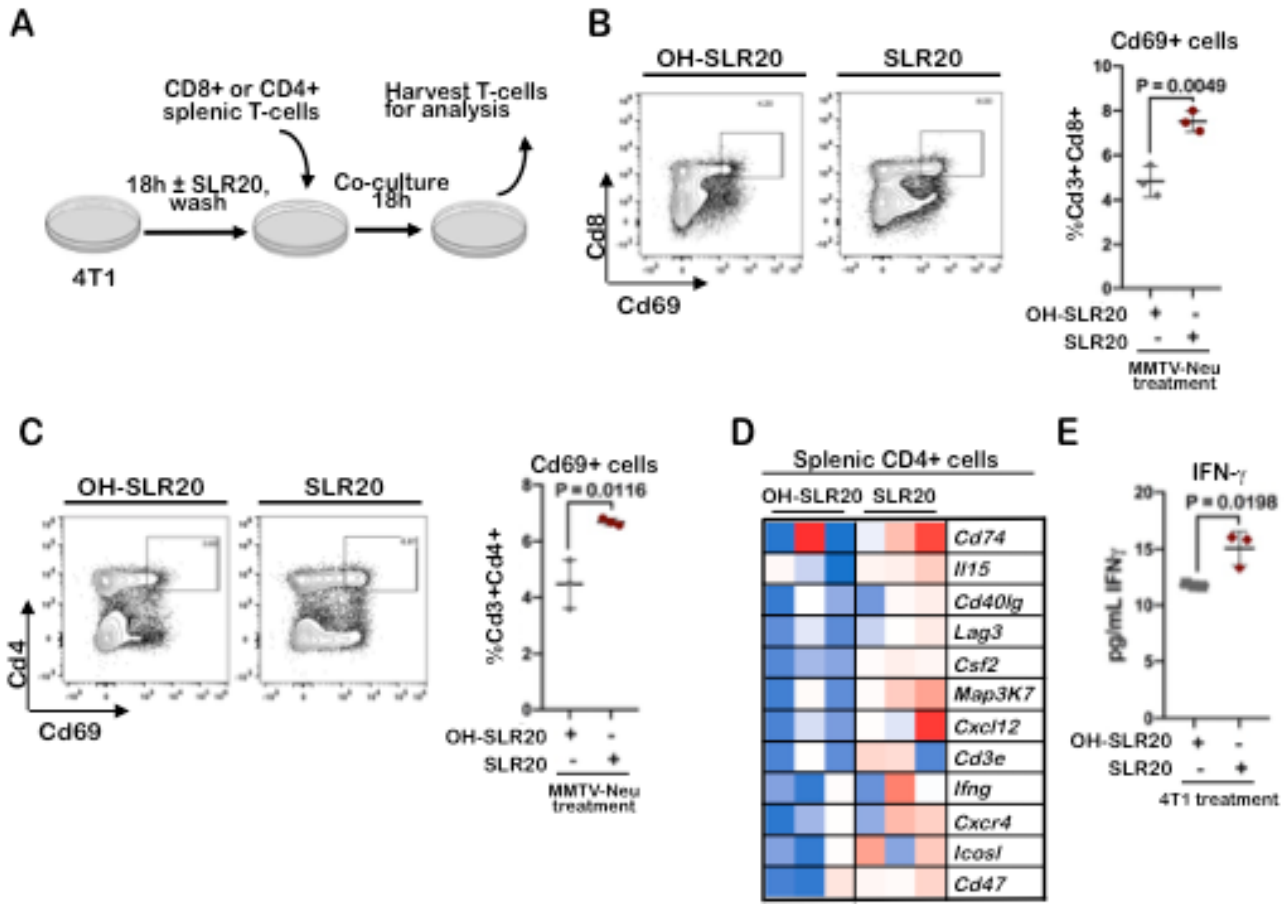

Figure 3.7 RIG-I signaling in breast cancer cells induces markers of T-cell activation.
A. Schematic of the experimental model used to measure the T-lymphocyte activation following co-culture with SLR20 or OH-SLR20 treated breast cancer cells. B-C. 18 hours after co-culture with treated breast cancer cells, $CD8^+$ and $CD4^+$ T-cells were assessed by flow cytometry to measure levels of activation marker CD69 on the cell surface. N=3. Student's t-test. D. 18 hours after effector $CD4^+$ T-cells were incubated in media conditioned by SLR20 or OH-SLR20 treated breast cancer cells, RNA was collected and assessed for expression of genes associated with T-cell activation (RT^2 Profiler PCR Array). Relative gene-expression values were calculated using the ddCq method, correcting for expression of *GAPDH*, and are shown as expression relative to the average value for each gene in OH-SLR20-transfected cells, as shown in the heat map. E. 18 hours after splenocytes were co-cultured with SLR20 or OH-SLR20 treated breast cancer cells, culture media was removed analyzed by ELISA to measure IFN-γ. N = 3. Student's t-test.

tumor volume was diminished in mice pre-treated with 4T1 lysates combined with SLR20 to less than half of what was measured in other treatment groups. Importantly, IHC analysis of tumor collected on day 16 (16 days after vaccination) revealed robustly increased tumor infiltration by $CD3^+$ cells in the tumors of mice immunized with SLR20 as the adjuvant (**Figure 3.10.C**). In contrast, tumors collected from mice vaccinated with saline or with OH-SLR20 as the adjuvant displayed no change in the burden of CD3+ TILs as compared to tumors grown in vehicle treated mice. These findings suggest that RIG-I signaling in the tumor microenvironment indirectly grooms T-cell phenotype and activity, enhancing T-cell function in the context of breast cancers.

Discussion

Studies of RIG-I activation in the cancer setting have typically focused on mechanisms that mediate anti-tumor innate immunity. Here, we present data illustrating the importance of T-cell mediated responses that occur in response to RIG-I activation. Using a synthetic RIG-I agonist, we demonstrated that RIG-I signaling coordinately upregulates cytotoxic FasL and Fas receptor in T-cells and tumor cells, respectively, to increase local T cell-mediated tumor cell death. Tumor cell RIG-I signaling increased MHC-I expression and antigen presentation by the tumor cells, while at the same time, drove effector T-cell activity. Using a modified tumor vaccination approach, we found a sustained impact of RIG-I signaling on T-cells that increased T-cell recruitment to subsequent tumors and reduced subsequent tumor growth. Although previous studies by several groups have established that RIG-I activated tumor cells can amplify anti-tumor innate immunity by increasing natural killer cell activity, and enhancing DC activity

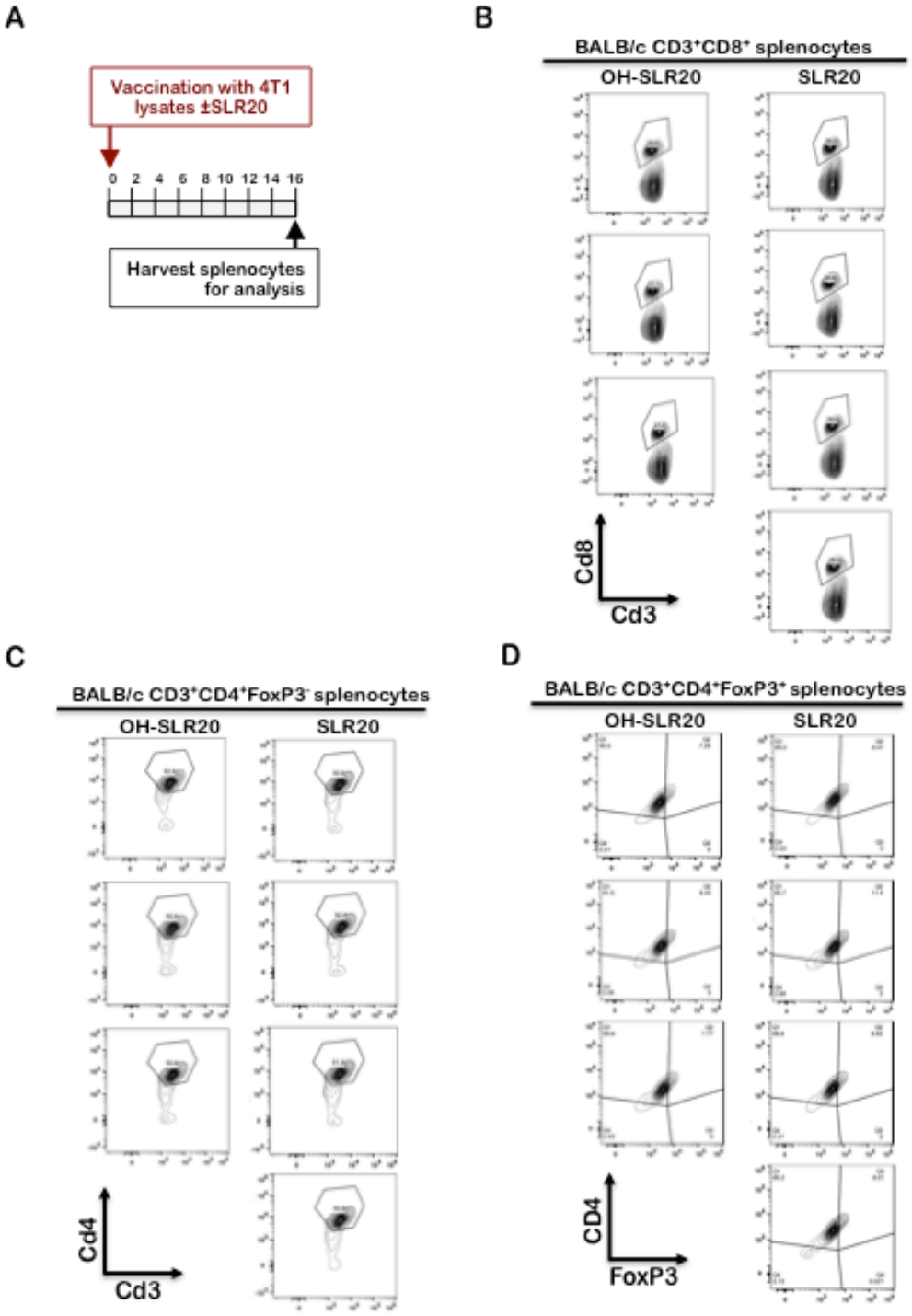

Figure 3.8 SLR20 Immunization does not alter splenic lymphocyte populations. A. Schematic of the experimental model used to measure splenocyte cytotoxicity analyzed in Figure 6A. B-D. 16 days after immunization, splenocytes were removed and assessed by flow cytometry to measure percentages of $CD8^+$ and $CD4^+$ effector T-cells and T-regulatory cells. N=3-4. Student's t-test.

(32, 117). Herein, we show that RIG-I signaling in tumor cells can promote certain aspects of T-cell mediated immunity.

We previously reported in mouse models of breast cancer that therapeutic delivery of a RIG-I agonist decreased tumor growth in vivo, due to tumor cell intrinsic apoptosis and pyroptosis. RIG-I signaling also resulted in robust expression of pro-inflammatory cytokines and increased recruitment of T-lymphocytes to the TME, suggesting that some tumor cells may be dying as a result of T-cells. To study the potential role of T-cells in treatment response to RIG-I agonists, we used a modified vaccination approach. Tumor challenge experiments showed that T-cell recruitment to tumors in vivo, and anti-tumor cytotoxic activity in cell culture, were amplified in mice pre-treated with a combination of RIG-I agonist and tumor lysate. These findings are consistent with previous studies showing that T-cell effector activity is increased following vaccination with a tumor antigen in combination with the MDA5/TLR3 dual agonist, poly-ICLC (89). These results suggest that RIG-I signaling augments adaptive immune responses against breast cancer cells.

A recent report identified $CD8^+$ and $CD4^+$ T-cells in the breast TME as largely exhausted with limited effector activity (113). Here we demonstrate that RIG-I agonist treated breast tumor cells promote an activated phenotype for effector T-cells. Thus, agonists of RIG-I may groom lymphocytes in the breast TME towards improved effector activity. Our study is consistent with a previous finding that Fas receptor and MHC-I are upregulated pancreatic cancer cells treated with a RIG-I agonist (32). In breast cancer cells, we showed that this effect is RIG-I dependent and also occurs *in vivo*, leading to

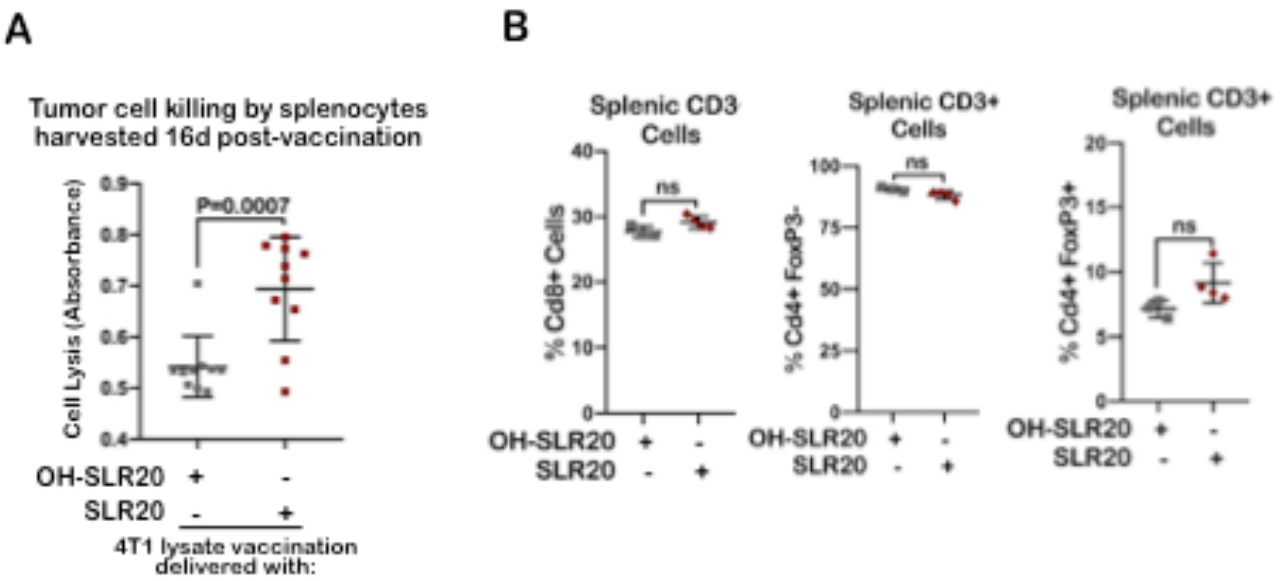

Figure 3.9 RIG-I signaling in immunization promotes lymphocyte killing. A. 16 days after immunization, splenocytes were removed and co-cultured with breast cancer cells for 2 hours. Cell lysis was quantified using a cytotoxicity assay that measures the release of LDH into the culture media. N = 10. Midlines are the average ±SD. Student's t-test. B. 16 days after immunization, splenocytes were removed and assessed by flow cytometry to measure percentages of $CD8^+$ and $CD4^+$ effector T-cells and T-regulatory cells. N=3-4. Student's t-test.

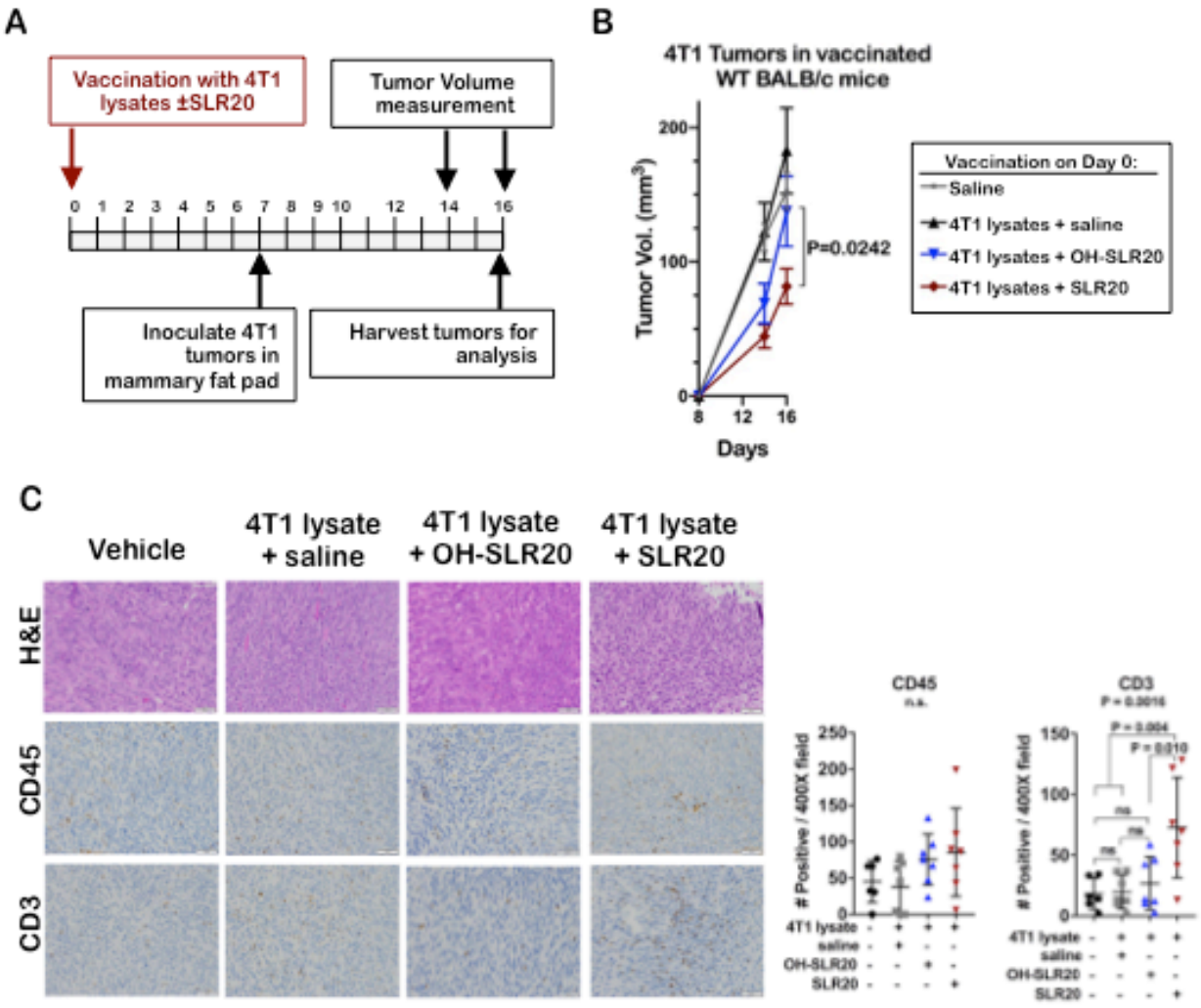

Figure 3.10 RIG-I signaling stimulates anti-mammary tumor immunity *in vivo*. A. Schematic of the experimental model used to measure post-vaccination tumor growth in BALB/c mice. B. Tumor volume was measured 14 and 16 days after vaccination. N = 9-10 per group. C. Histologic analysis of tumor sections using IHC. Representative images are shown. The number of CD45+ and CD3+ cells per 400× field was quantitated. Each point represents the average of three random fields per sample, N = 6-7. Midlines show average (±SD). Student's t-test.

increased recognition and killing of tumor cells in T-lymphocyte and breast cancer cell co-cultures.

In conclusion, we have demonstrated that RIG-I activation in breast cancer cells can promote T-lymphocyte activation and tumor cell targeting machinery, such as Fas receptor, Fas ligand and MHC-I. Moreover, we discovered that RIG-I signaling indirectly boosts T-cell mediated killing of breast cancer cells, improves T-cell recruitment to tumors, and decreases tumor growth through multiple mechanisms, including those that are tumor intrinsic and those that rely on innate and adaptive immunity. Overall, these findings warrant further studies of RIG-I agonists as a strategy to enhance the TME of immunologically cold tumors towards a more favorable phenotype.

CHAPTER IV

CONCLUSIONS AND FUTURE DIRECTIONS

RIG-I signaling and cell death

Investigating the molecular interactions and signaling of RIG-I like receptors (RLRs) in cancer is still a fairly recent undertaking, with most studies occurring within the past decade. The vast majority of research examining therapeutic RLR activation in cancer has concentrated on mechanisms that are involved in RLR-activated cell death, with particular focus on therapies targeting RIG-I and MDA5. Less attention has been given to RIG-I signaling's effect on the stromal and immune compartments in the tumor microenvironment (TME), an equally important component of RIG-I's therapeutic benefit. To date, there is no consensus on how RIG-I activates cell death in tumor cells. Different reports have presented evidence to support RIG-I activated cell death's dependence on a number of different pathways, including intrinsic (mitochondrial and caspase-9 dependent) and extrinsic (e.g. TRAIL, TNF, and FAS) apoptosis, LC3 dependent autophagy, MAPK inhibition, and inhibition of Akt/mTORC signaling (27, 32, 77, 114, 118-120). These studies exploring RIG-I mediated cell death span a diverse array of cancers, which suggests that RIG-I's activation of cell death may be nuanced, depending on the genetic and molecular attributes that are present within a particular malignancy.

In our study analyzing RIG-I activation in breast cancer, we found that RIG-I signaling an inflammatory type of programmed cell death called pyroptosis, which was previously unexplored in studies examining RIG-I agonists in cancer. Pyroptosis is an

inflammasome dependent form of cell death, which can be signaled by the formation of the RIG-I inflammasome (RIG-I/ASC) following RIG-I activation. In breast cancer, downstream effectors of the pyroptosis pathway were upregulated and activated following RIG-I agonist treatment, and assay markers of cell death (Annexin V and propidium iodide staining) were decreased upon inhibition of caspase-1, a pyroptotic activating caspase. Additionally, we found that apoptosis was also activated in breast cancer cells following RIG-I agonist treatment. Extrinsic apoptotic signaling factors (e.g. TNF, TRAIL, FAS) were increased and Annexin V staining was decreased upon inhibition of the extrinsic apoptotic signaling protein caspase-10. We did not investigate if pyroptosis was the predominant form of cell death, or if pyroptosis precedes apoptosis following RIG-I activation in breast cancer. It is possible that both occur simultaneously as it has been previously shown that RIG-I inflammasome formation and RIG-I/MAVS signaling are molecularly independent processes (72-73).

It is clear that more studies are needed to resolve the mechanisms behind RIG-I activated cell death in cancer cells. It is possible that the genetic landscape and molecular interactions existing within in a particular cancer may influence which cell death pathways are activated following RIG-I agonist treatment. Previous work identifying RIG-I complexes, e.g. RIG-I/ caspase-8 and RIG-I/ASC (72-73), gave mechanistic insight into pathways that were elicited to enact tumor cell death during RIG-I activation. One approach to further these studies would be to identify the RIG-I ‘interactome’, or the protein-protein interactions that occur following RIG-I activation, which may vary in different cancers.

It is also possible that RIG-I activation, when it is non-canonical, could signal alternative pathways to activate cell death in cancer. Depending on its localization, RIG-I has been shown to activate the transcription of an alternative set of cytokines, e.g. type III interferons (IFNs), when it is bound to MAVS on the surface of peroxisomes as opposed to MAVS on mitochondria (121, 127). Peroxisomal RIG-I activation, which is IRF1-mediated, and mitochondrial RIG-I activation, with is IRF3-mediated, work in tandem with one another to amplify the innate immune response, each one inducing its own unique troupe of inflammatory cytokines. RIG-I signaling from peroxisomes delivers a shorter, but rapid, immune response following RIG-I activation, while RIG-I mitochondrial signaling is more robust and long-term (127). This is one example of how alternative modes of RIG-I activation can preferentially activate different signaling pathways. Potentially, this phenomenon could be exploited, therapeutically, by designing RIG-I agonists who target the mode of activation that delivers the best therapeutic benefit.

Signaling crosstalk between RLR receptors has been shown to affect how RIG-I becomes activated. LGP2, the least studied RLR, negatively regulates RIG-I activation by blocking TRIM25-mediated polyubiquitylation of RIG-I (122). In our study on RIG-I activation in breast cancer, we analyzed genetic alterations in RIG-I via TCGA and found that only ~1.1% of breast cancers incurred genetic changes in the RIG-I gene *DDX58* (**Figure 2.2**)(114*)*, suggesting that therapeutically targeting RIG-I in breast cancers could be widely applicable. It is possible that genetic alterations in newly discovered negative regulators of RIG-I, e.g. LGP2, could alter the efficacy of RIG-I

agonists in certain cancers, indicating a need for more investigation of molecular interactions that could disrupt RIG-I signaling.

Currently, there is only one study that has explored whether RIG-I activated cell death is tumor cell specific (77). To our knowledge, RIG-I is globally expressed in every cell type, yet the mechanism behind RIG-I activated cell death has only been investigated in cancer cells. A study analyzing this topic in prostate cancer, demonstrated that RIG-I activation preferentially signaled cell death in prostate cancer cells, and did not signal cell death in non-malignant prostate cells (77). No mechanistic explanation for this result was presented in the study. It is possible that genetic alterations in certain cancers may assign some specificity in targeting RIG-I, but to date, this hypothesis has not been explored, and no study has analyzed how the genetic profile (e.g. amplification of negative regulators of RIG-I signaling, or nonsense mutations in RIG-I signaling partners such as MAVS) of a tumor can affect the therapeutic efficacy of a RIG-I agonist. Moreover, RIG-I activated cell death has not been reported in certain types of immune cells like natural killer cells (NKs) or T-lymphocytes, suggesting that there are cell intrinsic mechanisms, yet to be uncovered, which dictate the capabilities of RIG-I to signal cell death in specific cell populations.

RIG-I signaling and the tumor microenvironment

Aside from activating cell death, RIG-I like receptors (RLRs) can also signal an innate immune response in the tumor microenvironment (TME). Previous to our work, only two studies had investigated, in depth, the effects of RLR activation on tumoral innate immune populations, e.g. macrophages, dendritic cells (DCs), and natural killer

cells (NKs) (32, 117). Both reports presented evidence that RLR ligands and RLR activating viruses could increase classical activation and the expression of co-stimulatory molecules (e.g. CD80, CD86) in antigen presenting cells (APCs) either by direct treatment with an RLR ligand, or in co-culture with RLR activated tumor cells (32, 117). APCs co-cultured with RLR activated tumor cells were also shown to exhibit increased MHC-I and MHC-II expression and antigen presentation, as well as increased phagocytosis (117).

Previously, NK cells were the only lymphocyte population that had been examined, at length, in the context of therapeutic RLR activation in cancer. The majority of this work was generated in one study, which analyzed the effects RIG-I activation on NKs, DCs, and macrophages in ovarian cancer. This study revealed that NK cells, in co-culture with RLR activated tumor cells, exhibited increased markers of activation and degranulation (e.g. CD107a, IFN-γ), while also showing increased cytolytic activity against RLR activated ovarian cancer cells (117). Outside of these two studies, most reports investigating RLR activation in cancer focused solely on RIG-I's ability to activate cell death, and even within studies exploring RIG-I activation in the TME, extensive focus was given to how RLRs activate innate immunity with no analysis of how RLRs affect adaptive immunity in the cancer setting. Furthermore, neither of these studies specifically examine the activation of the RIG-I, as they both relied on MDA5 ligand, poly(I:C), in the majority of their studies on anti-tumor immunity.

The two aforementioned studies observed increases in APC activation in co-cultures with RLR activated tumor cells (32, 117). We observed similar effects in breast

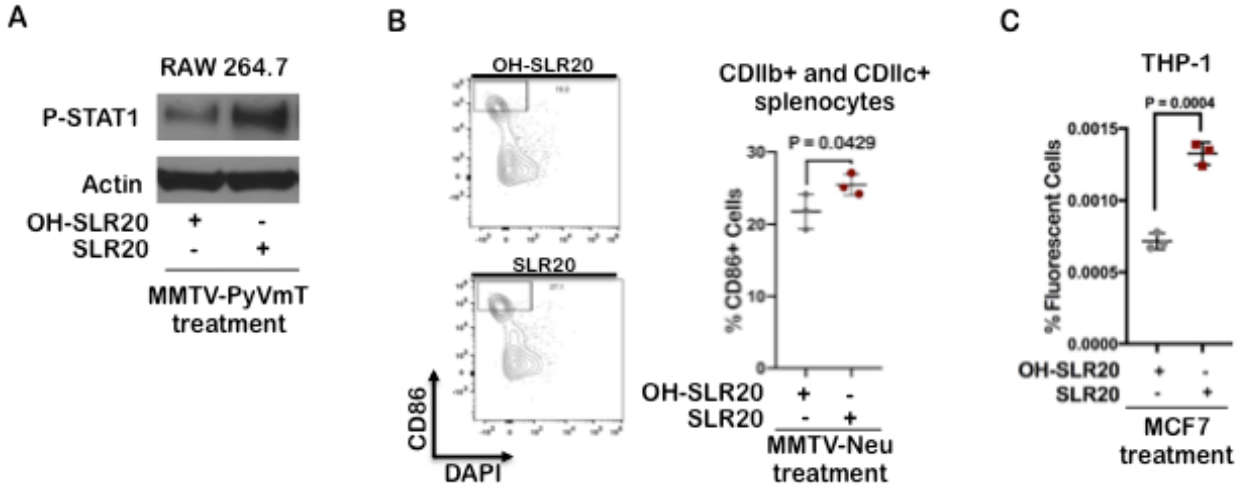

Figure 4.1 RIG-I signaling in breast cancer cells increases antigen presenting cell activation A. 18 hours after effector RAW 264.7 cells were incubated in media conditioned by SLR20 or OH-SLR20 treated PyVmT cells, RAW 264.7 cells were lysed and assayed by Western analysis. B. flow cytometry analysis of splenocytes 18 hours after co-culture with MMTV-Neu cells. N = 3. Midlines are the average ±SD. Student's t-test. C. MCF7 cells were transfected for 18 hours then stained (IncuCyte Phagocytosis, Essen Bioscience) and co-cultured with THP-1 cells for 24 hours. Phagocytosed MCF7 cells were analyzed via microscopy. N=3. Student's t-test.

cancer, using an agonist that specifically activates RIG-I, where we saw increased STAT1 phosphorylation (**Figure 4.1.A**) and increased expression of co-stimulatory molecule CD86 in antigen presenting monocytes either in co-culture with or in media conditioned by RIG-I activated breast cancer cells (**Figure 4.1.B**). Notably, APCs co-cultured with RIG-I activated breast cancer cells also exhibited increased phagocytic activity (**Figure 4.1.C**).

In our study, we also found that tumor infiltrating lymphocytes were increased following treatment with a RIG-I agonist. We attributed this increase in tumor infiltrating lymphocytes (TILs) to the elevated secretion of lymphocytic chemokines (e.g. CXCL11, RANTES) in breast cancer cells treated with a RIG-I agonist. RIG-I activation in breast cancer cells signaled increased T-cell activation, increased expression of molecules (e.g. FAS, FASL, and MHC-I) that mediate cytotoxic T-lymphocyte (CTL) killing, and increased CTL targeting of RIG-I agonist treated breast cancer cells. In our study, combinatorial treatment with breast cancer lysates and a RIG-I agonist resulted in decreased tumor growth and increased tumor reactive lymphocytes, demonstrating RIG-I's ability to amplify anti-tumor adaptive immune responses. These studies were the first to illuminate the effects of RIG-I agonist treatment on effector T-cell mediated responses against breast cancer cells and examine how RIG-I activation can potentially alter anti-tumor adaptive immunity.

While we have shown that RIG-I agonists have the ability to support effector T-cell responses in the TME, there is no guarantee that immunosuppressive T-regulatory cells (Tregs) will not disrupt effector T-cell activation and tumor cell killing in RIG-I activated tumors. T-regulatory cells have been shown, in some cancers, to be pro-

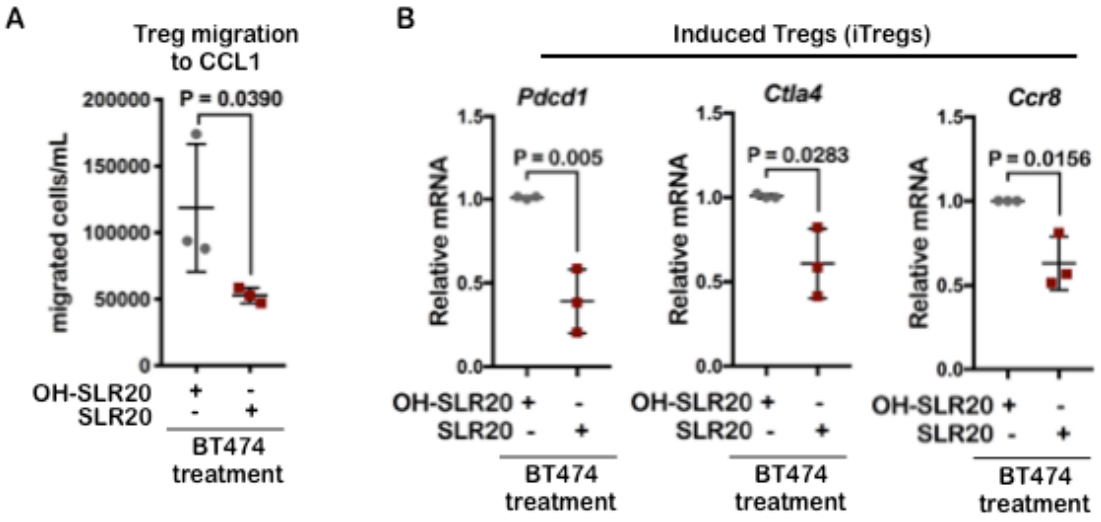

Figure 4.2 RIG-I signaling in breast cancer decreases Treg migration and differentiation A. BT474 and cells were treated with SLR20 or OH-SLR20 and cultured for 40 hours. Media from these cells was removed, filtered (0.2um) and added to freshly isolated, mouse splenic naïve $CD4^+$ T-cells (Miltenyi Biotec kit). Naïve $CD4^+$ T-cells were activated with plate bound anti-CD3e and anti-CD28 (BioXcell, 5ug/mL each) and media was supplemented with TGF beta (R&D, 5ng/mL) to induce Treg differentiation (iTreg). T-cells were treated with conditioned media for 5 days then collected for RT-qPCR analysis of Pdcd1, Ctla4, and Ccr8. N = 3. Midlines are the average ±SD. Student's t-test. B. Conditioned media, prepared as mentioned in A, was added to freshly isolated mouse Tregs (Miltenyi Biotec kit) then Tregs were plated in the upper chamber of 24-well 8um transwell plates (Corning) at 200,000 cells per well. Migration media consisted of RPMI/ 0.1% BSA/ CCL1 (R&D, 100ng/mL). Cells were incubated for 1.5hrs and cells in the migration media were counted using a hemocytometer.

tumorigenic in several ways, such as suppressing effector T-cell differentiation and serving as negative regulators for effector T-cell activation and killing. Presently, only one study has analyzed the effects of RLR activation on Tregs, but it mainly focused on direct RLR activation in Tregs, without exploring how Tregs were affected by RLR activation in cancer cells (123). Here, RLR activated Tregs exhibited reduced suppression of naïve T-cell differentiation into mature effector T-cells. Further, RLR activation was shown to inhibit TGF-β signaling in Tregs and disrupt Treg migration into tumors (123). The effects of RLR activation on Tregs in the TME is an area that continues to remain understudied, specifically in regard to RIG-I agonists. In breast cancer, we have some data showing that RIG-I activation in cancer cells can limit Treg migration toward a known tumoral Treg chemoattractant, CCL1 (**Figure 4.2.A**). Additionally, we have observed that Treg differentiation is disrupted when naïve T-cells are cultured in media conditioned by RIG-I agonist treated breast cancer cells, showing decreased markers of Treg maturation, e.g. PD-1, CTLA-4, and CCR8 (**Figure 4.2.B**). These studies suggest that RIG-I agonist can potentially reverse Treg mediated suppression of effector T-cells, yet more investigation is warranted to analyze mechanistically how RIG-I activation in tumors can alter Treg migration and activity in the tumor microenvironment.

When examining leukocyte infiltration in mammary tumors treated with a RIG-I ligand, we observed an increase in F4/80^{+} tumoral macrophages (114). Prior to our own studies, the impact of RIG-I signaling on tumor macrophage populations had not been reported. Tumor macrophages are often pro-tumorigenic in breast cancers, correlating with decreased overall survival for patients with cancer, and decreased response of

tumors to treatments (124-125). The pro-tumorigenic phenotype of tumor macrophages is due largely to their expression of immunosuppressive cytokines (e.g., TGF-β), diminished expression of antigen presenting machinery (MHC-I and II) and heightened expression of immune checkpoint proteins (PD-L1) (125-126). However, tumor macrophages could potentially be reprogrammed to express pro-inflammatory cytokines (IFN-beta), to upregulate antigen presenting machinery, and to upregulate pro-stimulatory molecules (e.g., CD86), given the plasticity of macrophage phenotype. We did not specifically profile tumor macrophage populations for their specific phenotype, or how RIG-I signaling might alter the phenotype from pro-tumorigenic to pro-inflammatory. Therefore, the field would greatly benefit from detailed studies examining the impact of RIG-I signaling on tumor macrophage phenotypes. However, our studies were the first to demonstrate that treatment of tumors in vivo with a RIG-I agonist resulted in potent recruitment of F4/80+ macrophages to tumors (**Figures 2.9** and **2.10**) (114)

Previous studies have examined the impact of the RLR agonist poly (I:C) on splenic dendritic cells (DCs) in tumor-bearing mice (32). These studies showed that, compared to mice treated with vehicle, poly(I:C) treated mice had increased expression of CD86 (co-stimulatory molecule) and MHC-II (antigen presenting and T-cell priming machinery) (32). We have not examined if the RIG-I agonist SLR20, like the RLR agonist poly (I:C), drives DC polarization towards this pro-inflammatory phenotype. It is possible that the increased responsiveness of T-cells to tumors that we observed in SLR20-treated mice is influenced to some degree by DCs, a professional antigen presenting cell that potently grooms T-cell adaptive immunity. Following immunization with tumor lysate, using SLR20 as an adjuvant, we saw reduced tumor growth and

increased TILs. Previous studies analyzing co-cultures of poly(I:C) treated DCs with naïve T-cells, reported increased DC-mediated T-cell priming (32). One approach to investigate if this occurs in vivo is to profile the phenotype of DCs within RIG-I agonist treated tumors and proximal lymph nodes to analyze changes in the expression of co-stimulatory molecules, MHC-I and –II, and type I IFN. It is possible that DC activation could be contributing to T-cell responses observed in our immunization studies. This hypothesis could be measured using an antigen specific system, e.g. ovalbumin (OVA)/OT-I. T-cell proliferation following RIG-I agonist treatment could be measured by performing an adopted transfer with labeled naïve T-cells from a donor OT-I mouse into RIG-I agonist treated mice bearing OVA expressing mammary tumors. Following depletion of DCs using targeted antibodies (e.g. anti-Cd11, -Cdllc, -MHC-II) T-cell proliferation could be measured, to see if a RIG-I agonist's effects on T-cell priming are DC specific.

Many studies have reported on the therapeutic benefit of RLR agonists as a monotherapy, but, previous to our study, none had explored the use of a RIG-I agonist in combined treatment, particularly with an immune-checkpoint inhibitor (ICI). ICIs have achieved success in cancers like melanoma and lung, but this has not been the case in breast cancers. Compared to patients with HER2 amplified (HER2+) and triple-negative breast cancer (TNBC), breast cancer patients who are estrogen receptor positive (ER+) had poorer responses (99, 128-130). It has been frequently reported that TNBCs, compared to other breast cancer subtypes, harbor more tumor infiltrating lymphocytes (TILs) and a higher mutational burden, two factors, which potentially lead to a tumor microenvironment (TME) that is more immunogenic and more pro-inflammatory (131-

132). Accordingly, TNBC is also more likely to express programmed death ligand 1 (PD-L1), a predictive marker for therapeutic efficacy in ICIs that target PD-L1 and programmed cell death protein 1 (PD-1) (133).

Based on our findings, we believe that therapeutic RIG-I activation in the mammary TME can create the conditions needed to overcome the poorly immunogenic phenotype found in many breast cancers. Our data demonstrated the use of a RIG-I agonist as a therapeutic 'switch' to reverse an immunologically silent breast TME, inhibit tumor growth, and increase therapeutic response to an immune checkpoint inhibitor (anti-PD-L1) (**Figures 2.4** and **2.9**) (114). One limitation of our study is that we only utilized one model [4T1 tumors (TNBC) in Balb/c mice]. Analyzing these effects in additional breast cancer models, with a longer treatment window, would further expand the scope of our investigation. This includes conducting studies in mouse models of other breast cancer subtypes, eg. MMTV-Neu tumors (HER2+), as well as immune-competent humanized mice that harbor tumors derived from human breast cancer cells. Examining how other ICIs, e.g. therapies that target PD-1, CTLA-4 or LAG-3, compare in combinatorial RIG-I agonist treatment is needed to confirm the consistency and specificity of our observations. Repeating these studies in RIG-I deficient tumors would confirm whether or not the effects observed in our study are RIG-I dependent.

We did not analyze the effect of combinatorial ICI and RIG-I agonist therapy on breast cancer metastasis. However, we did observe that RIG-I agonist treatment, alone, resulted in decreased tumor cell metastasis to the lungs. One limitation in this study lies in our delivery mechanism. SLR20 was injected intratumorally using a nanoparticle, therefore, it is possible that our observations are likely the result of decreased growth in

the primary tumor, with no direct affect on disseminated disease. In order to assess how a RIG-I agonist directly affects metastasized cells, systemic delivery methods for RIG-I agonist need to researched and developed for cancer treatment. This is evident, even in clinical trials assessing RIG-I agonist in cancer patients, where these agonists are delivered intratumorally using a commercial liposomal delivery reagent (NCT03065023 and NCT03739138). Both RIG-I agonist trials require the tumor to be “injectable” as eligibility criteria, which could potentially limit what cancers are investigated in these studies and also limit patient recruitment. Using a systemic delivery method, the effects of a RIG-I agonist on metastasis could be analyzed in other metastasis models for breast cancer, e.g. tail-vein injected tumor cells or breast cancer metastasis models, e.g. MMTV-PyMT mice.

Several cancer vaccine studies have shown an increase in therapeutic efficacy when using MDA5 ligand, poly-ICLC, as a vaccine adjuvant (79-82, 89). Our study in breast cancer revealed that a RIG-I agonist can augment the effects of immunization, showing increased tumor cell killing, ex vivo, in splenic lymphocytes isolated from mice immunized with a RIG-I agonist. In these same mice, we also observed decreased tumor growth and an influx of TILs. One of the major limitations of our study is our use of tumor lysate as the “cancer antigen.” Repeating these studies using an antigen-specific system, e.g. the ovalbumin (OVA)/OT-I system, would better support our observations and confirm the legitimacy our results. Additionally, our study would be more clinically relevant through the use of a known breast cancer antigen, e.g. HER2, or by taking a NeoVax approach, by profiling and synthesizing potential neoantigens that exists in breast cancers to be used in combination with a RIG-I agonist (134-135).

In regards to our immunization study, additional further analyses to determine if our effect is T-cell dependent must be completed. This can be achieved by depleting specific populations of lymphocytes, e.g. CD4+ or CD8+ effector T-cells, using targeted antibodies, or by incorporating T-cell deficient mice into these studies. It is also possible that humoral responses from B-cells within the tumor or proximal lymph nodes may potentially contribute to our observations. In an antigen specific model, e.g. OVA/OT-I, B-cell humoral responses can be assessed by isolating antibodies from the serum of immunized OT-I mice, and assaying these antibodies using an ELISA with plates coated with OVA antigen. To further investigate if B-cells are influenced by RIG-I activation, tumor B-cells can be assessed for activation markers, e.g. CD95 (FAS) and CD27.

Overall, immunotherapies, which rely on lymphocyte-mediated responses to administer an effect (e.g. ICIs and cancer vaccines) stand to gain from adjuvant use of a RIG-I agonist. Further studies are needed to fully resolve the mechanisms of RIG-I activated immunity in the TME. Future investigation should carefully assess the roles of intratumoral myeloid and lymphocyte populations in mediating anti-tumor immunity following RIG-I activation *in vivo*.

Concluding remarks

The data reported in this dissertation includes the first studies looking at therapeutic activation of the RLR, RIG-I, in breast cancer. Here, we reveal how RIG-I signals cell death in breast cancer and demonstrate RIG-I's anti-tumor effects including tumor growth inhibition, reduced metastasis, increased anti-tumor innate and adaptive

immune responses, and enhanced therapeutic efficacy of an ICI and cancer vaccine. Future studies are needed to further resolve how these effects are carried out mechanistically in breast and other cancers. Research advances in RIG-I agonist delivery and design can potentially move this therapy forward as a clinical option to promote anti-tumor immune responses in cancers that are immunosuppressed or immunologically silent.

REFERENCES

1. Pardoll DM. The blockade of immune checkpoints in cancer immunotherapy. Nat Rev Cancer. 2012;12:252–264.

2. Hodi FS, O'Day SJ, McDermott DF, Weber RW, Sosman JA, Haanen JB, Gonzalez R, Robert C, Schadendorf D, Hassel JC, Akerley W, van den Eertwegh AJ, Lutzky J, et al. Improved survival with ipilimumab in patients with metastatic melanoma. N Engl J Med. 2010;363:711–723.

3. Ellis PM, Vella ET, Ung YC. Immune Checkpoint Inhibitors for Patients With Advanced Non-Small-Cell Lung Cancer: A Systematic Review. Clin Lung Cancer. 2017;18:444–459 e441.

4. Luen S, Virassamy B, Savas P, Salgado R, Loi S. The genomic landscape of breast cancer and its interaction with host immunity. Breast. 2016;29:241–250.

5. Marincola FM, Jaffee EM, Hicklin DJ, Ferrone S. Escape of human solid tumors from T-cell recognition: molecular mechanisms and functional significance. Adv Immunol. 2000;74:181–273.

6. Garrido F, Algarra I. MHC antigens and tumor escape from immune surveillance. Adv Cancer Res. 2001;83:117–158.

7. Gatalica Z, Snyder C, Maney T, Ghazalpour A, Holterman DA, Xiao N, Overberg P, Rose I, Basu GD, Vranic S, Lynch HT, Von Hoff DD, Hamid O. Programmed cell death 1 (PD-1) and its ligand (PD-L1) in common cancers and their correlation with molecular cancer type. Cancer Epidemiol Biomarkers Prev. 2014;23:2965–2970.

8. Takeuchi O, Akira S. Pattern recognition receptors and inflammation. Cell. 2010;140:805–820.

9. Shalapour S, Karin M. Immunity, inflammation, and cancer: an eternal fight between good and evil. J Clin Invest. 2015;125:3347–3355.

10. Okamoto M, Tsukamoto H, Kouwaki T, Seya T, Oshiumi H. Recognition of Viral RNA by Pattern Recognition Receptors in the Induction of Innate Immunity and Excessive Inflammation During Respiratory Viral Infections. Viral Immunol. 2017;30:408–420.

11. Ishikawa H, Barber GN. STING is an endoplasmic reticulum adaptor that facilitates innate immune signalling. Nature. 2008;455:674–678.

12. Ishikawa H, Ma Z, Barber GN. STING regulates intracellular DNA-mediated, type I interferon-dependent innate immunity. Nature. 2009;461:788–792.

13. Chandra D, Quispe-Tintaya W, Jahangir A, Asafu-Adjei D, Ramos I, Sintim HO, Zhou J, Hayakawa Y, Karaolis DK, Gravekamp C. STING ligand c-di-GMP improves cancer vaccination against metastatic breast cancer. Cancer Immunol Res. 2014;2:901–910.

14. Li T, Cheng H, Yuan H, Xu Q, Shu C, Zhang Y, Xu P, Tan J, Rui Y, Li P, Tan X. Antitumor Activity of cGAMP via Stimulation of cGAS-cGAMP-STING-IRF3 Mediated Innate Immune Response. Sci Rep. 2016;6:19049.

15. Tang CH, Zundell JA, Ranatunga S, Lin C, Nefedova Y, Del Valle JR, Hu CC. Agonist-Mediated Activation of STING Induces Apoptosis in Malignant B Cells. Cancer Res. 2016;76:2137–2152.

16. Demaria O, De Gassart A, Coso S, Gestermann N, Di Domizio J, Flatz L, Gaide O, Michielin O, Hwu P, Petrova TV, Martinon F, Modlin RL, Speiser DE, Gilliet M. STING activation of tumor endothelial cells initiates spontaneous and therapeutic antitumor immunity. Proc Natl Acad Sci U S A. 2015;112:15408–15413.

17. Fu J, Kanne DB, Leong M, Glickman LH, McWhirter SM, Lemmens E, Mechette K, Leong JJ, Lauer P, Liu W, Sivick KE, Zeng Q, Soares KC, et al. STING agonist formulated cancer vaccines can cure established tumors resistant to PD-1 blockade. Sci Transl Med. 2015;7:283ra252.

18. Konno H, Yamauchi S, Berglund A, Putney RM, Mule JJ, Barber GN. Suppression of STING signaling through epigenetic silencing and missense mutation impedes DNA damage mediated cytokine production. Oncogene. 2018;37:2037–2051.

19. Xia T, Konno H, Ahn J, Barber GN. Deregulation of STING Signaling in Colorectal Carcinoma Constrains DNA Damage Responses and Correlates With Tumorigenesis. Cell Rep. 2016;14:282–297.

20. Pepin G, Gantier MP. cGAS-STING Activation in the Tumor Microenvironment and Its Role in Cancer Immunity. Adv Exp Med Biol. 2017;1024:175–194.

21. Yoneyama M, Kikuchi M, Natsukawa T, Shinobu N, Imaizumi T, Miyagishi M, Taira K, Akira S, Fujita T. The RNA helicase RIG-I has an essential function in double-stranded RNA-induced innate antiviral responses. Nat Immunol. 2004;5:730–737.

22. Loo YM, Gale M., Jr Immune signaling by RIG-I-like receptors. Immunity. 2011;34:680–692.

23. Goubau D, Schlee M, Deddouche S, Pruijssers AJ, Zillinger T, Goldeck M, Schuberth C, Van der Veen AG, Fujimura T, Rehwinkel J, Iskarpatyoti JA, Barchet W, Ludwig J, et al. Antiviral immunity via RIG-I-mediated recognition of RNA bearing 5′-diphosphates. Nature. 2014;514:372–375.

24. Hornung V, Ellegast J, Kim S, Brzozka K, Jung A, Kato H, Poeck H, Akira S, Conzelmann KK, Schlee M, Endres S, Hartmann G. 5′-Triphosphate RNA is the ligand for RIG-I. Science. 2006;314:994–997.

25. Linehan MM, Dickey TH, Molinari ES, Fitzgerald ME, Potapova O, Iwasaki A, Pyle AM. A minimal RNA ligand for potent RIG-I activation in living mice. Sci Adv. 2018;4:e1701854.

26. Schlee M, Roth A, Hornung V, Hagmann CA, Wimmenauer V, Barchet W, Coch C, Janke M, Mihailovic A, Wardle G, Juranek S, Kato H, Kawai T, et al. Recognition of 5′ triphosphate by RIG-I helicase requires short blunt double-stranded RNA as contained in panhandle of negative-strand virus. Immunity. 2009;31:25–34.

27. Besch R, Poeck H, Hohenauer T, Senft D, Hacker G, Berking C, Hornung V, Endres S, Ruzicka T, Rothenfusser S, Hartmann G. Proapoptotic signaling induced by RIG-I and MDA-5 results in type I interferon-independent apoptosis in human melanoma cells. J Clin Invest. 2009;119:2399–2411.

28. Liu LW, Nishikawa T, Kaneda Y. An RNA Molecule Derived From Sendai Virus DI Particles Induces Antitumor Immunity and Cancer Cell-selective Apoptosis. Mol Ther. 2016;24:135–145.

29. Rintahaka J, Wiik D, Kovanen PE, Alenius H, Matikainen S. Cytosolic antiviral RNA recognition pathway activates caspases 1 and 3. J Immunol. 2008;180:1749–1757.

30. Galluzzi L, Vitale I, Aaronson SA, Abrams JM, Adam D, Agostinis P, Alnemri ES, Altucci L, Amelio I, Andrews DW, Annicchiarico-Petruzzelli M, Antonov AV, Arama E, et al. Molecular mechanisms of cell death: recommendations of the Nomenclature Committee on Cell Death 2018. Cell Death Differ. 2018;25:486–541.

31. Ramos HJ, Gale M., Jr RIG-I like receptors and their signaling crosstalk in the regulation of antiviral immunity. Curr Opin Virol. 2011;1:167–176.

32. Duewell P, Steger A, Lohr H, Bourhis H, Hoelz H, Kirchleitner SV, Stieg MR, Grassmann S, Kobold S, Siveke JT, Endres S, Schnurr M. RIG-I-like helicases induce immunogenic cell death of pancreatic cancer cells and sensitize tumors toward killing by CD8(+) T cells. Cell Death Differ. 2014;21:1825–1837.

33. Glas M, Coch C, Trageser D, Dassler J, Simon M, Koch P, Mertens J, Quandel T, Gorris R, Reinartz R, Wieland A, Von Lehe M, Pusch A, et al. Targeting the cytosolic innate immune receptors RIG-I and MDA5 effectively counteracts cancer cell heterogeneity in glioblastoma. Stem Cells. 2013;31:1064–1074.

34. Poeck H, Besch R, Maihoefer C, Renn M, Tormo D, Morskaya SS, Kirschnek S, Gaffal E, Landsberg J, Hellmuth J, Schmidt A, Anz D, Bscheider M, et al. 5′-Triphosphate-siRNA: turning gene silencing and Rig-I activation against melanoma. Nat Med. 2008;14:1256–1263.

35. van den Boorn JG, Hartmann G. Turning tumors into vaccines: co-opting the innate immune system. Immunity. 2013;39:27–37.

36. Ellermeier J, Wei J, Duewell P, Hoves S, Stieg MR, Adunka T, Noerenberg D, Anders HJ, Mayr D, Poeck H, Hartmann G, Endres S, Schnurr M. Therapeutic efficacy of bifunctional siRNA combining TGF-beta1 silencing with RIG-I activation in pancreatic cancer. Cancer Res. 2013;73:1709–1720.

37. Pichlmair A, Schulz O, Tan CP, Naslund TI, Liljestrom P, Weber F, Reis e Sousa C. RIG-I-mediated antiviral responses to single-stranded RNA bearing 5′-phosphates. Science. 2006;314:997–1001.

38. Marques JT, Devosse T, Wang D, Zamanian-Daryoush M, Serbinowski P, Hartmann R, Fujita T, Behlke MA, Williams BR. A structural basis for discriminating between self and nonself double-stranded RNAs in mammalian cells. Nat Biotechnol. 2006;24:559–565.

39. Solis M, Nakhaei P, Jalalirad M, Lacoste J, Douville R, Arguello M, Zhao T, Laughrea M, Wainberg MA, Hiscott J. RIG-I-mediated antiviral signaling is inhibited in HIV-1 infection by a protease-mediated sequestration of RIG-I. J Virol. 2011;85:1224–1236.

40. Boelens MC, Wu TJ, Nabet BY, Xu B, Qiu Y, Yoon T, Azzam DJ, Twyman-Saint Victor C, Wiemann BZ, Ishwaran H, Ter Brugge PJ, Jonkers J, Slingerland J, Minn AJ. Exosome transfer from stromal to breast cancer cells regulates therapy resistance pathways. Cell. 2014;159:499–513.

41. Ranoa DR, Parekh AD, Pitroda SP, Huang X, Darga T, Wong AC, Huang L, Andrade J, Staley JP, Satoh T, Akira S, Weichselbaum RR, Khodarev NN. Cancer therapies activate RIG-I-like receptor pathway through endogenous non-coding RNAs. Oncotarget. 2016;7:26496–26515. doi: 10.18632/oncotarget.8420.

42. Zeng Y, Wang PH, Zhang M, Du JR. Aging-related renal injury and inflammation are associated with downregulation of Klotho and induction of RIG-I/NF-kappaB signaling pathway in senescence-accelerated mice. Aging Clin Exp Res. 2016;28:69–76.

43. Zhao L, Zhu J, Zhou H, Zhao Z, Zou Z, Liu X, Lin X, Zhang X, Deng X, Wang R, Chen H, Jin M. Identification of cellular microRNA-136 as a dual regulator of RIG-I-mediated innate immunity that antagonizes H5N1 IAV replication in A549 cells. Sci Rep. 2015;5:14991.

44. Karlsen TA, Brinchmann JE. Liposome delivery of microRNA-145 to mesenchymal stem cells leads to immunological off-target effects mediated by RIG-I. Mol Ther. 2013;21:1169–1181.

45. Barral PM, Sarkar D, Su ZZ, Barber GN, DeSalle R, Racaniello VR, Fisher PB. Functions of the cytoplasmic RNA sensors RIG-I and MDA-5: key regulators of innate immunity. Pharmacol Ther. 2009;124:219–234.

46. Bork P, Koonin EV. An expanding family of helicases within the 'DEAD/H' superfamily. Nucleic Acids Res. 1993;21:751–752.

47. Jankowsky E, Jankowsky A. The DExH/D protein family database. Nucleic Acids Res. 2000;28:333–334.

48. Saito T, Hirai R, Loo YM, Owen D, Johnson CL, Sinha SC, Akira S, Fujita T, Gale M., Jr Regulation of innate antiviral defenses through a shared repressor domain in RIG-I and LGP2. Proc Natl Acad Sci U S A. 2007;104:582–587.

49. Gack MU, Kirchhofer A, Shin YC, Inn KS, Liang C, Cui S, Myong S, Ha T, Hopfner KP, Jung JU. Roles of RIG-I N-terminal tandem CARD and splice variant in TRIM25-mediated antiviral signal transduction. Proc Natl Acad Sci U S A. 2008;105:16743–16748.

50. Gack MU, Shin YC, Joo CH, Urano T, Liang C, Sun L, Takeuchi O, Akira S, Chen Z, Inoue S, Jung JU. TRIM25 RING-finger E3 ubiquitin ligase is essential for RIG-I-mediated antiviral activity. Nature. 2007;446:916–920.

51. Gao D, Yang YK, Wang RP, Zhou X, Diao FC, Li MD, Zhai ZH, Jiang ZF, Chen DY. REUL is a novel E3 ubiquitin ligase and stimulator of retinoic-acid-inducible gene-I. PLoS One. 2009;4:e5760.

52. Oshiumi H, Matsumoto M, Hatakeyama S, Seya T. Riplet/RNF135, a RING finger protein, ubiquitinates RIG-I to promote interferon-beta induction during the early phase of viral infection. J Biol Chem. 2009;284:807–817.

53. Seth RB, Sun L, Ea CK, Chen ZJ. Identification and characterization of MAVS, a mitochondrial antiviral signaling protein that activates NF-kappaB and IRF 3. Cell. 2005;122:669–682.

54. Kawai T, Takahashi K, Sato S, Coban C, Kumar H, Kato H, Ishii KJ, Takeuchi O, Akira S. IPS-1, an adaptor triggering RIG-I- and Mda5-mediated type I interferon induction. Nat Immunol. 2005;6:981–988.

55. Meylan E, Curran J, Hofmann K, Moradpour D, Binder M, Bartenschlager R, Tschopp J. Cardif is an adaptor protein in the RIG-I antiviral pathway and is targeted by hepatitis C virus. Nature. 2005;437:1167–1172.

56. Matsuda A, Suzuki Y, Honda G, Muramatsu S, Matsuzaki O, Nagano Y, Doi T, Shimotohno K, Harada T, Nishida E, Hayashi H, Sugano S. Large-scale identification and characterization of human genes that activate NF-kappaB and MAPK signaling pathways. Oncogene. 2003;22:3307–3318.

57. Huang J, Liu T, Xu LG, Chen D, Zhai Z, Shu HB. SIKE is an IKK epsilon/TBK1-associated suppressor of TLR3- and virus-triggered IRF-3 activation pathways. EMBO J. 2005;24:4018–4028.

58. Chariot A, Leonardi A, Muller J, Bonif M, Brown K, Siebenlist U. Association of the adaptor TANK with the I kappa B kinase (IKK) regulator NEMO connects IKK complexes with IKK epsilon and TBK1 kinases. J Biol Chem. 2002;277:37029–37036.

59. O'Neill LA, Bowie AG. Sensing and signaling in antiviral innate immunity. Curr Biol. 2010;20:R328–333.

60. Panne D. The enhanceosome. Curr Opin Struct Biol. 2008;18:236–242.

61. Schroder M, Baran M, Bowie AG. Viral targeting of DEAD box protein 3 reveals its role in TBK1/IKKepsilon-mediated IRF activation. EMBO J. 2008;27:2147–2157.

62. Baum A, Garcia-Sastre A. Induction of type I interferon by RNA viruses: cellular receptors and their substrates. Amino Acids. 2010;38:1283–1299.

63. Kovacsovics M, Martinon F, Micheau O, Bodmer JL, Hofmann K, Tschopp J. Overexpression of Helicard, a CARD-containing helicase cleaved during apoptosis, accelerates DNA degradation. Curr Biol. 2002;12:838–843.

64. Kang DC, Gopalkrishnan RV, Wu Q, Jankowsky E, Pyle AM, Fisher PB. mda-5: An interferon-inducible putative RNA helicase with double-stranded RNA-dependent ATPase activity and melanoma growth-suppressive properties. Proc Natl Acad Sci U S A. 2002;99:637–642.

65. Cui Y, Li M, Walton KD, Sun K, Hanover JA, Furth PA, Hennighausen L. The Stat3/5 locus encodes novel endoplasmic reticulum and helicase-like proteins

that are preferentially expressed in normal and neoplastic mammary tissue. Genomics. 2001;78:129–134.

66. Yoneyama M, Kikuchi M, Matsumoto K, Imaizumi T, Miyagishi M, Taira K, Foy E, Loo YM, Gale M, Jr, Akira S, Yonehara S, Kato A, Fujita T. Shared and unique functions of the DExD/H-box helicases RIG-I, MDA5, and LGP2 in antiviral innate immunity. J Immunol. 2005;175:2851–2858.

67. Komuro A, Horvath CM. RNA- and virus-independent inhibition of antiviral signaling by RNA helicase LGP2. J Virol. 2006;80:12332–12342.

68. Rothenfusser S, Goutagny N, DiPerna G, Gong M, Monks BG, Schoenemeyer A, Yamamoto M, Akira S, Fitzgerald KA. The RNA helicase Lgp2 inhibits TLR-independent sensing of viral replication by retinoic acid-inducible gene-I. J Immunol. 2005;175:5260–5268.

69. Venkataraman T, Valdes M, Elsby R, Kakuta S, Caceres G, Saijo S, Iwakura Y, Barber GN. Loss of DExD/H box RNA helicase LGP2 manifests disparate antiviral responses. J Immunol. 2007;178:6444–6455.

70. de Veer MJ, Holko M, Frevel M, Walker E, Der S, Paranjape JM, Silverman RH, Williams BR. Functional classification of interferon-stimulated genes identified using microarrays. J Leukoc Biol. 2001;69:912–920.

71. Leaman DW, Chawla-Sarkar M, Jacobs B, Vyas K, Sun Y, Ozdemir A, Yi T, Williams BR, Borden EC. Novel growth and death related interferon-stimulated genes (ISGs) in melanoma: greater potency of IFN-beta compared with IFN-alpha2. J Interferon Cytokine Res. 2003;23:745–756.

72. Yu HB, Finlay BB. The caspase-1 inflammasome: a pilot of innate immune responses. Cell Host Microbe. 2008;4:198–208.

73. Poeck H, Bscheider M, Gross O, Finger K, Roth S, Rebsamen M, Hannesschlager N, Schlee M, Rothenfusser S, Barchet W, Kato H, Akira S, Inoue S, et al. Recognition of RNA virus by RIG-I results in activation of CARD9 and inflammasome signaling for interleukin 1 beta production. Nat Immunol. 2010;11:63–69.

74. Kubler K, Gehrke N, Riemann S, Bohnert V, Zillinger T, Hartmann E, Polcher M, Rudlowski C, Kuhn W, Hartmann G, Barchet W. Targeted activation of RNA helicase retinoic acid-inducible gene-I induces proimmunogenic apoptosis of human ovarian cancer cells. Cancer Res. 2010;70:5293–5304.

75. Hou J, Zhou Y, Zheng Y, Fan J, Zhou W, Ng IO, Sun H, Qin L, Qiu S, Lee JM, Lo CM, Man K, Yang Y, et al. Hepatic RIG-I predicts survival and interferon-alpha therapeutic response in hepatocellular carcinoma. Cancer Cell. 2014;25:49–63.

76. Li D, Gale RP, Liu Y, Lei B, Wang Y, Diao D, Zhang M. 5′-Triphosphate siRNA targeting MDR1 reverses multi-drug resistance and activates RIG-I-induced immune-stimulatory and apoptotic effects against human myeloid leukaemia cells. Leuk Res. 2017;58:23–30.

77. Kawaguchi Y, Miyamoto Y, Inoue T, Kaneda Y. Efficient eradication of hormone-resistant human prostate cancers by inactivated Sendai virus particle. Int J Cancer. 2009;124:2478–2487.

78. Jones M, Cunningham ME, Wing P, DeSilva S, Challa R, Sheri A, Padmanabhan S, Iyer RP, Korba BE, Afdhal N, Foster GR. SB 9200, a novel agonist of innate immunity, shows potent antiviral activity against resistant HCV variants. J Med Virol. 2017;89:1620–1628.

79. Zhu X, Nishimura F, Sasaki K, Fujita M, Dusak JE, Eguchi J, Fellows-Mayle W, Storkus WJ, Walker PR, Salazar AM, Okada H. Toll like receptor-3 ligand poly-ICLC promotes the efficacy of peripheral vaccinations with tumor antigen-derived peptide epitopes in murine CNS tumor models. J Transl Med. 2007;5:10.

80. Salem ML, El-Naggar SA, Kadima A, Gillanders WE, Cole DJ. The adjuvant effects of the toll-like receptor 3 ligand polyinosinic-cytidylic acid poly (I: C) on antigen-specific CD8+ T cell responses are partially dependent on NK cells with the induction of a beneficial cytokine milieu. Vaccine. 2006;24:5119–5132.

81. Salazar AM, Levy HB, Ondra S, Kende M, Scherokman B, Brown D, Mena H, Martin N, Schwab K, Donovan D, Dougherty D, Pulliam M, Ippolito M, et al. Long-term treatment of malignant gliomas with intramuscularly administered polyinosinic-polycytidylic acid stabilized with polylysine and carboxymethylcellulose: an open pilot study. Neurosurgery. 1996;38:1096–1103. discussion 1103-1094.

82. Rosenfeld MR, Chamberlain MC, Grossman SA, Peereboom DM, Lesser GJ, Batchelor TT, Desideri S, Salazar AM, Ye X. A multi-institution phase II study of poly-ICLC and radiotherapy with concurrent and adjuvant temozolomide in adults with newly diagnosed glioblastoma. Neuro Oncol. 2010;12:1071–1077.

83. Stupp R, Hegi ME, Mason WP, van den Bent MJ, Taphoorn MJ, Janzer RC, Ludwin SK, Allgeier A, Fisher B, Belanger K, Hau P, Brandes AA, Gijtenbeek J, et al. Effects of radiotherapy with concomitant and adjuvant temozolomide versus radiotherapy alone on survival in glioblastoma in a randomised phase III study: 5-year analysis of the EORTC-NCIC trial. Lancet Oncol. 2009;10:459–466.

84. Grossman SA, Ye X, Piantadosi S, Desideri S, Nabors LB, Rosenfeld M, Fisher J. Survival of patients with newly diagnosed glioblastoma treated with radiation

and temozolomide in research studies in the United States. Clin Cancer Res. 2010;16:2443–2449.

85. Okada H, Butterfield LH, Hamilton RL, Hoji A, Sakaki M, Ahn BJ, Kohanbash G, Drappatz J, Engh J, Amankulor N, Lively MO, Chan MD, Salazar AM, et al. Induction of robust type-I CD8+ T-cell responses in WHO grade 2 low-grade glioma patients receiving peptide-based vaccines in combination with poly-ICLC. Clin Cancer Res. 2015;21:286–294.

86. Dillon PM, Petroni GR, Smolkin ME, Brenin DR, Chianese-Bullock KA, Smith KT, Olson WC, Fanous IS, Nail CJ, Brenin CM, Hall EH, Slingluff CL., Jr A pilot study of the immunogenicity of a 9-peptide breast cancer vaccine plus poly-ICLC in early stage breast cancer. J Immunother Cancer. 2017;5:92.

87. Mehrotra S, Britten CD, Chin S, Garrett-Mayer E, Cloud CA, Li M, Scurti G, Salem ML, Nelson MH, Thomas MB, Paulos CM, Salazar AM, Nishimura MI, et al. Vaccination with poly(IC: LC) and peptide-pulsed autologous dendritic cells in patients with pancreatic cancer. J Hematol Oncol. 2017;10:82.

88. Tsuji T, Sabbatini P, Jungbluth AA, Ritter E, Pan L, Ritter G, Ferran L, Spriggs D, Salazar AM, Gnjatic S. Effect of Montanide and poly-ICLC adjuvant on human self/tumor antigen-specific CD4+ T cells in phase I overlapping long peptide vaccine trial. Cancer Immunol Res. 2013;1:340–350.

89. Sabbatini P, Tsuji T, Ferran L, Ritter E, Sedrak C, Tuballes K, Jungbluth AA, Ritter G, Aghajanian C, Bell-McGuinn K, Hensley ML, Konner J, Tew W, et al. Phase I trial of overlapping long peptides from a tumor self-antigen and poly-ICLC shows rapid induction of integrated immune response in ovarian cancer patients. Clin Cancer Res. 2012;18:6497–6508.

90. Rapoport AP, Aqui NA, Stadtmauer EA, Vogl DT, Xu YY, Kalos M, Cai L, Fang HB, Weiss BM, Badros A, Yanovich S, Akpek G, Tsao P, et al. Combination immunotherapy after ASCT for multiple myeloma using MAGE-A3/Poly-ICLC immunizations followed by adoptive transfer of vaccine-primed and costimulated autologous T cells. Clin Cancer Res. 2014;20:1355–1365.

91. Yuan D, Xia M, Meng G, Xu C, Song Y, Wei J. Anti-angiogenic efficacy of 5′-triphosphate siRNA combining VEGF silencing and RIG-I activation in NSCLCs. Oncotarget. 2015;6:29664–29674. doi: 10.18632/oncotarget.4869.

92. Buers I, Nitschke Y, Rutsch F. Novel interferonopathies associated with mutations in RIG-I like receptors. Cytokine Growth Factor Rev. 2016;29:101–107.

93. Lee-Kirsch MA. The Type I Interferonopathies. Annu Rev Med. 2017;68:297–315.

94. Trinchieri G. Type I interferon: friend or foe? J Exp Med. 2010;207:2053–2063.

95. Palmer CR, Jacobson ME, Fedorova O, Pyle AM, Wilson JT. Environmentally Triggerable Retinoic Acid-Inducible Gene I Agonists Using Synthetic Polymer Overhangs. Bioconjug Chem. 2018;29:742–747.

96. Miller KD, Siegel RL, Lin CC, Mariotto AB, Kramer JL, Rowland JH*, et al.* Cancer treatment and survivorship statistics, 2016. *CA Cancer J Clin* 2016,66:271-289.

97. Cimino-Mathews A, Foote JB, Emens LA. Immune targeting in breast cancer. *Oncology (Williston Park)* 2015,29:375-385.

98. Emens LA, Kok M, Ojalvo LS. Targeting the programmed cell death-1 pathway in breast and ovarian cancer. *Curr Opin Obstet Gynecol* 2016,28:142-147.

99. Nanda R, Chow LQ, Dees EC, Berger R, Gupta S, Geva R*, et al.* Pembrolizumab in Patients With Advanced Triple-Negative Breast Cancer: Phase Ib KEYNOTE-012 Study. *J Clin Oncol* 2016,34:2460-2467.

100. Garcia-Teijido P, Cabal ML, Fernandez IP, Perez YF. Tumor-Infiltrating Lymphocytes in Triple Negative Breast Cancer: The Future of Immune Targeting. *Clin Med Insights Oncol* 2016,10:31-39.

101. Luen SJ, Savas P, Fox SB, Salgado R, Loi S. Tumour-infiltrating lymphocytes and the emerging role of immunotherapy in breast cancer. *Pathology* 2017,49:141-155.

102. Wincott F, DiRenzo A, Shaffer C, Grimm S, Tracz D, Workman C*, et al.* Synthesis, deprotection, analysis and purification of RNA and ribozymes. *Nucleic Acids Res* 1995,23:2677-2684.

103. Zlatev I, Lackey JG, Zhang L, Dell A, McRae K, Shaikh S*, et al.* Automated parallel synthesis of 5'-triphosphate oligonucleotides and preparation of chemically modified 5'-triphosphate small interfering RNA. *Bioorg Med Chem* 2013,21:722-732.

104. Wilson JT, Keller S, Manganiello MJ, Cheng C, Lee CC, Opara C*, et al.* pH-Responsive nanoparticle vaccines for dual-delivery of antigens and immunostimulatory oligonucleotides. *ACS Nano* 2013,7:3912-3925.

105. Ciriello G, Gatza ML, Beck AH, Wilkerson MD, Rhie SK, Pastore A*, et al.* Comprehensive Molecular Portraits of Invasive Lobular Breast Cancer. *Cell* 2015,163:506-519.

106. Curtis C, Shah SP, Chin SF, Turashvili G, Rueda OM, Dunning MJ*, et al.* The genomic and transcriptomic architecture of 2,000 breast tumours reveals novel subgroups. *Nature* 2012,486:346-352.

107. Kohlway A, Luo D, Rawling DC, Ding SC, Pyle AM. Defining the functional determinants for RNA surveillance by RIG-I. *EMBO Rep* 2013,14:772-779.

108. Wallden B, Emond M, Swift ME, Disis ML, Swisshelm K. Antimetastatic gene expression profiles mediated by retinoic acid receptor beta 2 in MDA-MB-435 breast cancer cells. *BMC Cancer* 2005,5:140.

109. Venkatesh A, Nandigam H, Muccioli M, Singh M, Loftus T, Lewis D*, et al.* Regulation of inflammatory factors by double-stranded RNA receptors in breast cancer cells. *Immunobiology* 2017.

110. Liang H, Deng L, Hou Y, Meng X, Huang X, Rao E*, et al.* Host STING-dependent MDSC mobilization drives extrinsic radiation resistance. *Nat Commun* 2017,8:1736.

111. Nabet BY, Qiu Y, Shabason JE, Wu TJ, Yoon T, Kim BC*, et al.* Exosome RNA Unshielding Couples Stromal Activation to Pattern Recognition Receptor Signaling in Cancer. *Cell* 2017,170:352-366 e313.

112. Chandran SS, Klebanoff CA. T cell receptor-based cancer immunotherapy: emerging efficacy and pathways of resistance. *Immunol Rev* 2019, 290:127-147.

113. Plitas G, Konopacki C, Wu K, et al. Regulatory T-cells exhibit distinct Features in human breast cancer. *Immunity* 2016,45:1122-1134.

114. Elion DL, Jacobson ME, Hicks DJ, et al. Therapeutically Active RIG-I Agonist Induces Immunogenic Tumor Cell Killing in Breast Cancers. *Cancer Res* 2018,78:6183-6195.

115. Nguyen T, Russell J. The regulation of FasL expression during activation-induced cell death (AICD). *Immunol* 2001,103:426-434.

116. Bubenik J. Tumour MHC class I downregulation and immunotherapy. *Oncol Rep* 2003,10:2005-2008.

117. Kubler K, Pesch C, Gehrke N, et al. Immunogenic cell death of human ovarian cancer cells induced by cytosolic poly(I:C) leads to myeloid cell maturation and activates NK cells. *Eur J Immunol* 2011,41:3028-3039.

118. Szabo A, Fekete T, Koncz G, et al. RIG-I inhibits the MAPK-dependent proliferation of BRAF mutant melanoma cells via MKP-1. *Cellular Signaling* 2016, 28:335-347.

119. Li XY, Jiang LJ, Chen L, et al. RIG-I modulates Src-mediated AKT activation to restrain leukemic stemness. *Molecular Cell* 2014,53:407-419.

120. Tormo D, Checinska A, et al. Targeted activation of innate immunity for therapeutic induction of autophagy and apoptosis in melanoma cells. *Cancer Cell* 2009,16:103-114.

121. Odendall C, Dixit E, et al. Diverse intracellular pathogens activate type III interferon expression from peroxisomes. *Nat Immunol* 2014,15:717-726.

122. Quicke KM, Kim KY, et al. RNA Helicase LGP2 Negatively Regulates RIG-I Signaling by Preventing TRIM25-Mediated Caspase Activation and Recruitment Domain Ubiquitination. J Interferon *Cytokine Res* 2019.

123. Xu P, Bailey-Bucktrout S, Xi Y, et al. Innate antiviral host defense attenuates TGF-B function through IRF3-mediated suppression of smad signaling. *Molecular Cell* 2014,56:723-737

124. Poh A, Ernst M. Targeting macrophages in cancer: from bench to bedside. Front Oncol 2018,8:49.

125. Yang M, McKay D, Pollard J, Lewis C. Diverse functions of macrophages in different tumor microenvironments. Cancer Res 2018,78:5492-5503

126. Gordon SR, Maute RL, Dulken BW, et al. PD-1 expression by tumor-associated macrophages inhibits phagocytosis and tumor immunity. *Nature* 2018,545:495-499.

127. Dixit E, Boulant S, Zhang Y, et al. Peroxisomes are signaling platforms for antiviral innate immunity. *Cell* 2010,141:668-681.

128. Rugo HS, et al. Safety and Antitumor Activity of Pembrolizumab in Patients with Estrogen Receptor–Positive/Human Epidermal Growth Factor Receptor 2–Negative Advanced Breast Cancer. *Clin Cancer Res* 2018;24:2804-2811.

129. Dirix LY, et al. Avelumab, an anti-PD-L1 antibody, in patients with locally advanced or metastatic breast cancer: a phase 1b JAVELIN Solid Tumor study. *Breast Cancer Res Treat* 2018;167:671-686.

130. Emens LA, et al. Long-term Clinical Outcomes and Biomarker Analyses of Atezolizumab Therapy for Patients With Metastatic Triple-Negative Breast Cancer: A Phase 1 Study. *JAMA Oncol* 2018; doi:10.1001/jamaoncol.2018.4224

131. Loi S, et al. Prognostic and predictive value of tumor-infiltrating lymphocytes in a phase III randomized adjuvant breast cancer trial in node-positive breast cancer comparing the addition of docetaxel to doxorubicin with doxorubicin-based chemotherapy: BIG 02-98. *J Clin Oncol* 2013;31(7):860-867

132. Haricharan S, et al. Somatic mutation load of estrogen receptor-positive breast tumors predicts overall survival: an analysis of genome sequence data. *Breast Cancer Res Treat* 2014;146:211-220.

133. Cimino-Mathews A, et al. PD-L1 (B7-H1) expression and the immune tumor microenvironment in primary and metastatic breast carcinomas. *Hum Pathol* 2016;47:52-63.

134. Scanlan MJ, Jager D. Challenges to the development of antigen-specific breast cancer vaccines. *Breast Cancer Res* 2001;3:95-98

135. Ott P, Hu Z, Keskin D, et al. An immunogenic personal neoantigen vaccine for patients with melanoma. *Nature* 2017;547:217-221.